Ruamāhanga Airborne Aquifer Mapping Project: SkyTEM data processing and resistivity models

RL Kellett
T Brakenrig
AL Kirkby
DT Berhe
BS Keats
L Coup
F Sanders
M Herpe

GNS Science Consultancy Report 2024/60
June 2024

GNS SCIENCE
TE PŪ AO

DISCLAIMER

This report has been prepared by the Institute of Geological and Nuclear Sciences Limited (GNS Science) exclusively for and under contract to Greater Wellington Regional Council. Unless otherwise agreed in writing by GNS Science, GNS Science accepts no responsibility for any use of or reliance on any contents of this report by any person other than Greater Wellington Regional Council and shall not be liable to any person other than Greater Wellington Regional Council, on any ground, for any loss, damage or expense arising from such use or reliance.

Use of Data:

Date that GNS Science can use associated data: 1 July 2025

BIBLIOGRAPHIC REFERENCE

Kellett RL, Kirkby AL, Keats BS, Sanders F, Brakenrig T, Berhe DT, Coup L, Herpe M. 2024. Ruamāhanga Airborne Aquifer Mapping Project: SkyTEM data processing and resistivity models. Lower Hutt (NZ): GNS Science. 96 p. Consultancy Report 2024/60.

CONTENTS

FIGURES

TABLES

APPENDICES

APPENDIX FIGURES

APPENDIX TABLES

EXECUTIVE SUMMARY

The Ruamāhanga Airborne Aquifer Mapping Project is a multi-year initiative (2022–2025) jointly funded by the Kānoa Regional Economic Development & Investment Unit (Kānoa), Greater Wellington Regional Council (GWRC), Masterton District Council, Carterton District Council and South Wairarapa District Council. The project utilises airborne electromagnetic surveying technology (SkyTEM) to improve groundwater resource potential mapping and 3D modelling of the spatial extent of the aquifers within the Ruamāhanga Catchment in the Wairarapa Valley. The project is managed by GWRC on behalf of the group that provided funding. GNS Science (GNS) undertook technical support of the acquisition and leadership of the processing and interpretation. The technical outputs of this phase of the project were reviewed by the Aarhus University HydroGeophysics Group (HGG).

A total of 5684 km of SkyTEM data were collected over the Wairarapa Valley by SkyTEM Australia between 28 January and 2 March 2023. This report details the steps taken to remove electromagnetic noise and produce resistivity models from the acquired SkyTEM datasets. The project also included compiling the existing geoscience data and developing a framework for future hydrogeological interpretation of the modelled resistivity in the Ruamāhanga Catchment.

Both automatic and manual processing was carried out by GNS to remove electromagnetic noise from the SkyTEM low-moment and high-moment data. This processing was quality-checked by HGG. Post-processing was undertaken by GNS to remove any remaining artefacts and then a second quality check was undertaken by HGG. Using the retained data, spatially constrained inversions were performed, creating both smooth and sharp resistivity models. The resistivity models were delivered to GWRC in a range of formats compatible with GIS and geological modelling software.

An appraisal of the model was undertaken through a series of workshops where GNS worked with GWRC and its consultants to review the resistivity model and compare the results to the supporting geoscience information. These additional datasets include borehole lithology logs, the QMAP geology map, ground-based resistivity and electromagnetic measurements and seismic-reflection profiles.

The SkyTEM survey reveals a detailed 3D resistivity picture of the subsurface. The resistivity models have a layer thickness of 2–4 m in the near-surface and are discretised to a depth of 600 m. The standard depth of investigation varies from 22 m over low-resistivity ground to 670 m over highly resistive areas. Digital versions of the resistivity model have been provided to GWRC and images of the sections and slices through the resistivity model are presented in this report.

Hydrogeological interpretation of the 3D resistivity models is needed to make full use of the SkyTEM survey results. This follow-on work will be described in a separate report.

This page left intentionally blank.

1.0 INTRODUCTION

The Ruamāhanga Airborne Aquifer Mapping Project is a three-year initiative jointly funded by the Kānoa Regional Economic Development & Investment Unit (Kānoa; formerly the Provincial Growth Unit), Greater Wellington Regional Council (GWRC), Masterton District Council, Carterton District Council and South Wairarapa District Council. The project was originally designed to begin in 2019 and conclude in 2022. Delays due to COVID-19 meant that the project started in 2022. The project applies airborne electromagnetic (AEM) survey technology (SkyTEM) to improve the understanding of the hydrogeological units in the Ruamāhanga Catchment. The goal is to develop a more detailed groundwater resource-potential map and provide input for the next generation of 3D groundwater flow models within the Wairarapa Valley. To execute the project, GWRC engaged SkyTEM Australia to collect the AEM data and GNS Science (GNS) to process and interpret the data. GNS sub-contracted the Aarhus University HydroGeophysics Group (HGG) to provide an independent review of the data quality and processing steps. The key participants in the project are listed in Table 1.1. Phase 1 of the project was completed in June 2024 with the delivery of a resistivity model to GWRC. A second phase is planned that will develop a hydrogeological model and web-based mapping product.

SkyTEM is a specific airborne geophysical technique that uses transient (time-domain) electromagnetics (TEM) to investigate the shallow (up to ~500 m deep) electrical resistivity structure of the Earth. The resistivity structure can then be interpreted in terms of hydrogeological relevance to delineate potential groundwater aquifers and used to inform and improve existing geological/hydrological models. Data are collected using specialist equipment that is slung beneath a helicopter and flown at low elevations along closely spaced lines. A key advantage of this technique is that it enables a large amount of high-resolution data to be collected quickly and cost-effectively.

SkyTEM Australia collected AEM data in the Wairarapa Valley, commencing 28 January 2023 and ending 2 March 2023. This data collection is described by SkyTEM Australia Pty Ltd (2023). The field-data acquisition, production report, and datasets were reviewed by GNS and a letter report describing the survey was provided to GWRC (Kellett et al. 2023). The acquisition included AEM data and magnetic field data. The area covered by the survey included low-lying areas in southern Wairarapa (Lake Onoke, Lake Wairarapa and a small section offshore), five urban centres (Featherston, Martinborough, Carterton, Greytown and Masterton) and some elevated areas around the edges of the basin (Figure 1.1). In this report, we refer to the area covered by the survey as the Ruamāhanga Catchment, recognising that it is only the portion of the catchment that lies in the floor of the Wairarapa Valley.

The current report provides the background to the datasets delivered to GWRC as part of the first phase of the Ruamāhanga Airborne Aquifer Mapping Project. The report has three aims:

1. Provide a brief description of the SkyTEM data acquisition and the SkyTEM system.
2. Give a detailed description of the steps taken to develop resistivity models for the portion of the Ruamāhanga Catchment covered by the SkyTEM survey.
3. Describe the products delivered to GWRC as the outputs of Phase 1.

The report is structured in the following way:

- Sections 1 and 2 summarise the SkyTEM data collection.
- Processing and noise removal are described in Section 3.
- Inversion procedures used to develop the resistivity models are described in Section 4.

- The workshops and process undertaken to review the resistivity model are described in Section 5.
- Geophysical maps, cross-sections and digital deliverables are provided in Appendices 1–4 and described in Section 6.
- Section 7 summarises the additional geoscience data used to support the processing and development of the resistivity models.

A standard reporting template has been used as the basis for this report (e.g. HGG 2017; Rawlinson et al. 2021).

Table 1.1 Survey details.

SkyTEM Survey, Ruamāhanga Catchment	
Client	Greater Wellington Regional Council
Key Personnel	**GNS Science, New Zealand** Project lead/management: *Richard Kellett* Data processing, modelling and reporting: *Alison Kirkby, Brook Keats, Daniel Teke Berhe, Richard Kellett, Fiona Sanders, Maïwenn Herpe* **HGG Aarhus University, Denmark** Quality assurance: *Andy Kass, Jesper B Pedersen* **Greater Wellington Regional Council** Project lead: *Bruce Geden, Rebecca Morris* Project staff: *Rob van der Raaij, Lindsay Annear, Mike Thompson*
Locality	Ruamāhanga, Wairarapa, New Zealand
Survey Period	28 January – 2 March 2023
SkyTEM System	SkyTEM312
Line km acquired	5684 km (including repeated lines)
Line spacing	200 m and 400 m
Mean flight speed	98 km/h
Mean flight altitude of the TEM loop	44 m

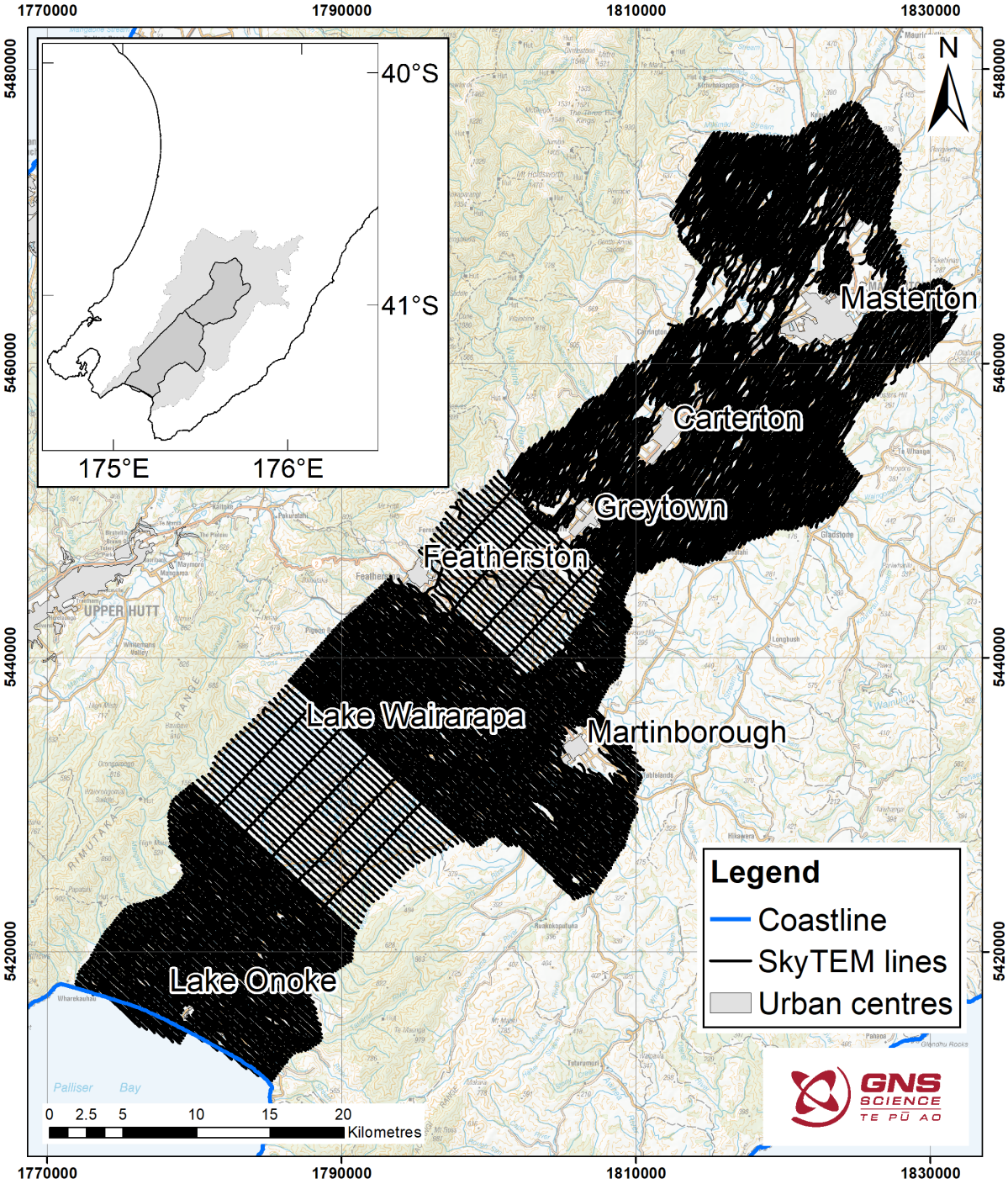

Figure 1.1 Location map of the Ruamāhanga Airborne Aquifer Mapping Project area. The inset map shows the lower North Island and the location of the survey area (dark grey) within the Ruamāhanga Catchment (light grey). The main map shows the flight lines and the main geographical features of the area.

2.0 THE SKYTEM SYSTEM

2.1 Overview

SkyTEM is a time-domain (transient) helicopter electromagnetic system designed for hydrogeophysical and environmental investigations. The following section contains a general introduction to the SkyTEM system. A more thorough description of the SkyTEM method can be found in Sørensen and Auken (2004). A description of the TEM method in general can be found in Nabighian and Macnae (1991) and Jørgensen et al. (2003).

2.1.1 Instrument

Figure 2.1 shows the SkyTEM system with the hexagonal frame slung beneath the helicopter. The lengths of the frame sides are approximately 12 m. The transmitter loop is mounted on the frame in an octagonal polygon configuration. To obtain a close-to-zero coupling to the primary magnetic field, the receiver coil (Figure 2.1) (also referred to as the Z coil or Z Rx coil) is placed at the back of the loop, approximately 2 m above the frame. Two lasers are placed on the frame, continuously measuring the distance to the ground surface below the loop, and two inclinometers measure the roll and pitch of the frame. Power is supplied by a generator placed on the sling cable between the helicopter and the loop, sufficiently away from the receiver to reduce noise. The positions of the various devices on the frame are shown in Figure 2.2 and listed in Table 2.1. A downward-facing camera is mounted on the helicopter to provide an additional check on the attitude of the loop and its location relative to features on the ground.

2.1.2 Measurement Procedure

The configuration of the system is customised for each survey. Measurements are carried out with one or two transmitter moments, depending on the target geology. The standard configuration uses a low (LM) and high (HM) transmitter moment, applied sequentially. For this survey, all data were acquired using interleaved LM and HM transmitter modes, consisting of 110 LM positive and negative pulse pairs at 275 Hz and 30 HM pulse pairs at 25 Hz, which repeats every 1.6 s (SkyTEM Australia Pty Ltd 2023). Data are recorded within ‘gates’, which are equivalent to specified time intervals. Lower-numbered gates (earlier times) correspond to information related to shallower depths than higher-numbered gates (later times). Standard processing utilises LM gates 9–26 and HM gates 16–38 (SkyTEM Australia Pty Ltd 2023). The numbering of the gates for LM and HM are independent. There is a significant overlap in the times of the LM and HM gates, with LM gates 23–26 corresponding to HM gates 16–24 (see Section 2.2: Tables 2.2, 2.3 and 2.4).

The flight altitude depends on the flight speed, the roughness of the terrain and the presence of obstacles such as towers, tall trees and buildings. The nominal flight altitude for this survey was 45–55 m (frame height). Over forested areas, the altitude is increased to maintain safe clearance over the treetops. The flight speed can be adjusted to a maximum of 120 km/hr to balance survey time, data density on the ground, smearing of data recovered at depth and a more stable levelling of the transmitter loop. For the present survey, a mean speed of 98 km/hr was used.

Apart from GPS, attitude, altitude and TEM data, several instrument parameters are monitored and stored for quality-control use when the data are processed.

2.1.3 Depth of Investigation

The depth of investigation (DOI) for the SkyTEM system is defined as the depth for which data can be reliably used, given that the signal strength decreases over time, which equates to depth in the subsurface. The DOI depends on the transmitter moment, geological setting, background noise level, flight speed and altitude (as air is highly resistive). Normally, a DOI of between 150 and 500 m can be achieved. The DOIs are estimated for each resistivity model during the inversion process (see Section 4.5).

2.2 Technical Specification

The system instrument set-up is shown in Figure 2.2. The positioning of the instruments and the corners of the octagon described by the transmitter coil are listed in Table 2.1. The origin is defined as the centre of the transmitter coil.

The SkyTEM system was configured in a standard two-moment set-up: LM and HM. The specifications of these are summarised in Tables 2.2–2.4. See SkyTEM Australia Pty Ltd (2023) for further details.

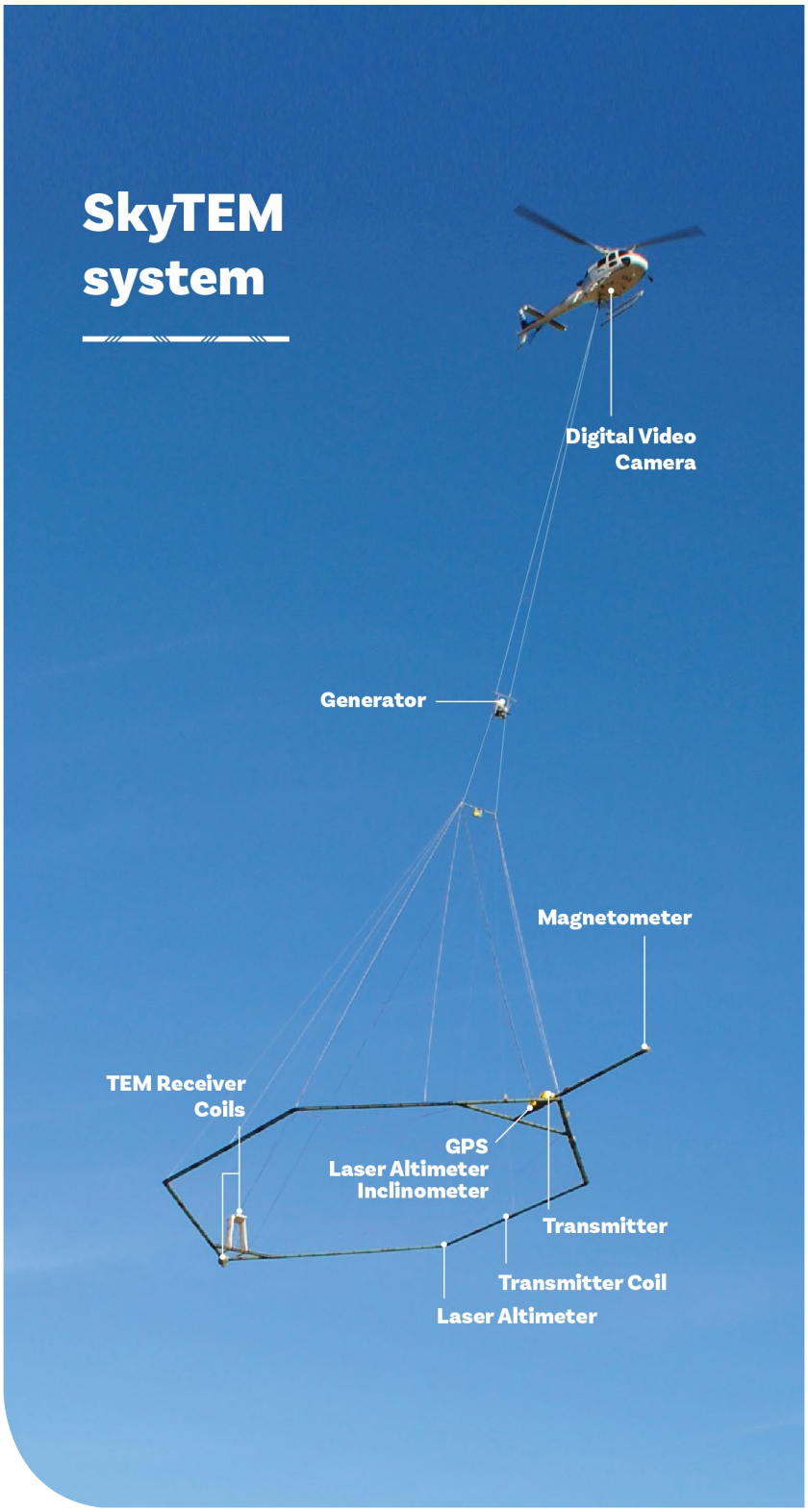

Figure 2.1 The SkyTEM312 system. The transmitter frame holds the transmitter loop, inclinometers, laser-altimeters, receiver coils and instrumentation. For a detailed instrument set-up, see Figure 2.2. Figure from SkyTEM Australia Pty Ltd.

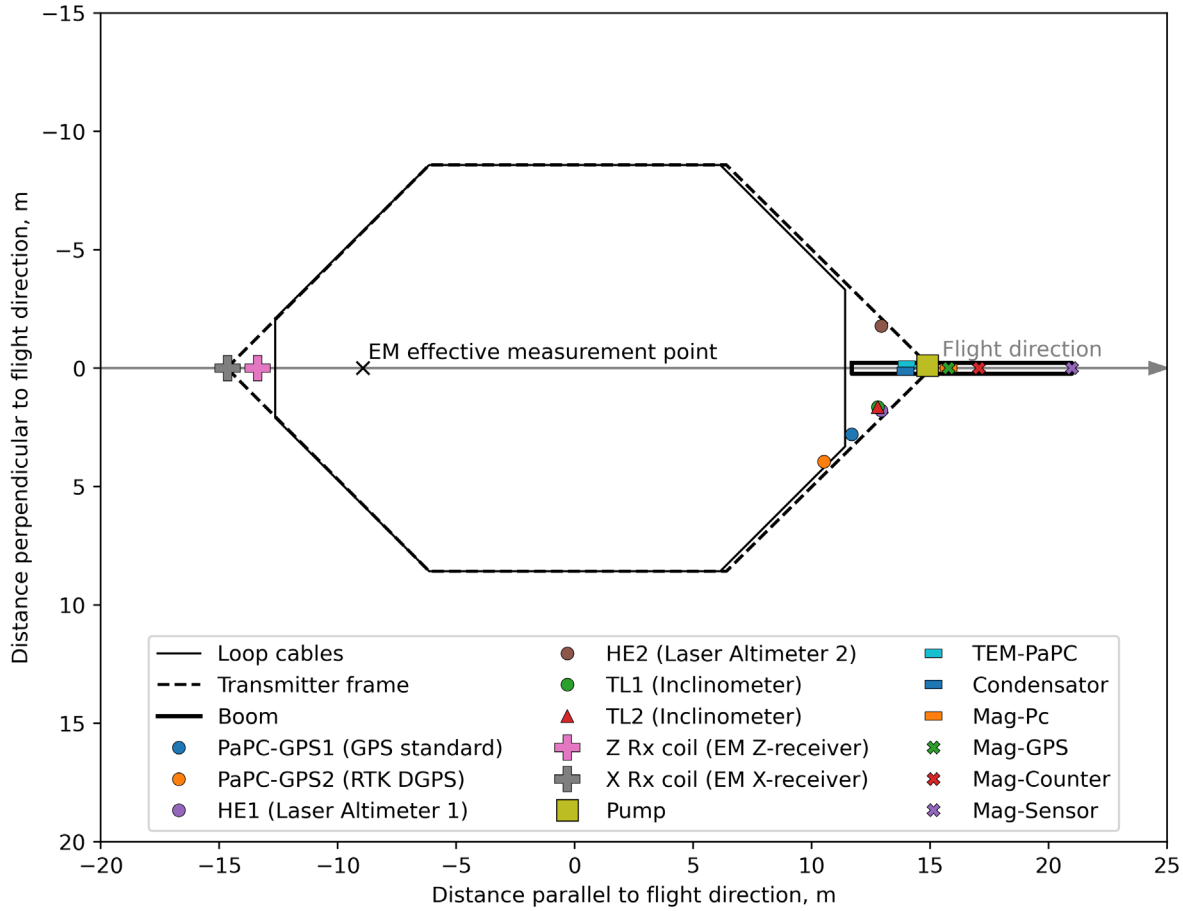

Figure 2.2 Instrument set-up for the SkyTEM312 system used. Modified from SkyTEM Australia Pty Ltd (2023).

Table 2.1 Summary of equipment and transmitter coil corner positioning. The origin is defined as the centre of the transmitter coil. Z is positive towards the ground. EM = electromagnetic.

Unit	X (m)	Y (m)	Z (m)
PaPC-GPS1 (GPS standard)	11.68	2.79	-0.16
PaPC-GPS2 (RTK DGPS)	10.51	3.95	-0.16
HE1 (Laser Altimeter 1)	12.94	1.79	-0.12
HE2 (Laser Altimeter 2)	12.94	-1.79	-0.12
TL1 (Inclinometer)	12.79	1.64	-0.12
TL2 (Inclinometer)	12.79	1.64	-0.12
Z Rx coil (EM Z-receiver coil)	-13.39	0.00	-2.00
X Rx coil (EM X-receiver coil)	-14.65	0.00	0.00
Loop corner 1	-12.64	-2.10	0.00
Loop corner 2	-6.14	-8.58	0.00
Loop corner 3	6.14	-8.58	0.00
Loop corner 4	11.41	-3.31	0.00
Loop corner 5	11.41	3.31	0.00
Loop corner 6	6.14	8.58	0.00
Loop corner 7	-6.14	8.58	0.00
Loop corner 8	-12.64	2.10	0.00

Table 2.2 Summary of low-moment and high-moment transmitter (Tx) and receiver (Rx) specifications.

Parameter	Low Moment	High Moment
Number of turns	2	12
Transmitter area	342.0 m^2	342.0 m^2
Tx current	~ 6 A	~ 110 A
Tx peak moment	~ 4100 Am^2	~ 454,700 Am^2
Repetition frequency	275 Hz	25 Hz
Tx-on-time	0.8 ms	5.0 ms
Tx-off-time	1.018 ms	15.0 ms
Duty cycle	44%	25%
Gate time interval (centres)	2.415 µs – 0.861 ms	436.415 µs – 13.187 ms
Parameter	**X**	**Z**
Rx coil effective area	115.5 m^2	325 m^2
Rx coil low pass cut-off frequency	348.3 KHz	203.6 KHz

Table 2.3 SkyTEM312 low-moment (LM) channel times. All gate times are relative to the start of the transmitter current ramp down. Gates 3–8 are within the ramp-down time (see Section 4.1).

LM Gate Number	Gate Width (µs)	Gate Open (µs)	Gate Centre (µs)	Gate Close (µs)
3	1.57	1.63	2.415	3.20
4	1.57	3.63	4.415	5.20
5	1.57	5.63	6.415	7.20
6	1.57	7.63	8.420	9.20
7	1.57	9.63	10.410	11.20
8	2.57	11.63	12.920	14.20
9	3.57	14.63	16.415	18.20
10	4.57	18.63	20.915	23.20
11	5.57	23.63	26.415	29.20
12	7.57	29.63	33.415	37.20
13	9.57	37.63	42.415	47.20
14	12.57	47.63	53.915	60.20
15	15.57	60.63	68.415	76.20
16	19.57	76.63	86.415	96.20
17	24.57	96.63	108.915	121.20
18	30.57	121.63	136.915	152.20
19	50.57	152.63	177.915	203.20
20	50.57	203.63	228.915	254.20
21	50.57	254.63	279.915	305.20
22	100.57	305.63	355.915	406.20
23	100.57	406.63	456.915	507.20
24	100.57	507.63	557.915	608.20
25	151.57	608.63	684.415	760.20
26	201.57	760.63	861.415	962.20

Table 2.4 SkyTEM312 high-moment (HM) channel times. All gate times are relative to the start of the transmitter current ramp down.

HM Gate Number	Gate Width (μs)	Gate Open (μs)	Gate Centre (μs)	Gate Close (μs)
16	19.57	426.63	436.415	446.20
17	24.57	446.63	458.915	471.20
18	30.57	471.63	486.915	502.20
19	50.57	502.63	527.915	553.20
20	50.57	553.63	578.915	604.20
21	50.57	604.63	629.915	655.20
22	100.57	655.63	705.915	756.20
23	100.57	756.63	806.915	857.20
24	100.57	857.63	907.915	958.20
25	151.57	958.63	1034.415	1110.20
26	201.57	1110.63	1211.415	1312.20
27	252.57	1312.63	1438.915	1565.20
28	353.57	1565.63	1742.415	1919.20
29	403.57	1919.63	2121.415	2323.20
30	504.57	2323.63	2575.915	2828.20
31	707.57	2828.63	3182.415	3536.20
32	807.57	3536.63	3940.415	4344.20
33	1009.57	4344.63	4849.415	5354.20
34	1211.57	5354.63	5960.415	6566.20
35	1415.57	6566.63	7274.415	7982.20
36	1819.57	7982.63	8892.415	9802.20
37	2019.57	9802.63	10812.415	11822.20
38	2729.57	11822.63	13187.415	14552.20

3.0 PROCESSING

3.1 Pre-Processing – Primary Field Compensation

The magnetic field coupling between the receiver coils and transmitter loops is continuously hardware-monitored, providing a separate value for the magnetic field coupling during each transient sounding. High-altitude data are collected at an elevation of greater than 400 m altitude to identify the response of the system in the absence of electrical conductors. These data are used to remove the primary field during raw data correction in a process known as Primary Field Compensation (PFC). The PFC enables accurate modelling and inversion of the very early time gates, and some on-time gates in the LM, to yield shallow geological information (Auken et al. 2020).

PFC-corrected data and LM system response were provided by SkyTEM Australia Pty Ltd (2023).

3.2 Workflow

The software package AGS Seequent Workbench (Workbench) was used for processing the SkyTEM data.

The aim of this processing was to prepare data for the geophysical inversion modelling. The processing primarily includes filtering and averaging of data, as well as culling and discarding distorted or noisy data.

The data processing can be summarised in four steps:

1. **Import of SkyTEM data into a fixed database structure:** SkyTEM Australia provide data in a range of formats (SkyTEM Australia Pty Ltd 2023). The raw data are supplied as binary files with some additional ASCII system files. These files can be imported into the workstation and processing can be applied from scratch. Alternatively, a pre-processed version is provided in an ASCII file that contains the critical data in columns. The columns include flight numbers, line numbers, GPS positions, measurement date and time, transmitter loop tilt, laser elevation, transmitter currents, powerline monitor signal, HM and LM amplitudes (TEM voltage) for each window for each receiver component, estimates of the uncertainty, and the magnetic field data.
2. **Automatic processing:** Automatic processing was applied to the GPS, altitude, tilt and TEM voltage data. This automatic processing removes points that were deemed likely to be influenced by noise based on set thresholds on data characteristics, for example, gradients in the dB/dt curve. Further details of automatic filtering is provided in Sections 3.5 and 3.6.
3. **Manual processing:** Inspection and editing of the results of the automatic processing for the data types in question.
4. **Post-processing and quality-checking of the data processing**, including utilising preliminary inversion results.

All data are recorded with a common time stamp. For this survey, the data were provided at intervals of 0.2 s. This time stamp is used to link position, geometry and electromagnetic voltage data. The time stamp is given as the UTC time. A sample interval of 0.2 s equates to a spacing of between 5 and 7 m for a flying speed of between 90 and 100 km/hr. This interval is smaller than necessary to image the ground at the resolution of the system and results in very large files that make the processing slow. In order to speed up the processing without sacrificing spatial resolution, the data were re-sampled at 1 s intervals.

The survey area is divided into two blocks, described as the ‘Main block’ and ‘Masterton block’. The Main block was flown on lines oriented 130/310° (relative to True or Geographic North), with areas around the Martinborough and Featherston townships avoided due to safety issues of flying over built-up areas. The Masterton block was flown on lines oriented 030/210° (relative to True or Geographic North). Parts of this block were not flown around suburbs, hobby farms and stables adjacent to Masterton, Carterton and Greytown, leaving some larger gaps than anticipated. Several tie-lines were flown to tie the Main and Masterton blocks. The Main block extended out to 1 km offshore and covered Lake Wairarapa. Several tie-lines were also flown across the Masterton block north of Carterton (SkyTEM Australia Pty Ltd 2023). Processing was undertaken on each block separately using the same workflow. Figure 3.1 shows the locations of the Main and Masterton blocks.

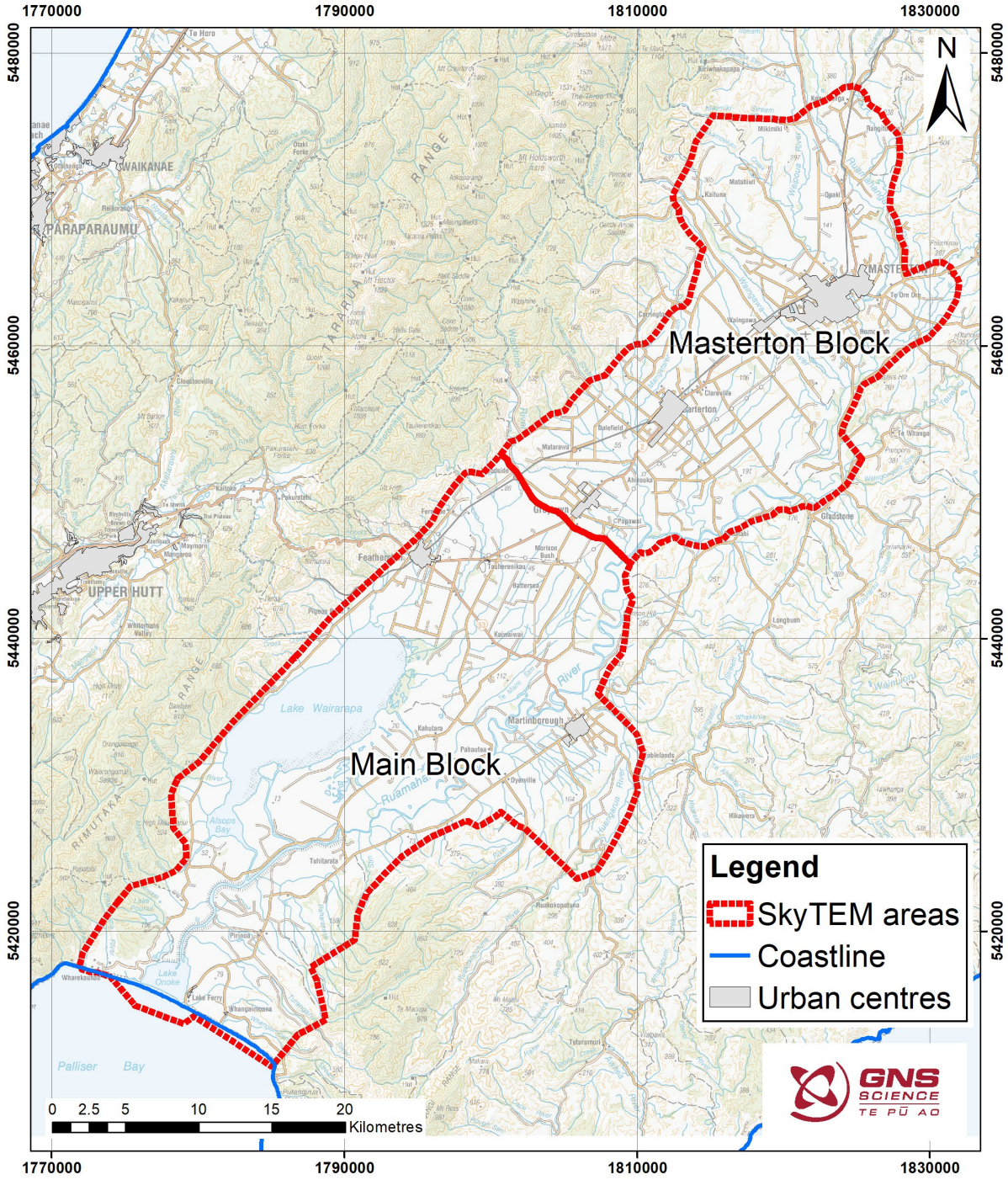

Figure 3.1 Location of the SkyTEM survey divided on the Main (southern) and Masterton (northern) blocks.

In the following section, a short description of the processing of the different data types is presented. A more thorough description of the SkyTEM data processing can be found in Auken et al. (2009).

3.3 GPS Positioning

The TERRASTAR HP (high-precision) real-time differential correction service was used to provide a real-time input to the channel GP2 (SkyTEM Australia Pty Ltd 2023).

The GP2 GPS data were shifted to the optimal measurement point of the SkyTEM system, which is approximately two-thirds of the distance from the centre of the frame towards the receiver coil. In this survey, the GPS data are shifted 8.9 m from the centre of the loop towards the rear of the system (Figure 2.2).

3.4 Roll and Pitch Data

SkyTEM Australia utilise the roll and pitch of the frame to correct the altitude of the frame and effective area of the transmitter loop for the voltage data calculation. It is presumed that the frame is rigid and so the roll and pitch of the transmitter and receiver coils are identical. Pitch and roll will affect the orientation of the electromagnetic field relative to the ground surface. It will also affect the distance measured by the laser altimeters. These corrected data are provided in the XYZ files, so no additional attitude corrections were required.

3.5 Altitude Data

The distance between the transmitter coil and the ground is measured with two independent lasers. If the terrain is flat and the loop horizontal, the altitude calculated from the two lasers should be the same and is the most accurate measurement of the distance from the loop to the ground. The elevation of the transmitter loop is also measured with GPS receivers. Figure 3.2 shows an altitude data example over some hilly topography and the Ruamāhanga River east of Carterton. During automatic filtering, a Digital Elevation Model (DEM) was also used. This DEM is used by Workbench, along with the GPS elevation values, to calculate a GPS-based altitude. Here, ‘altitude’ means height above the ground, while ‘elevation’ means height above sea level. This GPS altitude was not used directly but was utilised as a guideline during manual altitude user edits. The DEM utilised was a 10-m-resolution DEM derived from a 1-m-resolution LiDAR elevation model available over the entire Wellington area.

The aim of the altitude data processing is to remove laser reflections that do not come from the ground but typically bounce off the tree canopy and other above-ground features (e.g. large buildings). The processing is based on the fact that reflections from treetops result in an apparently lower altitude than reflections from the surface. Automatic filtering of the altitude data was followed by a manual inspection and correction.

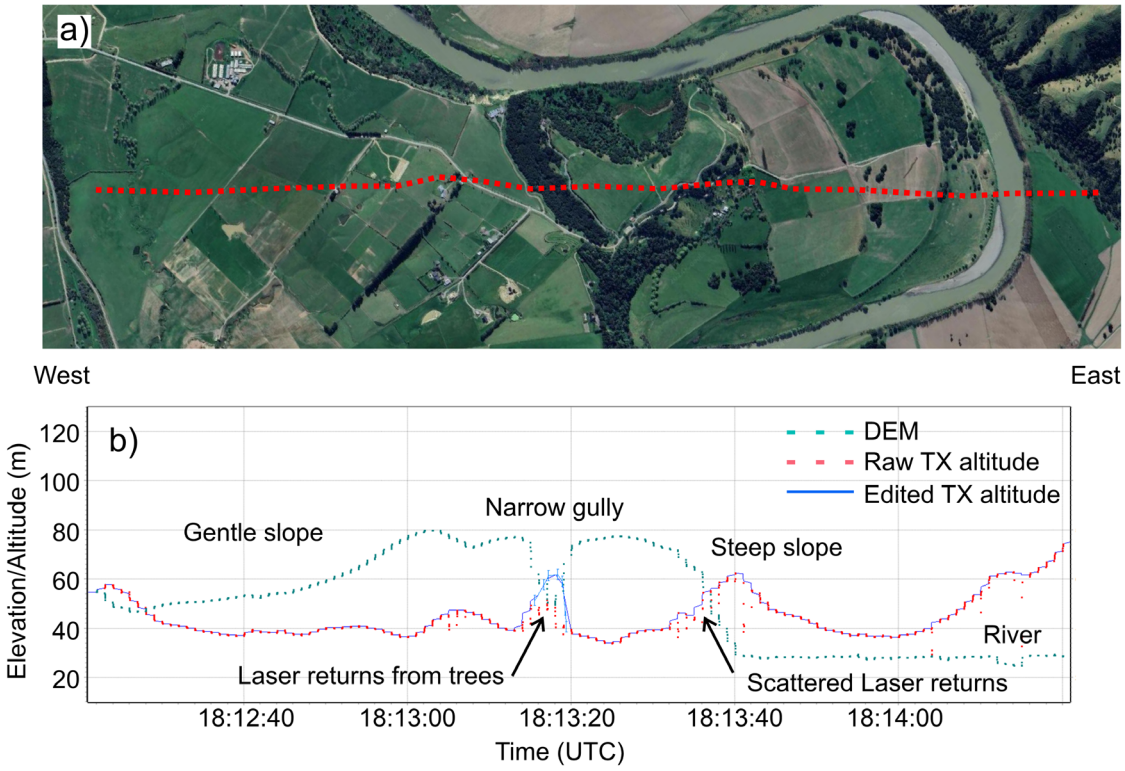

Figure 3.2 Example of the altitude data from a flight line. (a) The air photo shows the location of the line across the Ruamāhanga River. (b) The section shows the DEM as elevation (teal dashed line), original laser altitude (red dashed line) and final edited laser altitude (blue solid line). The narrow gully cause laser returns from the tops of the trees, producing an incorrect altitude. The helicopter climbs over powerlines and trees alongside the roads, as well as to avoid steep topography at the eastern end of the line.

3.6 Voltage Data

The voltage data were gathered continuously along flight lines alternating between the LM and HM modes. Voltage data were collected by induction coils (x Rx and z Rx), whose output voltage is proportional to the time derivative of the secondary magnetic field created by the current induced in the ground (Nabighian and Macnae 1991).

The voltage is normalised by the magnetic dipole moment of the transmitter and is expressed in units of *V/(A*turns*m^4)*, where *turns* is the number of loops of wire around the frame and *A* is the current. The processing of voltage data was carried out in a two-step system: an automatic and a manual part. In the former, data were corrected for the transmitter/receiver tilt, and automatic filters applied that were designed to cull coupled or noise-influenced data. As part of the processing undertaken by SkyTEM Australia, some lateral smoothing of the voltage curves is undertaken prior to them being sampled at 5 Hz and saved as XYZ files.

Electromagnetic noise can be from capacitive couplings (e.g. buried cables), galvanic couplings (e.g. grounded power lines or fences), noise at specific frequencies, spikes and white noise. The size/extent of such a coupling will differ depending on the resistivity of the underlying geology. If not removed, such noise will appear as artefacts within resistivity models developed from the data, such as the appearance of non-geological low-resistivity areas. Automatic processing procedures are not always able to effectively remove electromagnetic noise. The manual inspection and removal of coupled data is therefore essential to obtain high-quality end results. The manual processing included identifying patterns of noise caused by roads, powerlines, houses, railways and farm and vineyard infrastructure. We utilised a series of GIS layers of powerlines, provided under a data

license agreement from PowerCO; topographic data (LINZ 2011); geological data (Heron 2024) and a Google Earth hybrid base map in the AGS Workbench software were used to help guide the processor's expectations of noise source locations. The sources of couplings evident in the data were not always possible to identify from these maps and datasets, but they correspond to most of the couplings evident in the data. Figure 3.3 shows an example of strongly coupled data.

In addition to couplings, the late-time part of the sounding curves in both HM and LM displays white noise, reflecting the point where the signal level is not distinguishable above the noise level. Failure to remove this data can lead to artefacts in inversions, although this is often compensated for by high error bars on the late-time data. Therefore, following removal of couplings, the late-time part of the signal was removed from the data below a lower amplitude threshold. Figure 3.4 shows an example of data with significant amounts of electromagnetic noise.

Processing of the voltage data was undertaken by four geophysicists (Table 1.1). Individual approaches to removing the noise varied slightly between the four staff, but a series of reviews ensured that the manual editing was consistent across both staff and the HM and LM channels. In most cases, the coupling was present in both the HM and LM data. In some cases, the noise was present in the LM data, but the deeper-looking HM data were not influenced by the noise. On rare occasions, the coupling was present in the HM data, but the LM data were apparently free of interference. In general, the data were cut out of both moments using the same window to ensure that the inversion models were not biased to either shallow or deep resistivity structure. To provide the option of utilising early time gates in the inversion modelling (providing higher near-surface resolution; see Section 4), LM gates 4–8 were enabled within the dataset after several passes of manual processing. The rejection windows used for the LM data were used for the early time gates (4–8).

Rapid changes in helicopter altitude or orientation can also impact data quality due to the pitch/roll of the equipment not able to be completely corrected for. This noise is particularly relevant towards the ends of lines where the helicopter performed a turning manoeuvre, as sufficient data may not have been trimmed to compensate for this. Data considered to be impacted too heavily by such changes were also removed.

After an initial round of processing, a series of inversions were tested to provide some initial results for interpretation. It became immediately apparent that the 0.2 s interval data were over-sampled and the large number of data points for the survey made processing prohibitively slow. A decision was made to re-sample the raw data to 1 s intervals, while preserving the detailed noise removal.

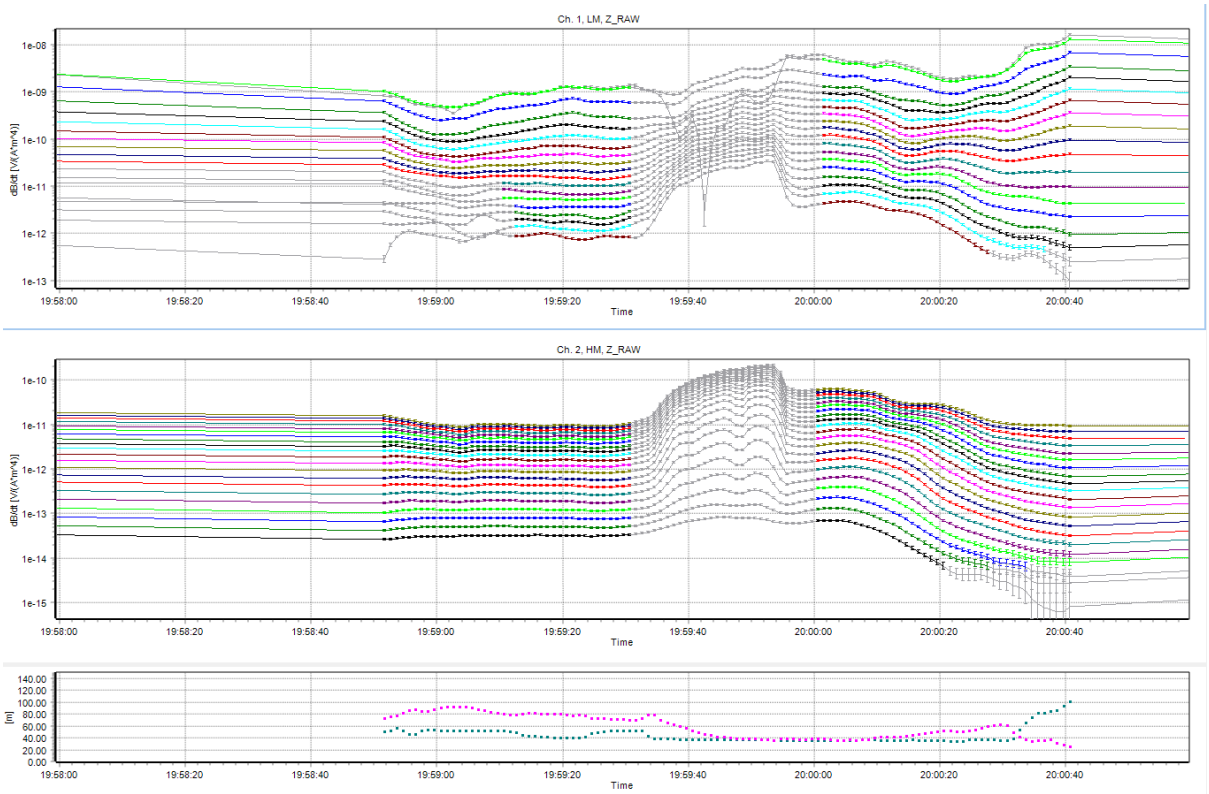

Figure 3.3 Data section example with coupled data. The section displays three minutes (~2.5 km) of data. The top panel is the raw LM data for channels 8–26. The middle panel is the HM data for channels 16–36. The lower panel is the altitude (pink) and DEM (teal). Both the LM and HM channels show a zone of coupling between 19:59:30 and 20:00:00 that has been removed (light grey). These data are affected by a large horticultural operation with covered trees. The LM data are affected by noise in the late gates at the left-hand side of the plot.

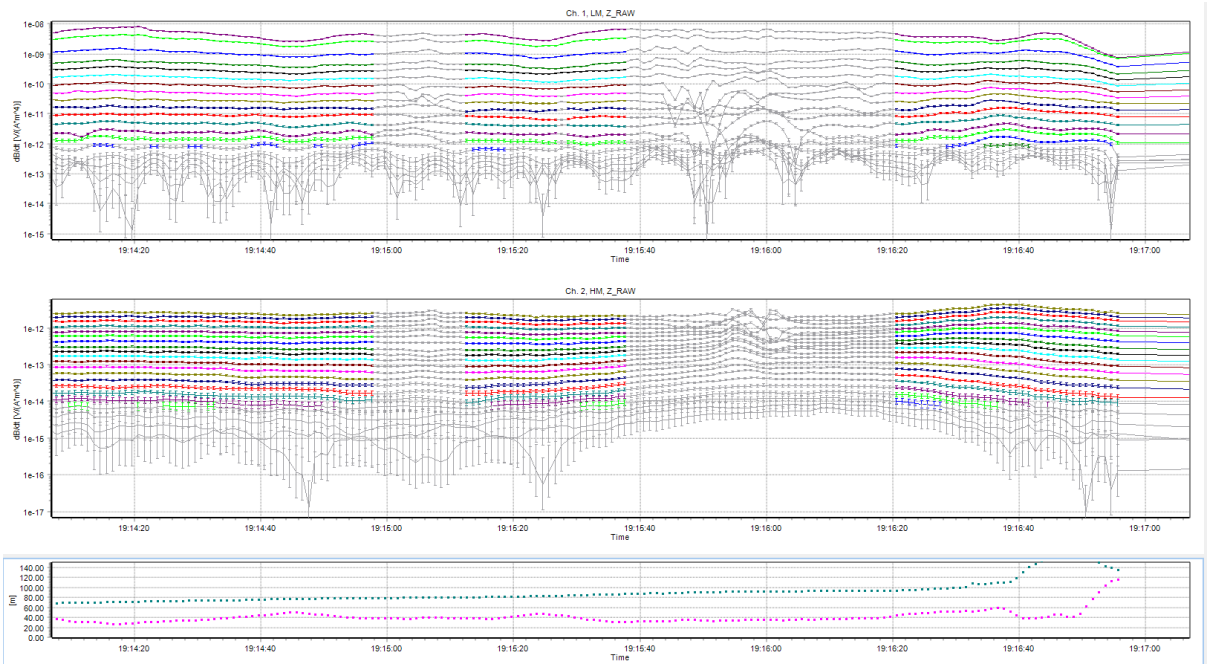

Figure 3.4 Data section example with noisy electromagnetic data. The section displays three minutes (~2.5 km) of data. The top panel is the raw LM data for channels 8–26. The middle panel is the HM data for channels 16–36. The lower panel is the altitude (pink) and DEM (teal). The LM channel shows two zones of noise across all windows that have been removed from processing (grey). The HM noise is more isolated, but the same window of data has been removed (grey). The bottom three gates for both moments fall below the threshold and have been removed. The end of the flight line is seen at the right-hand side.

3.7 Quality Checking and Post-Processing

A team of four GNS staff undertook the manual voltage processing following guidelines established by HGG (2011). On completion of the processing, the entire dataset was quality-checked by the GNS Technical Leader (Table 1.1). The data were viewed at time windows ranging from approximately three minutes to the entire flight (two hours) for quality-checking and to assist with an alternate view of the data trends and behaviour. The quality-checker worked through all datasets manually and made manual edits where needed (adding or deleting data points). The entire dataset was divided into two parts based on the amount of data and dominant flight direction (Figure 3.1). After each set of data were processed and reviewed by GNS, the processing was reviewed by staff from HGG.

Following the manual inspection of the voltage data, post-processing was undertaken. This process involved calculating preliminary Laterally Constrained Inversions (LCI) for all data (see Section 4.2 for further details). These preliminary resistivity models were inspected alongside a range of quality assurance maps that presented parameters indicating the presence of noisy data. The primary quality-assurance parameters were the mis-fit between observed data and model response (data residual), anomalous elevation changes in the LCI, and sudden lateral changes in the DOI (see Section 5 for further details). Consistent removal of electromagnetic coupling anomalies on lines that cross a powerline or road was the focus of one round of quality-control review. Further manual edits to remove or add voltage data were performed with the aim of reducing all residuals.

4.0 INVERSION

Mathematical inversion is the calculation of the cause (m) of a set of observations (d_{obs}). It is called an inverse problem because it starts with the effects (observations) and then calculates the causes. In this work, a resistivity model of the earth (upper ~500 m of the subsurface geology) is calculated (m) based on the recorded SkyTEM data (d_{obs}) using established electromagnetic equations [$F(m)$].

$$d_{obs} = F(m)$$

For such a complex and non-unique (multiple solutions can fit the observed data) mathematical problem, a direct solution is not able to be calculated. Therefore, an iterative procedure is used to reach a minimum mis-fit (difference) between modelled [$d_{est} = F(m_{est})$] and observed data (d_{obs}). This is a minimisation problem (a mathematical problem that searches for the smallest value, or global minimum), for which there are different algorithms available to improve computational efficiencies, with the objective being to find a global minimum. In this case, the inversion uses a 1D full non-linear damped least-squares solution (or Levenberg-Marquardt algorithm). The algorithm starting point is set by initial parameter estimates (prior values). If there are multiple minima present, then inappropriate prior values may bias the result to only find a local minimum; thus, prior values close to the true global minimum may be required to achieve the true global minimum. However, the algorithm is generally robust in terms of typically finding a solution, even if it starts very far from the final minimum.

Inversion of the dataset and evaluation of the inversion results were carried out using the Aarhus Workbench software package. The underlying inversion code (AarhusInv) was developed by the HydroGeophysics Group, Aarhus University, Denmark (Auken et al. 2015).

Model development using mathematical inversion is a non-unique process and follows an iterative process:

1. A starting (initial) resistivity model is created.
2. Using this resistivity model, an electromagnetic forward model is utilised to calculate the resultant voltage data.
3. The residual between the measured voltage data and estimated voltage data from the forward model is calculated.
4. The resistivity model is adjusted using rules imposed by the regularisation scheme applied (e.g. imposed prior knowledge, constraints between soundings, smooth/sharp requirements).
5. Steps 2–4 are repeated until the residual reaches a defined threshold value that is considered to be the global minimum, until the mis-fit is not decreasing or until the maximum number of iterations is reached.

The inversion is a 1D full non-linear damped least-squares solution in which the transfer function of the instrumentation is modelled. The transfer function includes turn-on and turn-off ramps, front gate, low-pass filters and transmitter and receiver positions. The flight altitude contributes to the inversion scheme as a model parameter, with the laser altimeter readings included as a constrained prior value.

The inversion settings for the sharp and smooth inversions in Workbench are listed in Table 4.1, and the layer structure is shown in Table 4.2.

Table 4.1 Inversion settings, smooth/sharp spatially constrained inversion set-up.

Item		Value
Software	AGS Seequent Workbench Version	6.9.0
Model set-up	Number of layers Starting resistivities (ohm.m) Thickness of first layer (m) Depth to last layer (m) Thickness distribution of layers	40 30 1.0 600.0 Log increasing with depth
Smooth model: constraints/ prior constraints	Lateral constraints on resistivities (factor) Reference distance (m) Power law Vertical constraints on resistivities (factor) Prior, thickness Prior, resistivities Prior on flight altitude (m) Lateral constraints on flight altitude (factor) Minimum number of gates per moment Data misfit calculated on: Log Rho or Rho	1.3 (Medium) 40 0.75 2.0 (Medium) Fixed Unconstrained +/- 2.0 1.3 5 Rho
Sharp model: constraints/ prior constraints	Lateral constraints on resistivities (factor) Lateral sharpness Reference distance (m) Power law Vertical constraints on resistivities (factor) Vertical sharpness Prior, thickness Prior, resistivities Prior on flight altitude (m) Lateral constraints on flight altitude (factor) Minimum number of gates per moment Data misfit calculated on: Log Rho or Rho	1.04 (Medium) Auto 40 0.75 1.12 (Medium) Auto Fixed Unconstrained +/- 2.0 1.3 5 Rho

Table 4.2 Layer structure used for resistivity models. The last layer thickness is modelled as an infinite half-space.

Layer	Thickness (m)	Depth to Bottom of Layer (m)
1	1.0	1.0
2	1.1	2.1
3	1.2	3.4
4	1.4	4.7
5	1.5	6.3
6	1.7	8.0
7	1.9	9.9
8	2.1	12.1
9	2.4	14.5
10	2.7	17.1
11	3.0	22.1
12	3.3	23.4
13	3.7	27.1
14	4.1	31.2
15	4.6	35.8
16	5.1	41.0
17	5.7	46.7
18	6.4	53.1
19	7.1	60.2
20	7.9	68.1
21	8.8	76.9
22	9.9	86.8
23	11.0	97.8
24	12.3	110.0
25	13.7	123.7
26	15.2	139.0
27	17.0	156.0
28	19.0	174.9
29	21.1	196.0
30	23.6	219.6
31	26.3	245.9
32	29.3	275.2
33	32.7	307.9
34	36.4	344.3
35	40.6	385.0
36	45.3	430.3
37	50.5	480.8
38	56.4	537.2
39	62.8	600.0
40	Infinity	-

4.1 System Response Modelling

System response modelling enables early time data (early gates) to be used when they would normally be excluded, thus improving near-surface resolution of the resistivity models. With the system response modelling scheme (Auken et al. 2020), the waveform, low-pass filters, etc., are not modelled separately but instead as a system response measured for the specific SkyTEM set-up. This approach enables accurate modelling of gates in the ramp-down time.

For this survey, five extra gates (4–8) located during ramp down were included in the inversion (Figure 4.1). The uncertainty of these data points was increased to 1.2 standard deviations (STD), which adds an additional 20% uncertainty compared to the 1.0 STD uncertainty utilised by the majority of the data points.

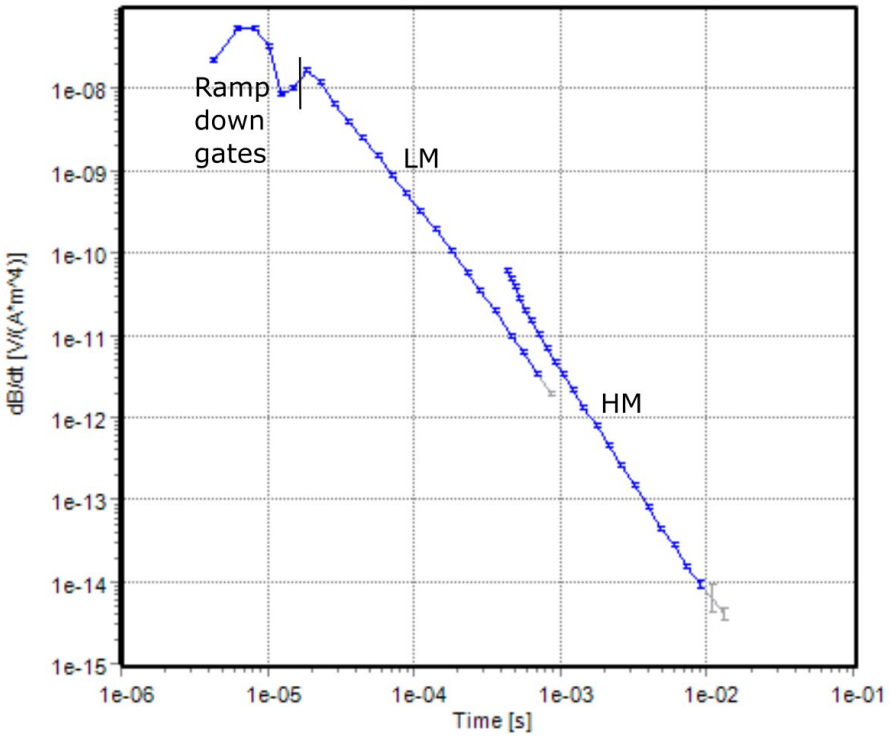

Figure 4.1 High-moment (right curve – HM) and low-moment (left curve – LM) dB/dt sounding curves. The gates left of the black line are located within the ramp-down time. The sign can often be reversed depending on the shallow resistivity structure of the ground.

4.1 Laterally Constrained Inversion

The LCI scheme is used for preliminary inversions of the SkyTEM data as part of the processing workflow. The LCI scheme uses constraints between the 1D models along flight lines. Ramp-down gates 4–8 were not utilised for LCI inversions because the LCI inversion was used primarily to review data quality over the entire study area during post-processing and quality checks.

4.2 Spatially Constrained Inversion

The SCI scheme was used for the final inversions of the SkyTEM data. The SCI scheme uses constraints between the 1D models both along and across the flight lines, as shown in Figure 4.2. The constraints are scaled according to the distance between soundings.

The network of constraints is designed using a Delaunay triangulation, which connects natural neighbour models. For line-oriented data, the Delaunay triangulation results in a model being connected to the two neighbour models at the flight line and typically 2–3 models at the adjacent flight lines (Figure 4.3).

Constraining the parameters laterally in an SCI enhances the resolution of resistivities and layer interfaces, particularly for the layers that are poorly resolved by independent inversion of the soundings in the initial LCI.

SCI set-up parameters for this survey are also listed in Table 4.1.

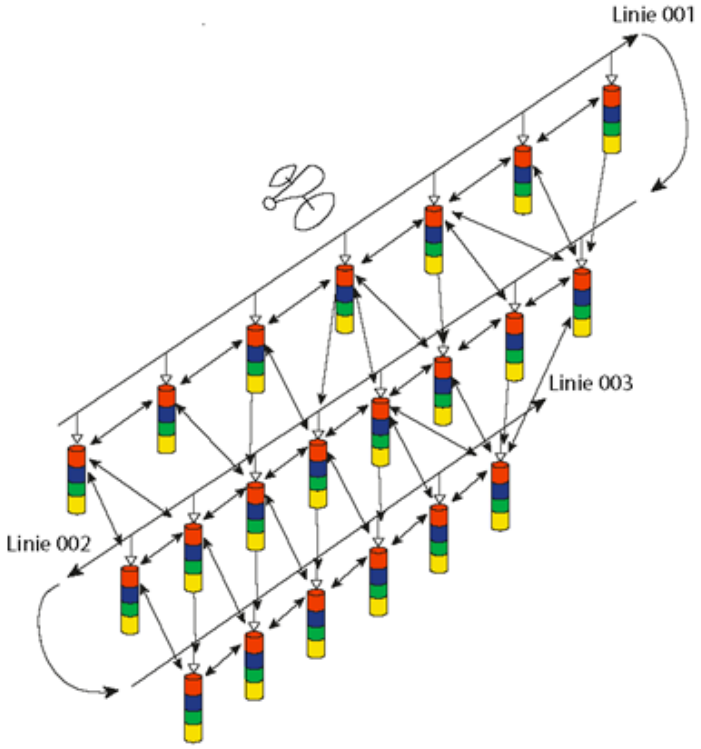

Figure 4.2 Schematic presentation of the spatially constrained inversion set-up. Constraints connect not only soundings located along the flight line, but also those across them. Figure from HGG (2017).

The SCI was undertaken in stages because of computational limitations associated with the large number of measurements. Figure 4.4 shows a map of the survey area with polygons used to mask the SCI models. The Main block was divided into three areas. The onshore part of the Main block was divided into two areas with approximately four flight lines of overlap.

The offshore part was inverted as a separate area, with no overlap onto the onshore area. The offshore area included Lake Onoke due to the high salinity in the tidal water body. The parameters for the SCI in the offshore area were tailored for the low-resistivity surface layer. The top 1 m was fixed at 0.3 ohm.m (typical resistivity for seawater), while the remaining layers were allowed to vary from a starting value of 30 ohm.m (Table 4.2). The contrast in resistivity across the coast and between Lake Onoke and the surrounding land is large and produced some anomalies that cannot be modelled using the LCI or SCI process. The effect of this coastal signature was reduced by preventing any lateral constraints across the coastal boundary.

The Masterton block was also inverted in two parts, with some lines from the Main block included to allow a smooth overlap with the southern part of the survey. The SCI models were stitched together, removing any duplicated models. The stitching was performed along a seam that divided the zone of overlap in half. Comparison of the models within the overlap zone indicated that the differences between different SCI runs in the overlapped region was very small.

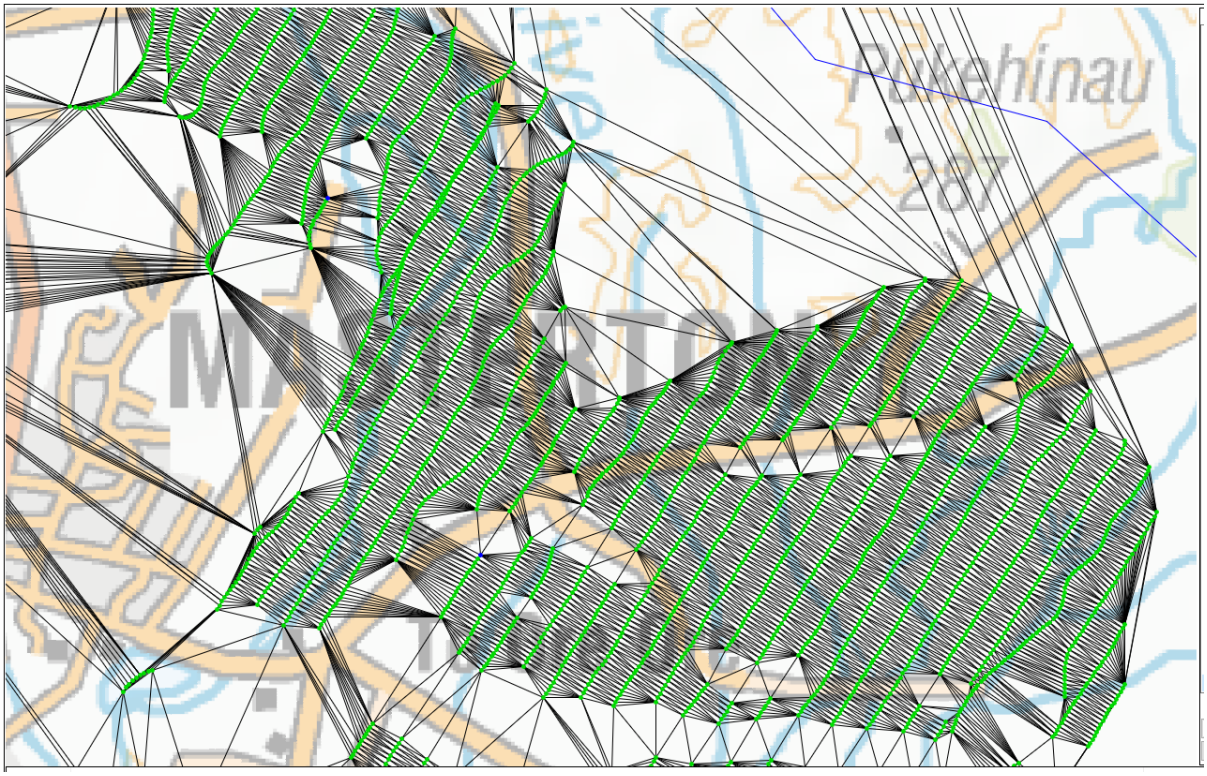

Figure 4.3 Example set-up of the spatially constrained inversion network. The green points are the model positions. The black lines show the constraints created with the Delaunay triangles. The flight line distance in this example is 200 m.

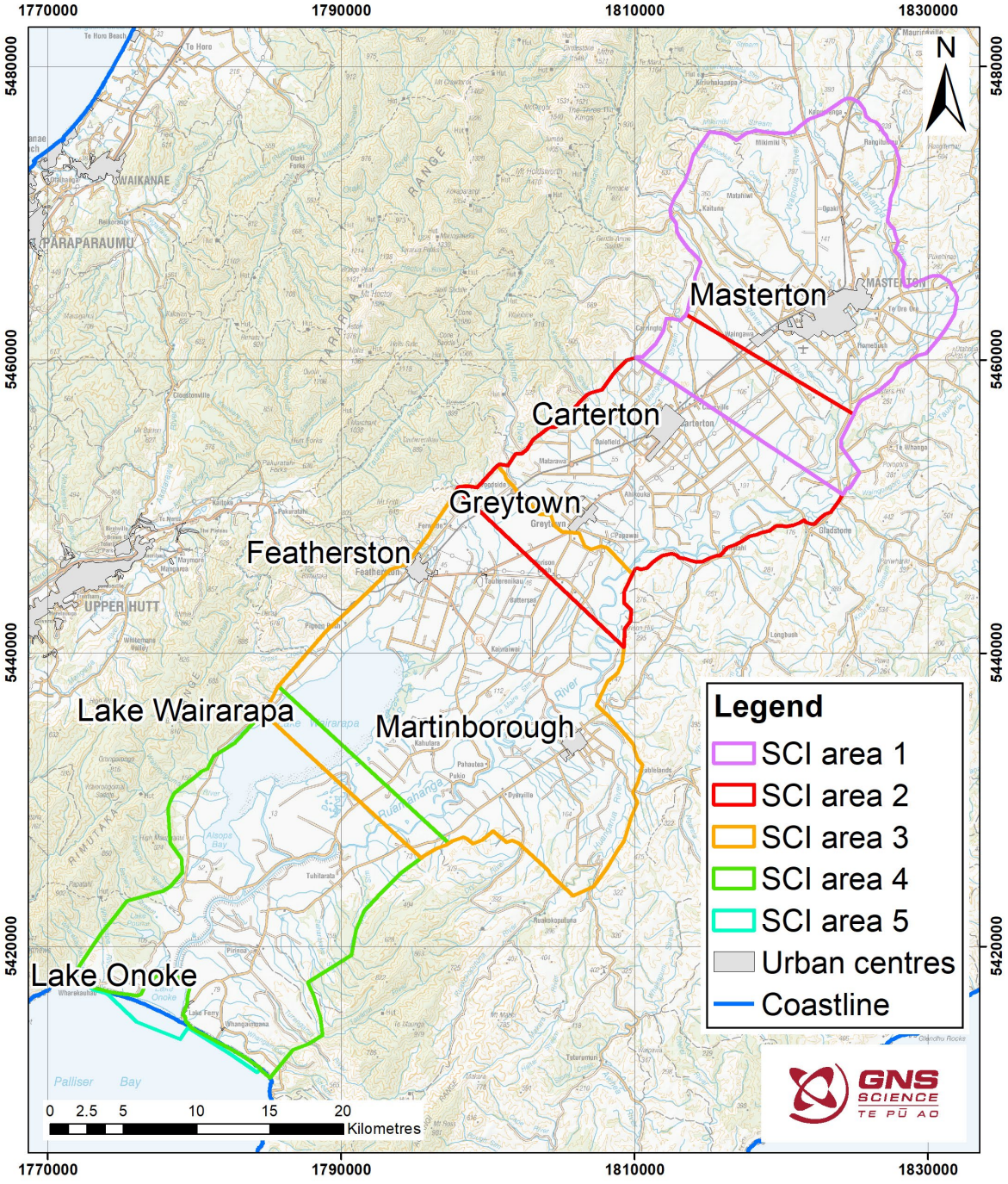

Figure 4.4 Map of the survey area showing the polygons used to divide the spatially constrained inversion up into parts for more efficient processing. Areas 1, 2, 3 and 4 are overlapped to produce a smooth merge between the areas. The offshore area (Area 5) including Lake Onoke does not overlap Area 4.

4.3 Smooth, Sharp Inversion

Both smooth and sharp model inversions were carried out. Both inversion types used the SCI set-up and same model layers (Table 4.2), but the regularisation scheme was different.

A smooth model is a many-layered model that uses a fixed layer structure (logarithmically increasing layer thicknesses), and the inversion scheme solves for the resistivity of each layer. The smooth regularisation scheme penalises the resistivity changes, resulting in the smoothest resistivity transitions both vertically and horizontally, as seen in Figure 4.5. As such, sharp geological layer boundaries may appear diffuse, and picking geological layer boundaries is subjective. However, inclined layer sequences are more readily detected.

A sharp model uses the same model discretisation as the smooth model, but the model regularisation scheme is different. The sharp model regularisation scheme penalises the number of resistivity changes above a certain size, instead of the absolute resistivity changes (as in the smooth model regularisation scheme). The sharp model regularisation scheme therefore results in a model with few, but relatively sharp, resistivity transitions. This allows for relative abrupt changes in resistivities, while using the fixed-layer thicknesses of the smooth model. An example is shown in Figure 4.5. Both the smooth model and sharp model can explain the SkyTEM-observed data equally well, so are both valid versions of the subsurface.

Assuming a geological layered environment, picking geological layer boundaries will be less subjective in a sharp model compared to a smooth model.

Attempts were made to invert the offshore block using the sharp constraints. Additional work will be required to determine the combination of constrains or starting models that can produce a model with a suitable data residual and a realistic resistivity model of the seawater depth and subsurface. The smooth model for the offshore regions provides a suitable resistivity structure for any further interpretation.

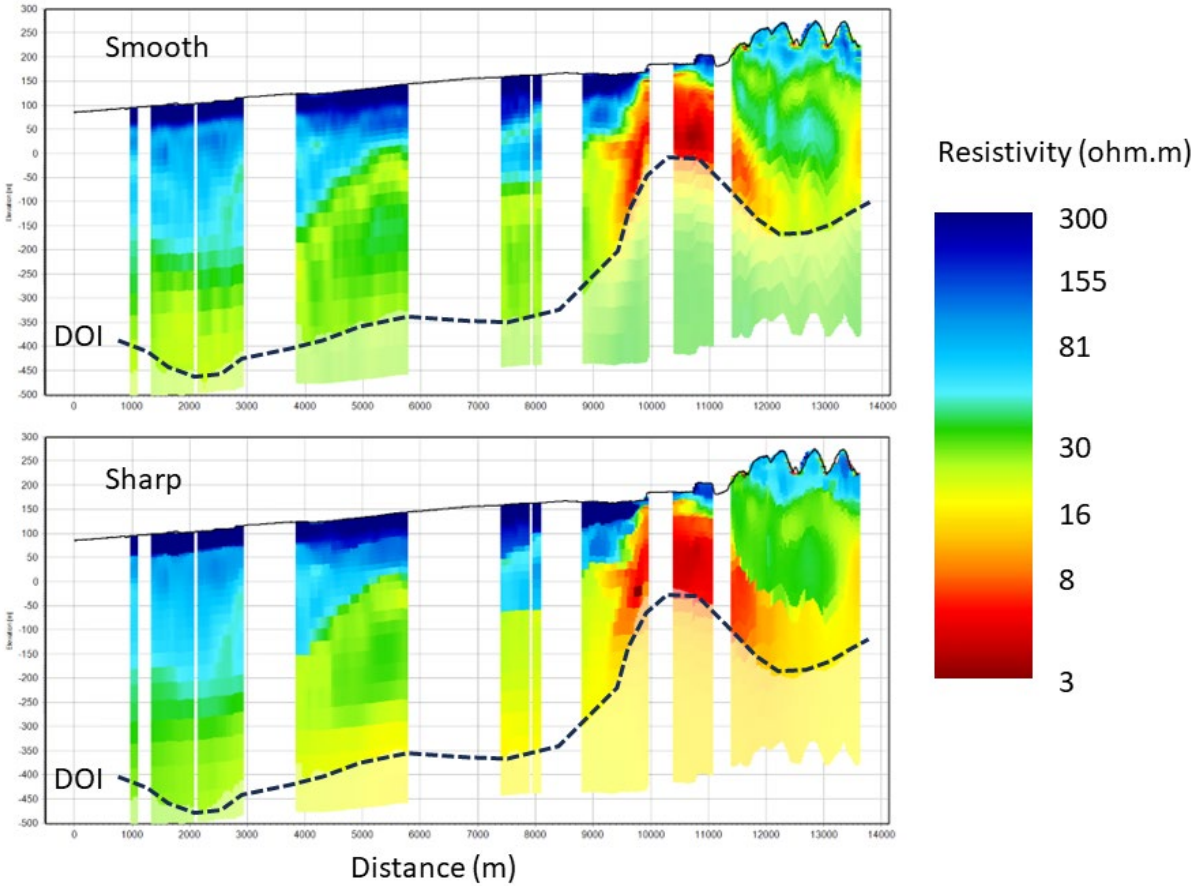

Figure 4.5 Profile examples of a smooth (upper panel) and sharp (lower panel) inversion of the same SkyTEM dataset, showing resistivity in ohm.m. The dashed lines show the standard depth of investigation (DOI; see Section 4.4). The sections are very similar, but some boundaries are more obvious in the sharp model (e.g. the base of the surficial high-resistivity layer [dark blue] and the top of the 16–20 ohm.m layer [yellow] at depth on the right-hand side of the section).

4.4 Depth of Investigation

For each resistivity model, a DOI is estimated as described in Christiansen and Auken (2012). The DOI calculation takes into account the SkyTEM system transfer function, the number of data points, the data uncertainty and the resistivity model.

Electromagnetic fields are diffusive, and there is no discrete depth where information on the resistivity structure stops. There are several ways to calculate the DOI depending on thresholds. In this study, we have adopted the standard DOI. As a guideline, the resistivity structures below the standard DOI value are very weakly determined by the data and should normally be disregarded. Figure 4.5 shows the standard DOI as a dashed line, and the cells below the line are semi-transparent to indicate the uncertainty in resolving the resistivity. Note that, under the low-resistivity zone at the right-hand side of the section, the DOI is shallow (<200 m deep), while, under the very high-resistivity layers on the left-hand side of the section, the DOI is much deeper (>400 m). Table 4.3 provides the details on the DOI standard for the resistivity models.

The standard DOI estimates are included as point theme maps in Appendix 1. The cross-sections in Appendix 2 are blanked in depth at the DOI standard values. The resistivity models are blanked below the DOI standard value when compiling the mean resistivity maps. The software also computes a more conservative estimate of the DOI designed to identify the limit of maximum confidence in the resolved structure. The conservative DOI behaved in a similar way to the standard DOI, but we found that realistic resistivity structures at depth were being masked by the more conservative DOI and so have decided to only present the standard parameter.

Table 4.3 Standard depth of investigation.

Depth of Investigation	Smooth Model (m)	Sharp Model (m)
Minimum	22	26
Maximum	658	673
Mean	382	394
Median	395	406

5.0 WORKSHOPS

As part of the deliverables for the Ruamāhanga Airborne Aquifer Mapping Project, GNS ran two sets of workshops for GWRC and its consultants. Workshop 1 was held on 26–27 October 2023 and Workshop 2 was held on 4–5 April 2024.

Workshop 1 had the following aims:

- Establish the main relationships between resistivity models and lithological units in the southern part of the survey.
- Finalise parameters for the remaining resistivity model development.

Two days were focused on a review of the processing and LCI resistivity models for the Main block. To support the presentation of the resistivity models to the client, a range of additional geoscience data was included in the study. The borehole logs, GroundTEM and DC resistivity surveys were used to illustrate how the resistivity models relate to the geology. The supporting geoscience data are discussed in more detail in Section 7. The southern area included the area around Lake Ferry, where saline intrusion was a concern for GWRC. The review of the SkyTEM data focused on sections that covered the transition from the offshore to the onshore and crossed Lake Onoke (Figure 5.1). The workshop also focused on the Turanganui and Tauanui Valleys, where deeper aquifers were being targeted for water supply (Figure 5.1). While the focus of the workshops was to identify the key features being imaged by the SkyTEM, there was a keen interest in comparing the preliminary models to the results previously presented by Kellett et al. (2022). A series of maps of resistivity slices and resistivity sections were presented at the workshop. Appendix 2 sections South 1 and South 4 illustrate the data from this region.

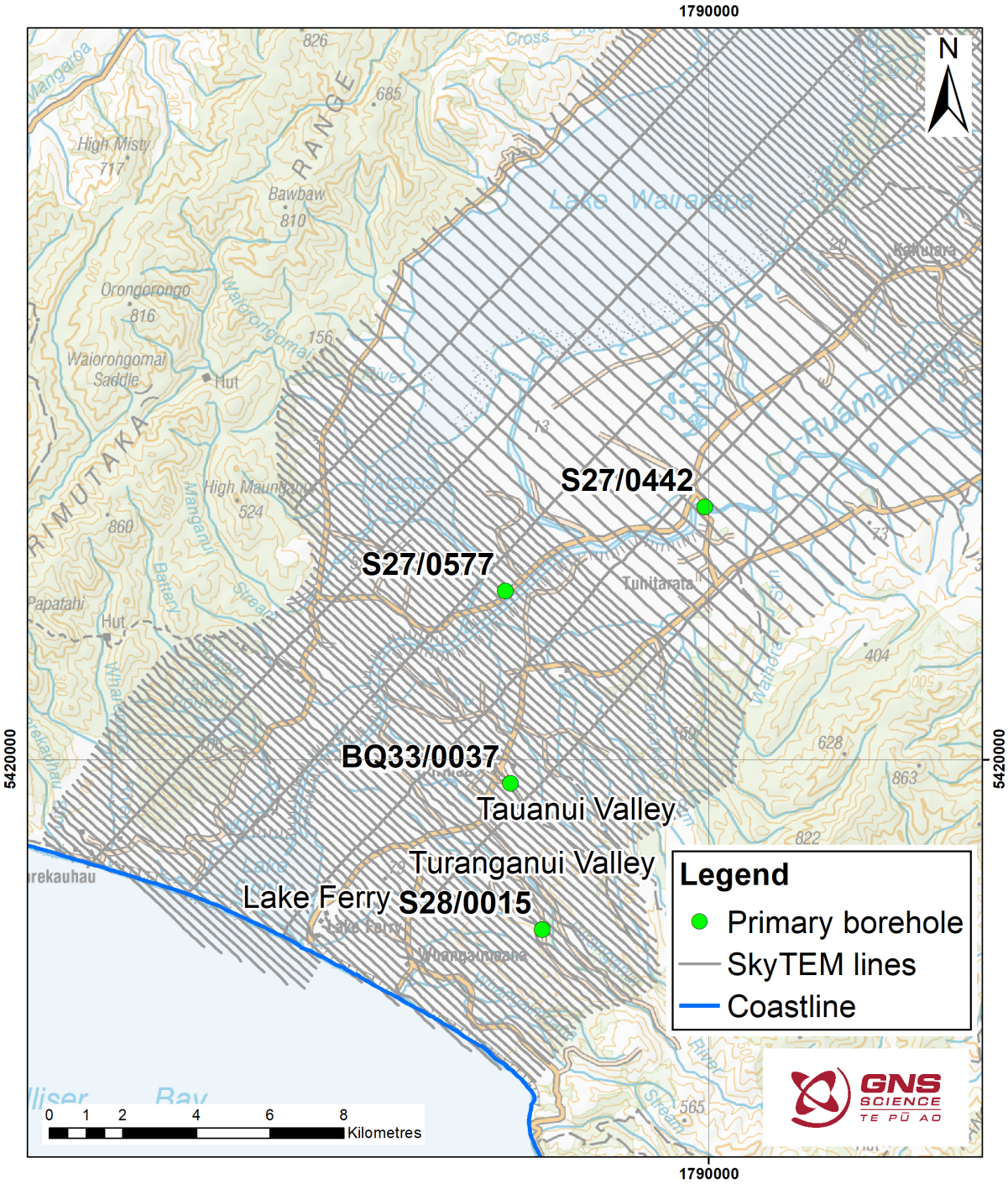

Figure 5.1 Map of Main block in the southern Ruamāhanga Catchment showing areas for evaluation of the resistivity model. Primary boreholes and location names identify the focus areas.

Workshop 2 had the following aims:

- Establish the main relationships between resistivity models and lithological units in the northern part of the survey.
- Finalise the formats for delivery of the resistivity models.
- Identify options for the hydrogeological model development.
- Scope out the web-based mapping tool and requirements to provide public access to the models.

One day was focused on the Masterton block, with an emphasis on the resistivity structure in the Te Ore Ore and Parkvale areas (Figure 5.2). A series of resistivity slices and resistivity sections helped illustrate the relationship between the SkyTEM models and the existing GroundTEM and DC resistivity, as well as some key boreholes. Appendix 2 sections North 5 and North 6 illustrate the data from these areas. The second day provided an opportunity to explore the different versions of the resistivity model that could be exported from the processing software, as well as the different versions of web-based mapping products being used by other projects.

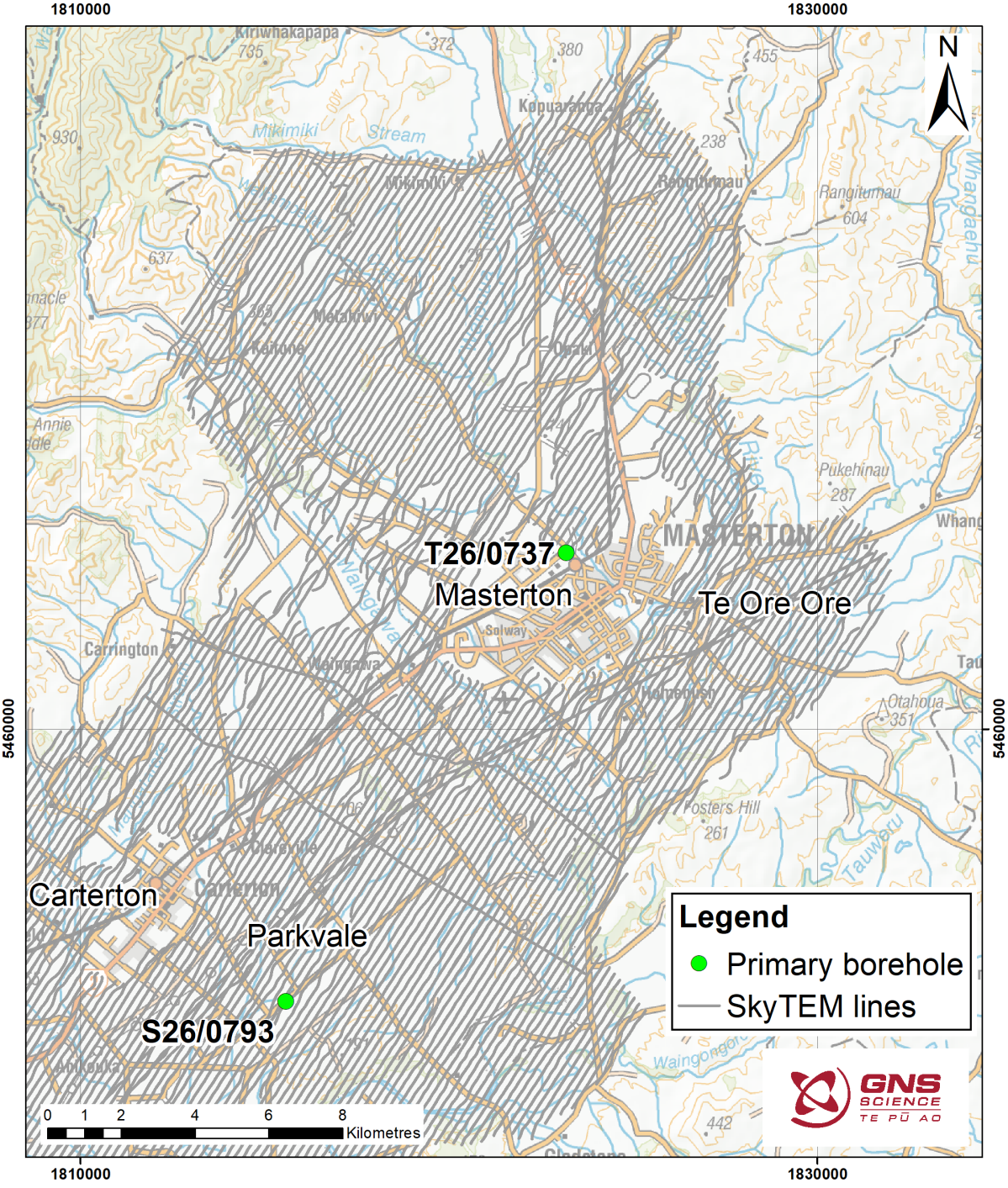

Figure 5.2 Map of Masterton block in the Northern Ruamāhanga Catchment showing areas of focused evaluation of the resistivity model. Te Ore Ore and Parkvale basins were reviewed in detail.

6.0 MAPS AND CROSS-SECTIONS

To visualise the resistivity structures in the mapping area, a series of maps (quality-control maps and resistivity maps) and cross-sections were created. These maps and sections were used extensively in the two workshops to provide guidance on the quality of the resistivity models in the areas being reviewed. A sub-set of the maps and sections are provided in this report.

The following sections describe the maps and sections that are included in the Appendices.

6.1 Location Map, Quality-Control Maps

The location map and quality-control maps described below are included in Appendix 1. Each map is shown in two parts, representing the Main block (Ruamāhanga South) and Masterton blocks (Ruamāhanga North).

6.1.1 Model Location and Flight Lines

This map shows the actual flight lines. Black dots mark where data were discarded due to line turns or noise. Blue dots mark where data were kept and inverted to a resistivity model.

6.1.2 Moment Indication

This map shows whether both LM and HM data are present. In general, both moments were present for the whole survey.

6.1.3 Flight Altitude

This map shows the processed flight altitudes from the laser altimeters (distance from the frame to the ground). The flight altitude reflects the necessary safe distance to the ground, treetops, etc.

6.1.4 Data Residual

The data residual describes how well the obtained SCI resistivity models explain the recorded data (how well the data are fitted). The data residual values are normalised with the data standard deviation, so a data residual below 1 corresponds to a fit within one standard deviation.

Two data residual maps are shown in Appendix 1 for the smooth and sharp inversion results. In general, the data residuals are very good (<0.6), which is expected for this type of environment and geological setting. There are some isolated areas that have relatively high data residual values (>1.5). These high values are associated with one or more of the following low-signal ground responses (resistive ground), a high flight altitude and rapid lateral changes in resistivity, such as at the coast.

In the offshore block, the data residual for the flight lines over the sea are anomalously high but the data residual over Lake Onoke is low. Both areas have saline water in the shallow section. One possibility is that, offshore, the depth of the seabed changes rapidly from zero to greater than 15 m, while the depth of Lake Onoke is relatively constant. Another possibility is the effect of ocean waves on the data or the inversion. As described in Section 4.3, there are no sharp inversions of the offshore data.

6.1.5 Number of Data Points

This map shows the number of data points (time gates from both HM and LM) in use for each resistivity model. Areas with smaller numbers of data points in the inversion correlate to areas with a low signal level (very resistive areas) and/or relatively high flight altitude. The minimum number of data points used in any single sounding is 7. The maximum number of data points available in any single sounding curve is 44 (23 LM and 21 HM gates).

6.1.6 Depth of Investigation

The DOI estimates for the smooth and sharp model inversion results (see Section 4.5 for a description of the DOI calculation) are shown in Appendix 1 as a map. The DOI is shown as a depth below the ground surface.

6.1.7 Altitude Difference Maps

The altitude difference is the amount that the inversion process needs to adjust the elevation of the transmitter loop and receiver to optimise the data residual. In general, a model can be determined with minimum mis-fit and less than 1 m of elevation shift. The maps shown in Appendix 1 have less than 1 m of altitude shift, except over the seawater, where changes of up to 2.5 m are required to fit the data.

6.2 Cross-Sections

The final resistivity models are a 3D volume of data. They can be presented as cross-sections and as slices. The cross-sections are useful because they provide a way of illustrating the relationships between the resistivity model and key boreholes. A selection of these is included in Appendix 2. Each section shows the smooth 1D models, which are blanked at the standard DOI value.

6.3 Mean Resistivity Maps

The final models have been delivered in layers so that they can be imported into Geographic Information Systems (GIS). To make depth or horizontal slices, the mean resistivity in the depth or elevation intervals is calculated for each resistivity model and then interpolated to a regular grid.

Figure 6.1 shows how the resistivities of the layers in a model influence the calculation of the mean resistivity in a depth interval [A, B]. d_0 is the surface; d_1, d_2 and d_3 are the depths to the layer boundaries in the model; and ρ_1, ρ_2, ρ_3 and ρ_4 are the resistivities of the layers.

The model is subdivided into sub-thicknesses $\Delta t_{1–3}$. The mean resistivity (ρ_{vertical}) is calculated as:

$$\rho_{vertical} = \frac{\rho_1 \cdot \Delta t_1 + \rho_2 \cdot \Delta t_2 + \rho_3 \cdot \Delta t_3}{\Delta t_1 + \Delta t_2 + \Delta t_3}$$

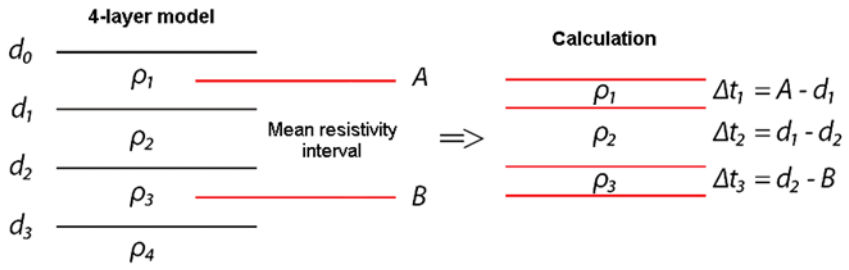

Figure 6.1 Illustration of how the resistivities of layers influence the mean resistivities in a depth interval [A:B]. Figure from HGG (2017).

In general terms, the mean resistivities in a depth interval are calculated using the equation:

$$\bar{\rho} = \frac{\sum_{i=1}^{n} \rho_i \cdot \Delta t_i}{\sum_{i=1}^{n} \Delta t_i}$$

where *i* runs through the interval from 1 to the number of sub-thicknesses. The mean resistivity calculated by the above formula (ρ_{vertical}) is named the vertical mean resistivity, which is equal to the total resistance if a current flows vertically through the interval.

Resistivity mapping with a horizontal transmitter coil only generates horizontal current flows in the ground. It is therefore most correct to perform the mean resistivity calculation with respect to a horizontal current flow in the mean resistivity interval. The horizontal mean resistivity ($\rho_{\text{horizontal}}$) is equal to the reciprocal of the mean conductivity (σ_{mean}) and is calculated as:

$$\rho_{horizontal} = \frac{1}{\sigma_{mean}} = \left[\frac{\sum_{1=1}^{n} \left(\frac{1}{\rho_i}\right) \cdot \Delta t_i}{\sum_{i=1}^{n} \Delta t_i} \right]^{-1}$$

For this survey, horizontal mean resistivity themes have been generated from the following models (masl = metres above sea level mbgl = metres below ground level):

1. Smooth model in elevation above sea level (from -600 masl to +360 masl).
2. Smooth model in depth below ground surface (from 0 to 600 mbgl).
3. Sharp model in elevation above sea level (from -600 masl to +360 masl).
4. Sharp model in depth below ground surface (from 0 to 600 mbgl).

The interpolation of the mean resistivity values to regular grids was performed by Kriging interpolation, with a node spacing of 50 m and a search radius of 800 m. The grids were then masked to remove values that were more than 300 m from a measured data point.

For the models that represent the resistivity at slices relative to sea level, a large number of layers are required to cover the change in elevation across the survey area from 0 masl at the coast to 350 masl in the northwest. The depth interval needs to be fine for all values above zero in order to capture the finely resolved resistivity structure in the near surface (150 layers). However, for practical reasons, the minimum depth interval used in the elevation slices (4 m) is larger than the minimum vertical cell size in the SCI inversions (1 m).

For the models that represent the depths below ground level, the layering used in the inversion, rounded to the nearest metre, was adopted for the gridding (40 layers).

Some examples of the mean resistivity maps are placed in Appendix 3.

6.4 Deliverables

All digital maps and data are geo-referenced to coordinate system New Zealand Transverse Mercator (NZTM 2000) and New Zealand Vertical Datum 2020 (NZVD2016). Further details on the dataset formats are provided in Appendix 4.

6.4.1 Primary Outputs

The primary outputs are the full resistivity models, which are delivered in readily accessible fixed format text files:

- *workbench_xyz**SCI_combined_All_smooth_inv.xyz*
- *workbench_xyz**SCI_combined_All_sharp_inv.xyz*

The data that contributed to the inversion models and mode responses (synthetic data) are also provided in ASCII format.

- *workbench_xyz**SCI_combined_All_smooth_dat.xyz*
- *workbench_xyz**SCI_combined_All_smooth_syn.xyz*
- *workbench_xyz**SCI_combined_All_sharp_dat.xyz*
- *workbench_xyz**SCI_combined_All_sharp_syn.xyz*

Additionally, the AGS Seequent Workbench projects are delivered, which contain the raw data, processed data, inversion results, theme maps and profiles. The three Workbench projects are:

- **Main Block:** *WB_Ruamāhanga_AEM_S_1Hz.7z*
- **Masterton Block:** *WB_Ruamāhanga_AEM_N_1Hz.7z*
- **Combined:** *WB_Ruamāhanga_AEM_1Hz.7z*

Each workspace holds both the smooth and sharp inversion results. Proprietary AGS Seequent Workbench software is required to open the files. This workspace could be utilised in the future for any changes, such as new DEM models and re-inversions.

6.4.2 Alternative Outputs

Additional versions of the final resistivity model are provided for use in a range of geological mapping software:

- Resistivity models in Leapfrog Pseudo-borehole format (e.g. for importing into Seequent Leapfrog Software) for both the sharp and smooth model:
  - \ *Merged_SCI_smooth_MOD.csv*
  - *Merged_SCI_smooth_MOD_collar.csv*
  - *Merged_SCI_smooth_MOD_survey.csv*
  - *Merged_SCI_sharp_MOD.csv*
  - *Merged_SCI_sharp_MOD_collar.csv*
  - *Merged_SCI_sharp_MOD_survey.csv*

- Mean resistivity maps for both smooth and sharp models in depth (mbgl) and elevation (masl) intervals (*XXXm_YYYm* corresponds to the interval from XXX m to YYY m) as ArcGIS ASCII grid files:
  - *\MRESD_smooth\XXXm_YYYm.asc*
  - *\MRESD_sharp\XXXm_YYYm.asc*
- Mean resistivity maps for both smooth and sharp models in depth (mbgl) and elevation (masl) intervals (*XXXm_YYYm* corresponds to the interval from XXX m to YYY m) as ESRI ArcPro 2.9 geodatabases and layer files for immediate use in ARC Pro as raster images:
  - *\MRESD_smooth\XXXm_YYYm.gdb*
  - *\MRESD_sharp\XXXm_YYYm.gdb*

7.0 PRIMARY AND SUPPORTING DATASETS

As part of the process of planning the SkyTEM survey (Kellett et al. 2020) a range of supporting geoscience datasets were evaluated. These data are then used along with the input data from SkyTEM and the DEM to develop the resistivity model.

7.1 Input Datasets

The primary input datasets from the AEM survey were provided to GWRC as part of the SkyTEM Australia Pty Ltd (2023) report (see Section 1).

7.2 Supporting Geoscience Data

The main supporting dataset is the DEM that is used as part of the altitude processing, inversions and resistivity model production. A range of geological and geophysical data were also compiled to support the evaluation of the inversion models and provide reference material for the workshops. These data will be valuable for the next phase of work, which will include the construction of a hydrogeological model. This section provides a brief description of the supporting geoscience data collated as part of this report.

7.2.1 Digital Elevation Model

The area is completely covered by LiDAR data collected from 2013 to 2020 (LINZ 2011). Figure 7.1 shows a shaded relief image of the DEM. The resulting DEM for the survey area was down-sampled to 10 m resolution for use in the SkyTEM processing.

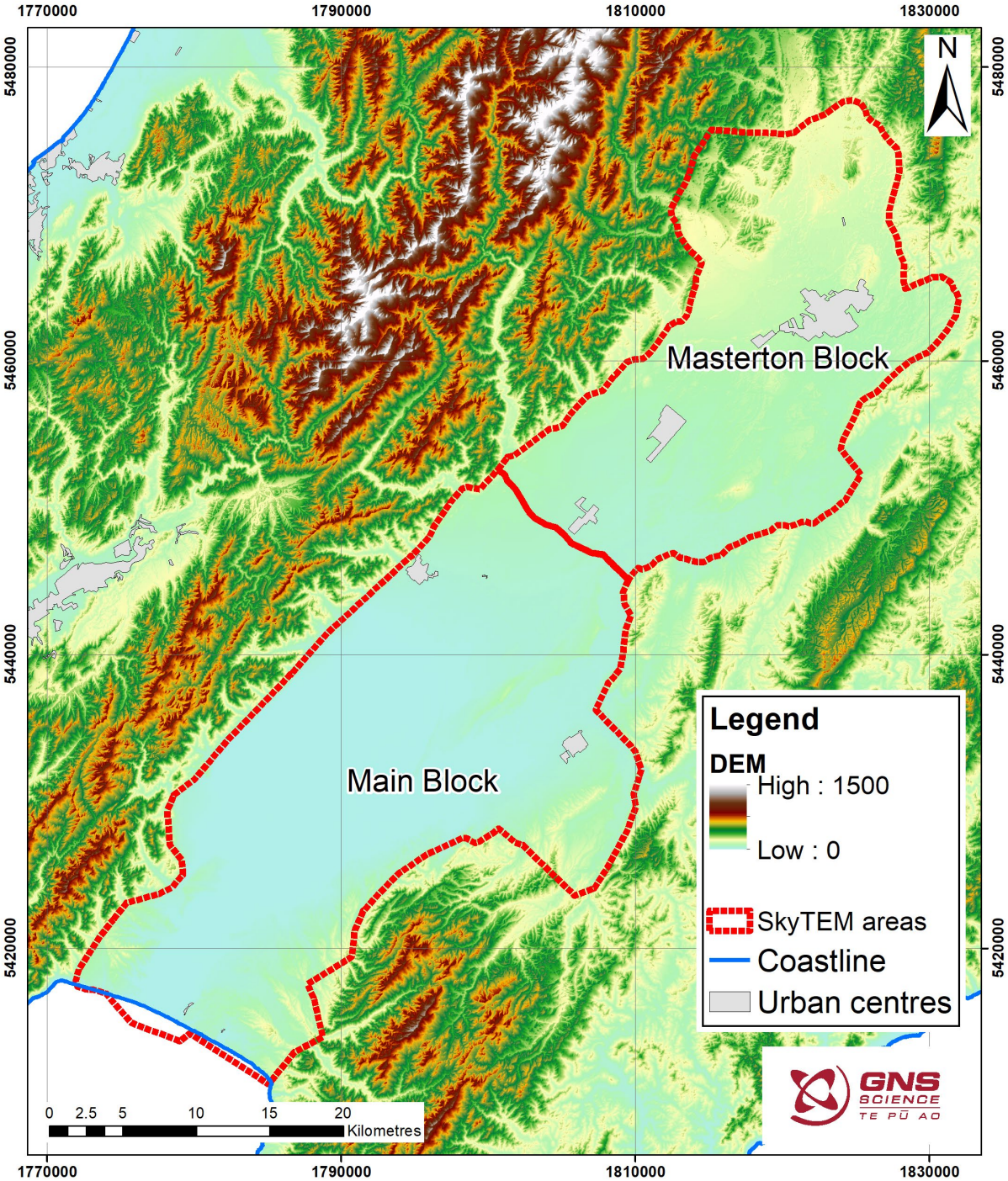

Figure 7.1 Map of the SkyTEM survey coverage within the Ruamāhanga Catchment and the digital elevation model (DEM).

7.2.2 Geological Maps

There are a wide range of published maps in the study area. The SkyTEM survey covers the Wellington (Begg and Johnston 2000) and Wairarapa (Lee and Begg 2002) sheets of the 1:250,000-scale QMAP series (Heron 2024). The maps are available in digital format as vectors and raster images and are used to support the interpretation of the SkyTEM data (Figure 7.2). More detailed geological mapping has been undertaken in the Wairarapa Valley (see references within Begg and Johnston [2000] and Lee and Begg [2002]) but the QMAP geology sheets provide sufficient detail for any future interpretation of the SkyTEM data (Kellett et al. 2022).

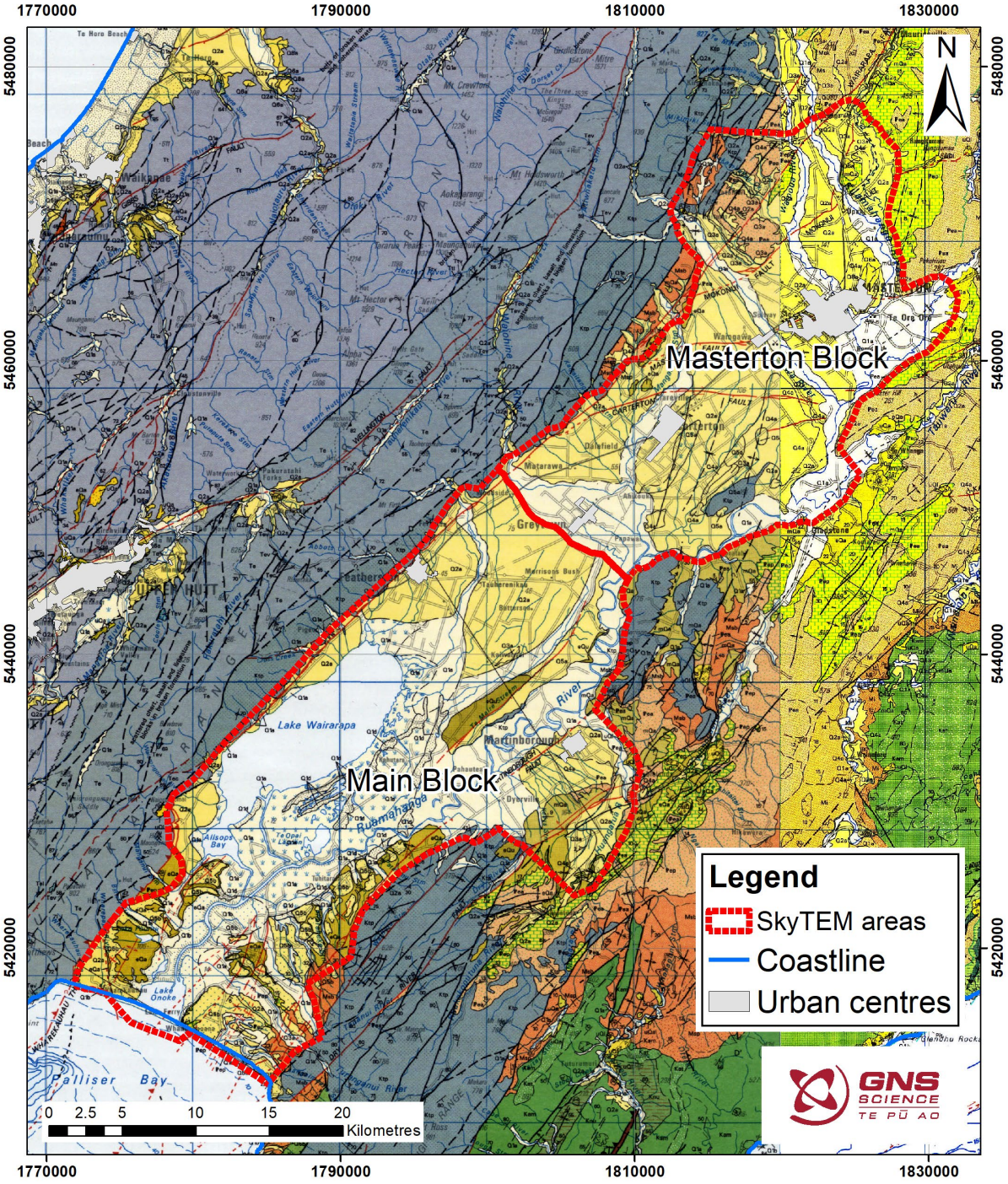

Figure 7.2 1:250,000-scale geological map of New Zealand for the wider survey area (Heron 2024). For the geological legend, refer to Begg and Johnston (2000) and Lee and Begg (2002).

7.2.3 Airborne Magnetic Data

The SkyTEM system includes a total field magnetometer that measures the intensity of Earth's magnetic field. The data are collected continuously on all flight lines and can be processed to produce a map of the variations in Total Magnetic Intensity (TMI). The International Geomagnetic Reference Field (IGRF) at the time of acquisition is removed to show local field variations across the survey area. The details are given in SkyTEM Australia Pty Ltd (2023). The data shown in Figure 7.3 is a smoothed version of the product delivered by SkyTEM Australia.

The magnetic field is sensitive to lateral and vertical changes in the concentration of magnetic minerals in the rocks. The changes in the shallow subsurface produce high-intensity, short, spatial wavelength anomalies, and the changes in the deeper part of the section produce a broader anomaly. Magnetic minerals such as magnetite, ilmenite and titanomagnetite are common in igneous and metamorphic rocks, producing very strong anomalies. The variation in the magnetic properties of sedimentary rocks is subtle and usually results from changing provenance of the sediment. Gravel and sand deposits that include clasts eroded from volcanic, plutonic or metamorphic basement often retain the magnetic minerals and can be mapped in the subsurface by their magnetic anomaly.

Man-made sources of magnetic anomalies can often dominate a magnetic anomaly map and are difficult to filter out. Powerlines, houses, buildings, vehicles and railway tracks produce anomalies that are much stronger than the geological signal. The map shown in Figure 7.3 shows some evidence for the main power line and railway crossing diagonally from the southwest to the east through the Wairarapa. The change in flight-line direction between the Main and Masterton blocks is an obvious feature in the data.

The primary purpose of a SkyTEM survey is to collect TEM data, so the magnetic data acquisition is secondary. There are still some line levelling anomalies in the magnetic data in the southern part of the survey area. Collecting additional tie lines to improve the levelling between flights would not have been cost-effective. Additional processing such as the reduction to pole, calculation of vertical and horizontal gradients, and inversion can be used to further investigate the source of the magnetic anomalies.

A previous dataset was collected by Lakes Oil in 2008 (Holdgate 2008) as part of a petroleum exploration project (Figure 7.4). The data show similar regional trends and the localised influence of buildings and other infrastructure. The Lakes Oil data have been levelled with the SkyTEM magnetic data to demonstrate the correlation of the anomalies.

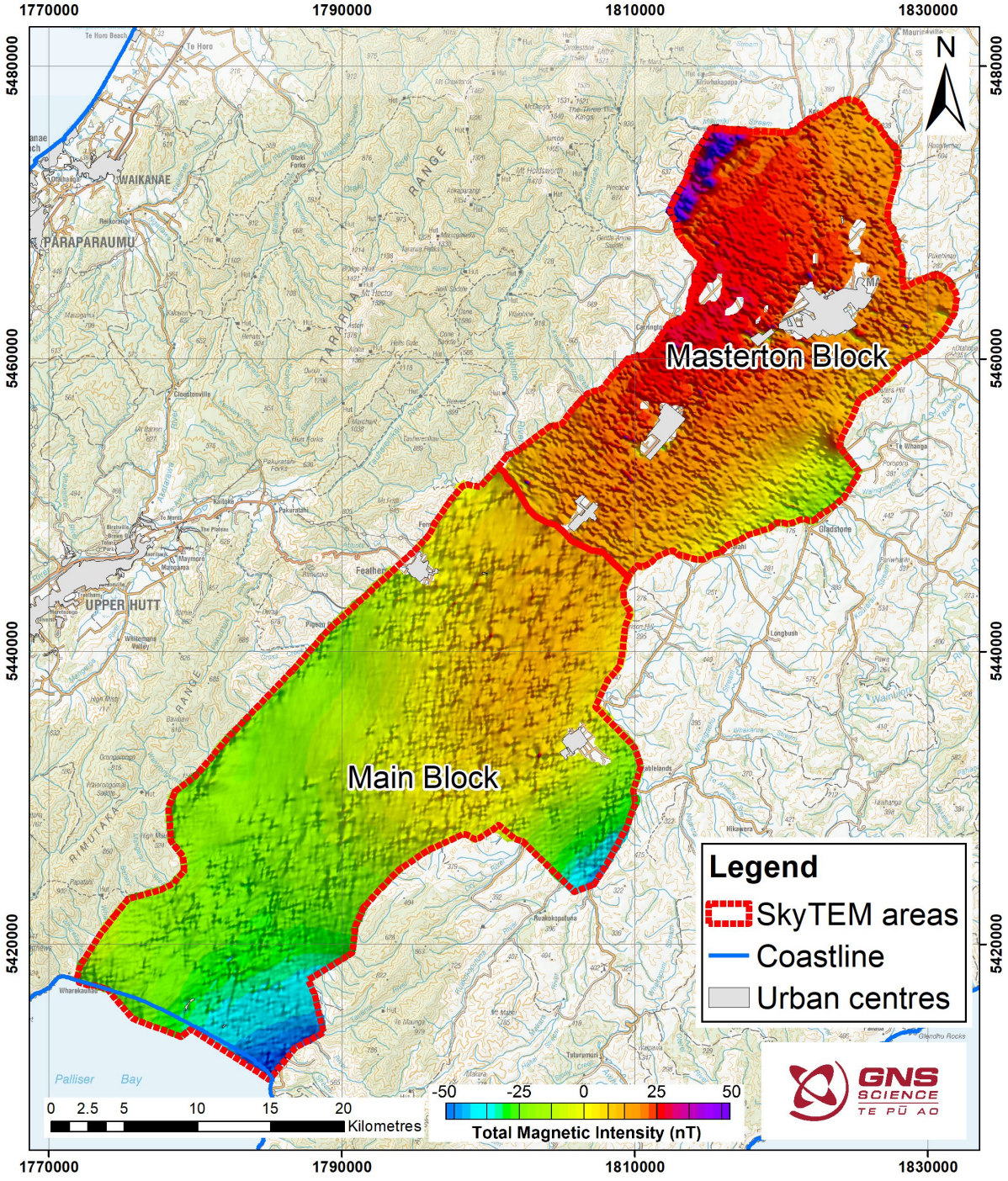

Figure 7.3 SkyTEM airborne magnetic data (total magnetic intensity with International Geomagnetic Reference Field removed in nanotesla) collected during the SkyTEM survey.

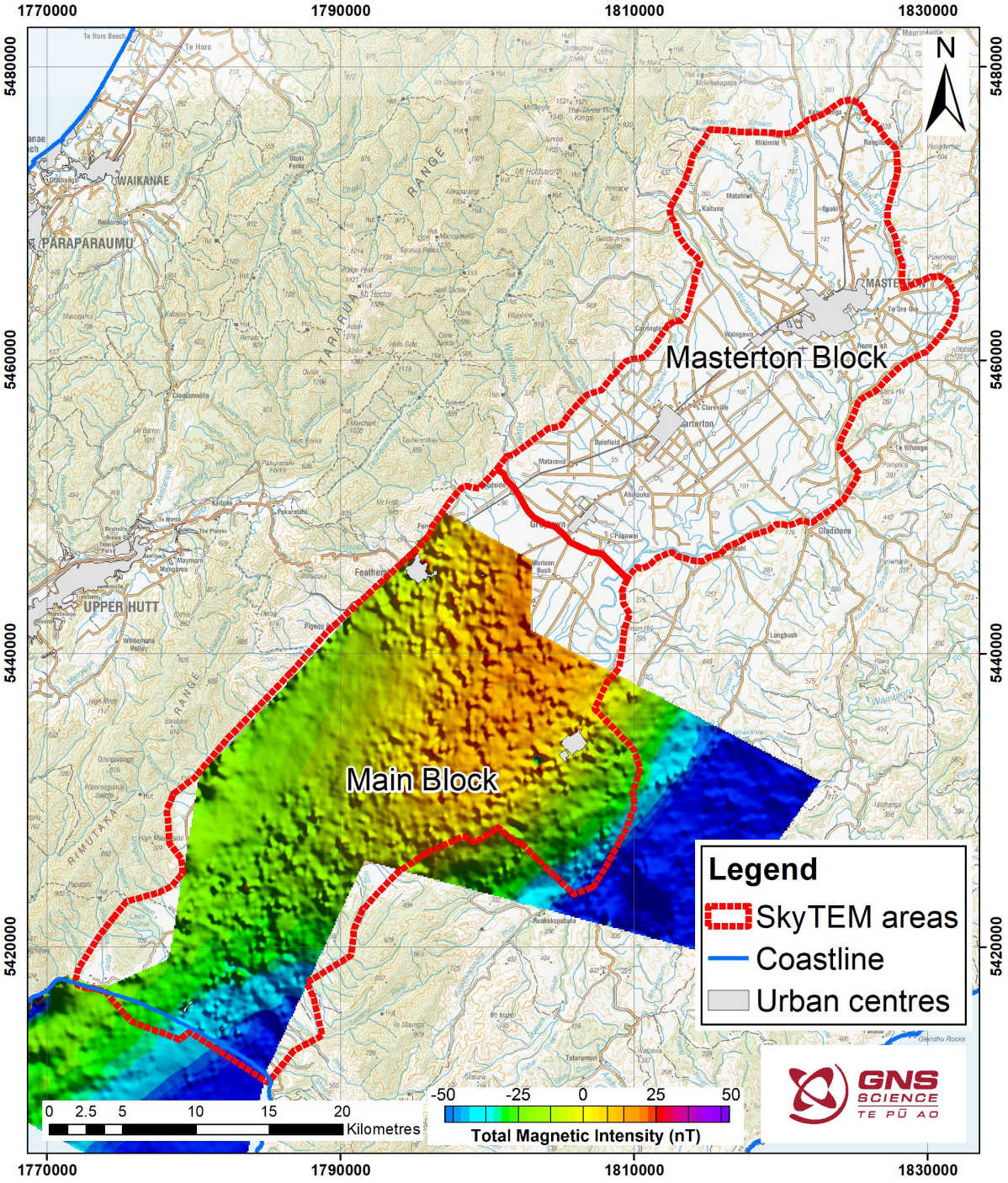

Figure 7.4 Lakes Oil airborne magnetic data (total magnetic intensity with International Geomagnetic Reference Field removed in nanotesla) collected during the 2008 survey.

7.2.4 GroundTEM Data

Ground-based TEM (GroundTEM) soundings have been made within the Ruamāhanga Catchment in three campaigns. In 2020, a set of eight soundings were conducted at a reconnaissance level in preparation for the SkyTEM survey design (Kellett et al. 2020). In 2022, 12 soundings were made in the Pirinoa area of southern Wairarapa (Kellett et al. 2022). During the acquisition of the SkyTEM in 2023, an additional five soundings were made in the central and northern parts of the field area. The sites are located at key wells across the area so that the detailed geology provided by the borehole logs can be compared to the models derived from the GroundTEM and closest SkyTEM models (Figure 7.5).

The GroundTEM data collected in 2020 and 2022 were collected using the Zonge TEM and NanoTEM system (Kellett et al. 2020, 2022), and the sites collected in 2023 utilised an ABEM WalkTEM system. All of the data have been processed separately using AGS Seequent SPIA software with a smooth and layered 1D inversion routine (Auken et al. 2015). The smooth 1D models for the NanoTEM and TEM soundings were exported in a standard ASCII format for importing into the SkyTEM processing and interpretation software (Workbench). Kellett et al. (2022) provides examples of the processed data and models.

Prior to the acquisition of the SkyTEM data, the GroundTEM soundings provided a valuable dataset to help determine the optimal configuration of the SkyTEM system. The resistivity model for each sounding was used to develop an initial relationship between electrical resistivity and lithology. The GroundTEM produce resistivity profiles that are similar in resolution to the SkyTEM inversions, so provide a valuable link between the geology derived from the well and the resistivity derived from the SkyTEM survey.

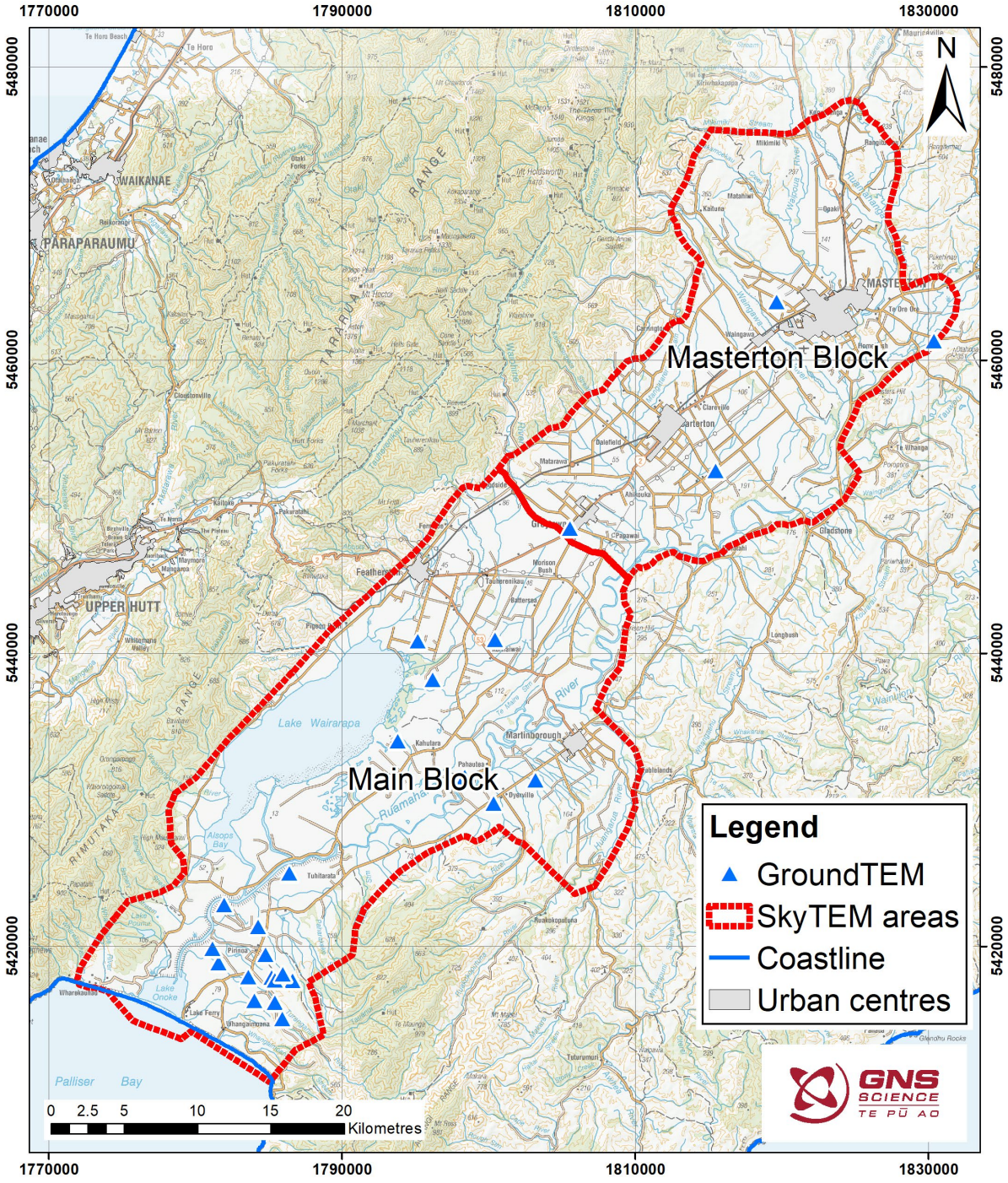

Figure 7.5 The locations of GroundTEM soundings undertaken prior to and during the SkyTEM survey. Most of the measurements are located at key boreholes across the study area.

7.2.5 Direct Current Resistivity Data

Electrical resistivity surveys have been used for groundwater exploration in New Zealand since the mid-1960s (Risk 1974). The data can be collected as individual soundings primarily using a Schlumberger array. Schlumberger resistivity soundings provide a 1D model of the resistivity structure at the centre of the measurement array. In more recent times, the data are collected on a continuous profile, providing a 2D array of measurements that can be processed to yield a resistivity cross-section. This technique is referred to as Electrical Resistivity Tomography (ERT) (Dahlin 2001).

Various groups, including the Ministry of Works (White 1982) and the Regional Council have collected a total of 124 Schlumberger soundings in the Wairarapa Valley (Figure 7.6). These data are available from GWRC as tables of data and graphs of sounding plots, with the approximate location of the site.

As part of this project, the raw data from the Schlumberger soundings have been digitised from the figures or tables and modern inversion methods used to generate new models. One-dimensional (1D) modelling software was used to derive 20-layer smooth models for each site (Cockett et al. 2015). These models were then imported into the AGS Seequent Workbench software for comparison with borehole lithology logs and the SkyTEM models. Kellett et al. (2022) provide a detailed description of some of the datasets and their use in mapping the aquifers in the southern part of the study area.

GNS collected two ERT lines in the Pirinoa region as part of the 2022 survey (Kellett et al. 2022). The two sections provided valuable control on the SkyTEM models in the Turanganui and Tauanui valleys (Figure 7.6) and were used in Workshop 1 to support the evaluation of the resistivity model. Similarly, the large number of resistivity soundings in the Te Ore Ore basin to the northeast of Masterton were used in the Workshop 2, where the Masterton block was evaluated.

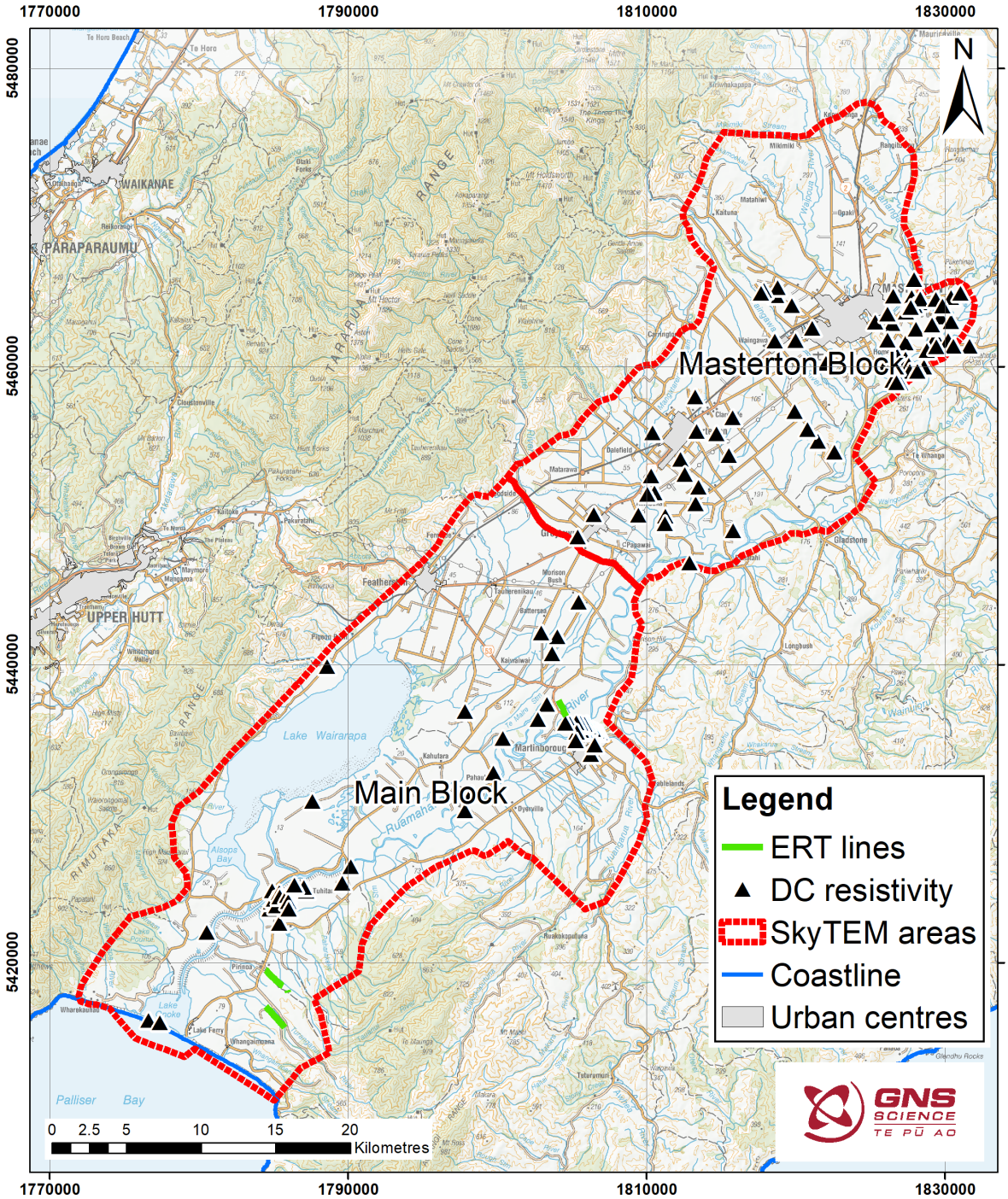

Figure 7.6 Electrical resistivity surveys across the field area include legacy DC resistivity soundings (green points) and Electrical Resistivity Tomography (ERT) lines (green) collected as part of the SkyTEM design.

7.2.6 Seismic Reflection Data

Seismic reflection surveys have been undertaken by the Department of Scientific and Industrial Research (DSIR) Geophysics Division, in collaboration with Victoria University of Wellington. The primary aim of the survey was research into the tectonics of the East Coast fold and thrust belt. Figure 7.7 shows the location (in green) of the five individual seismic lines across the SkyTEM survey area near Martinborough and south of Masterton. The data were collected in three different projects in 1986, 1988 and 2002 using the DSIR 48 Channel SERCEL system and a combination of mini-sosie and dynamite sources. Details of each seismic programme are given in Cape (1989), Cape et al. (1990) and Nicol et al. (2002).

Several of these seismic lines have been reprocessed by petroleum exploration companies to improve the imaging of the stratigraphy and structure (Excel Geophysical Services Ltd 2013).

All seismic lines are available in digital format for incorporation into the SkyTEM interpretation.

In addition to the regional exploration seismic data, there have been several high-resolution shallow seismic surveys undertaken in the Wairarapa Valley for engineering, hydrogeology and active fault mapping. Figure 7.7 shows the locations of the surveys, which comprise:

- A shallow reflection survey for groundwater undertaken by ScanTEC in 2010 east of Carterton and Southeast of Featherston (Watson 2008a, 2008b).
- A shallow reflection survey for liquefaction studies undertaken by Southern Geophysical near Blundell's barrage on the lower Ruamāhanga River (Streeter 2005).
- A shallow refraction survey over the Wairarapa Fault west of Lake Onoke (Rollo 1992).
- A shallow refraction survey at Whangimoana (Hicks 1974).

Most of these data are only available as scanned images of the sections. The seismic data are valuable for identifying layering in the sediments that may correspond with contacts mapped in the SkyTEM data. The seismic method is also capable of mapping faults that might be subtle features in the SkyTEM data.

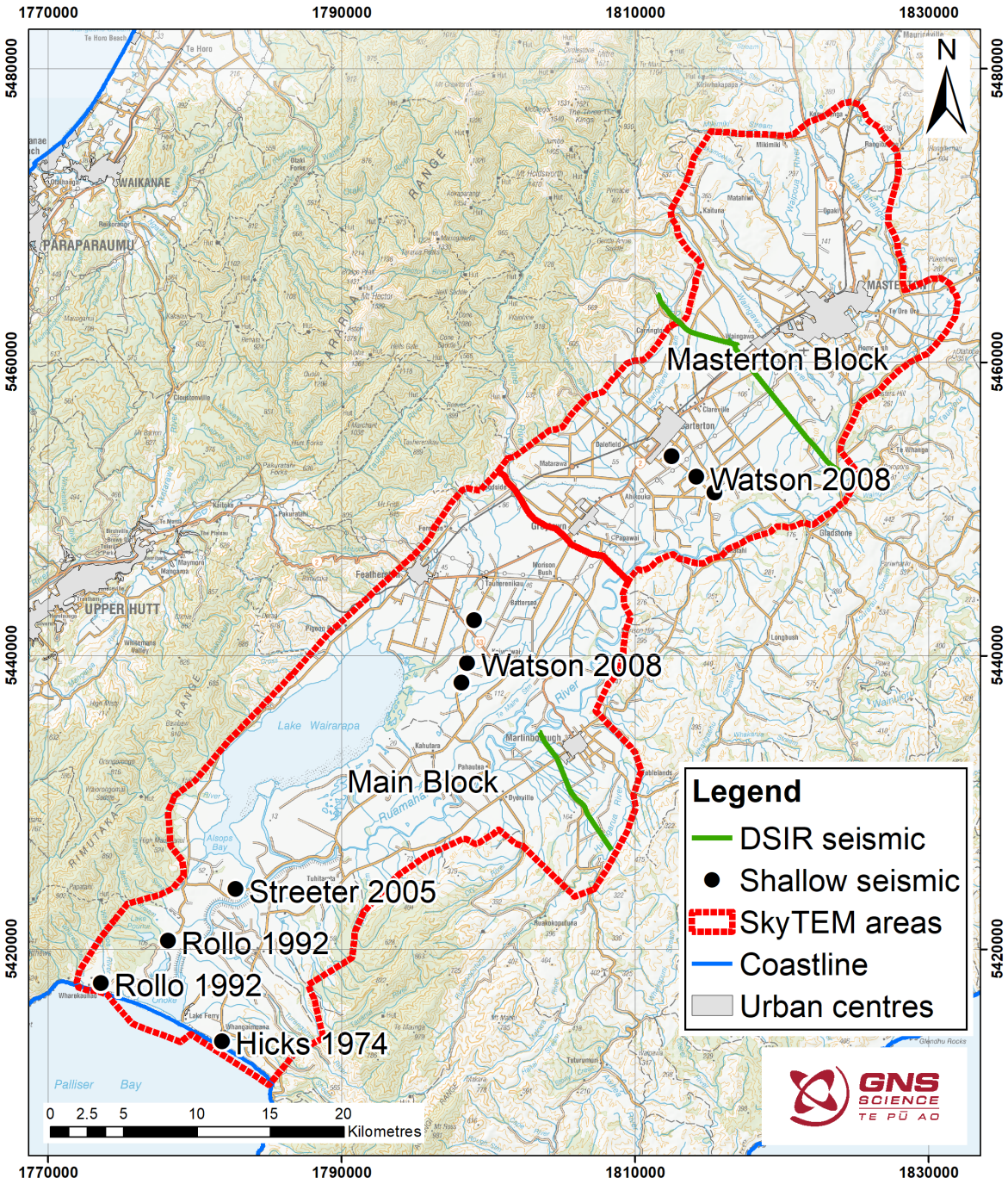

Figure 7.7 Seismic reflection lines collected by DSIR between 1986 and 1988 for tectonic studies, shown as green lines. The locations of various shallow seismic studies conducted for engineering, groundwater, and active faulting studies are shown as points.

7.2.7 Magnetotelluric Data

The magnetotelluric method utilises natural fluctuations in Earth's magnetic and electric fields to map the subsurface resistivity structure. It is primarily used for regional tectonic studies where the resistivity of the top 2–25 km of the crust are imaged (Heise et al. 2013). The method can also be used for exploration of sedimentary basins, geothermal systems and mineral deposits where more detailed information is required in the top 0.5–2 km.

Over the last 30 years, there have been several magnetotelluric surveys in the Wairarapa (Figure 7.8). Some of the older surveys (Ingham et al. 2001; McLoughlin et al. 2002) have large station spacing and utilised low frequencies, so are less useful for supporting the SkyTEM

data. The survey undertaken by Rollo (1992) near Lake Onoke has close station spacing, but the available data are limited. There are two surveys that collected a dense set of data on profiles across the Wairarapa Valley (Ingham 2014; Heise et al. 2013). These sections can be re-inverted to focus on the shallow resistivity structure. They provide some important constraints on the structure of the basement and the prominent fold and thrust structure in the sedimentary basin that potentially extend to the surface.

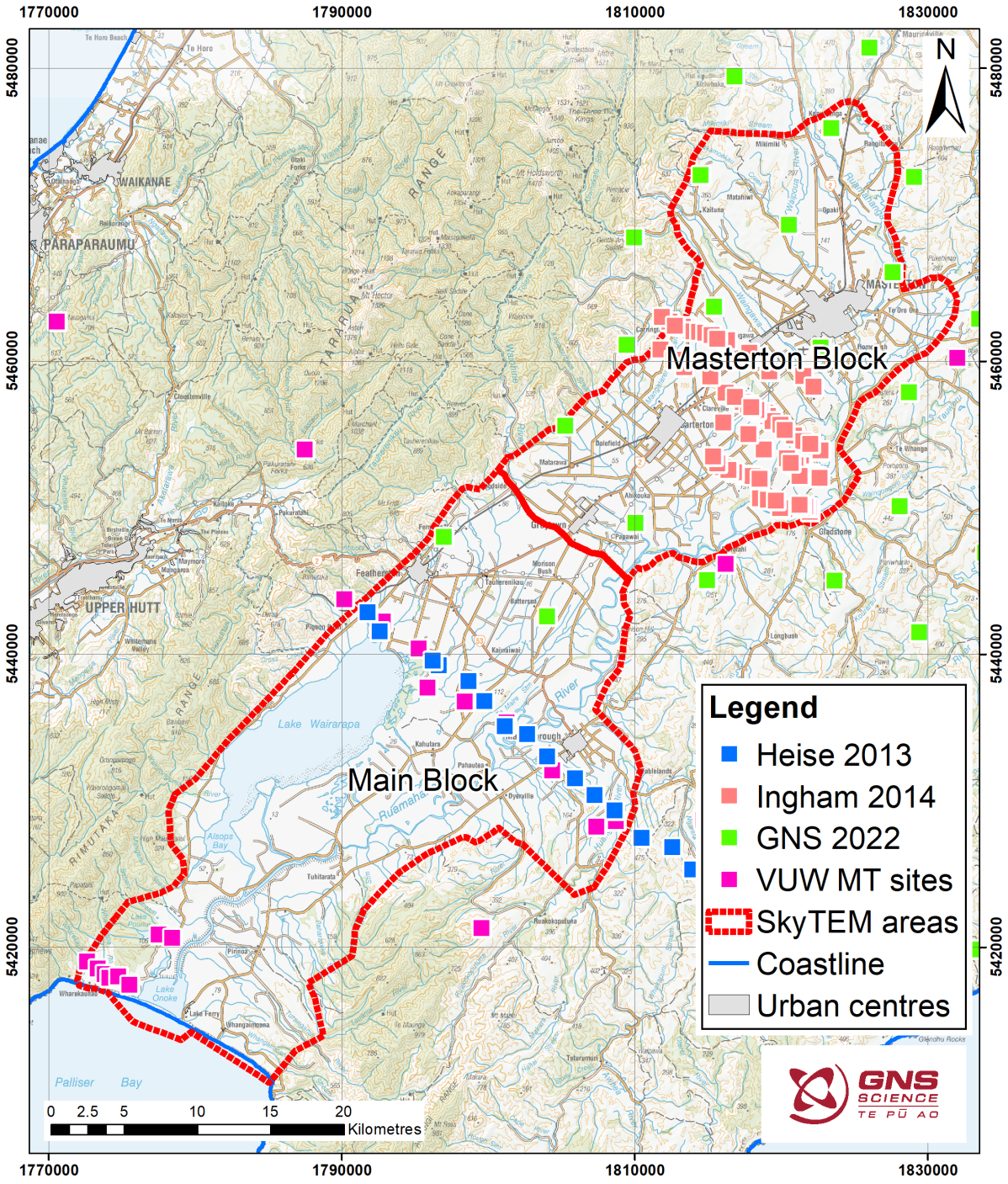

Figure 7.8 Location of the magnetotelluric sites across the Wairarapa valley. The VUW MT sites are old sites collected prior to 2000. The detailed surveys on profiles (Ingham [2014] and Heise et al. [2013]) have been collected with modern equipment and provide some control on the deep resistivity structure of the SkyTEM models.

7.2.8 Groundwater Boreholes

The GWRC well database[1] (accessed 1 July 2023) contained 3456 boreholes within the limits of the SkyTEM area (Figure 7.9). This database includes both bore construction and lithological information. Of all these bores in the survey area, 3195 bores have depth information. The mean bore depth of these bores is 15 m, and the median and mode of the bore depths are 9 m and 6 m, respectively (Figure 7.10).

Lithological information is available from 1953 boreholes within the GWRC database. This information within the database is variable in terms of the level of detail of the descriptions and the accuracy of the depths. Within the bore lithological dataset, obvious data-entry errors have been corrected.

Based on previous experience in the Hawke's Bay projects (Tschritter et al. 2022), there are two potential sources of uncertainty inherent in these lithological borehole log descriptions:

1. The encountered lithologies are usually described by commercial drillers during the drilling and not experienced geologists, resulting in non-standardised, potentially inaccurate, descriptions that commonly do not include a geological unit or formation.
2. Data-entry errors resulting from the manual transfer of borehole logs from often non-digital sources into the borehole log database.

Additionally, bore location errors may arise from incorrect surveying of the locations, from conversion of historically used spatial reference systems with low location accuracy and from data-entry errors.

The primary role of the boreholes in this present study is to provide some initial validation of the resistivity models and a correlation with the main hydrogeological units. In future projects, the borehole data will be used for a more detailed interpretation of the resistivity model and development of a hydrogeological model. The database has been divided into three sub-sets (primary, secondary, tertiary) based on the following criteria:

- **Borehole depth:** Deeper boreholes provide constraints over more of the SkyTEM model.
- **Presence of detailed lithological information:** Finer divisions and more detailed descriptions in the lithological log help build up a more detailed view of the variations in lithology within units.
- **Proximity to SkyTEM data and supporting geophysical data:** Boreholes that are within 100 m of a SkyTEM, GroundTEM or DC resistivity model point are valuable because they help bridge the gap between the resistivity model and the lithology. Interpolating more than 100 m from a borehole to the SkyTEM risks mis-interpreting lateral changes in the geology.

7.2.8.1 Primary Borehole Logs

This dataset comprises 17 boreholes that are greater than 50 m deep and have lithological descriptions that are reliable based on the level of detail and consistency. GroundTEM surveys were undertaken at some of these boreholes to provide detailed resistivity information. These boreholes ranged in depth from 50 to 177 m.

1 https://data-gwrc.opendata.arcgis.com/datasets/wells-and-bores/explore

7.2.8.2 Secondary Borehole Logs

This dataset comprises 108 boreholes. The lithological information was typically less detailed than the primary sub-set. The depths of the boreholes ranged from 11 to 93 m, but the deeper wells were in areas already covered by the primary dataset.

7.2.8.3 Tertiary Borehole Logs

This dataset comprises the remaining 1828 boreholes. While still very valuable to reviewing the lateral changes in geology across the Ruamāhanga Catchment, they were shallow and contained less detailed lithological information. These boreholes ranged in depth from 1.3 to 49 m.

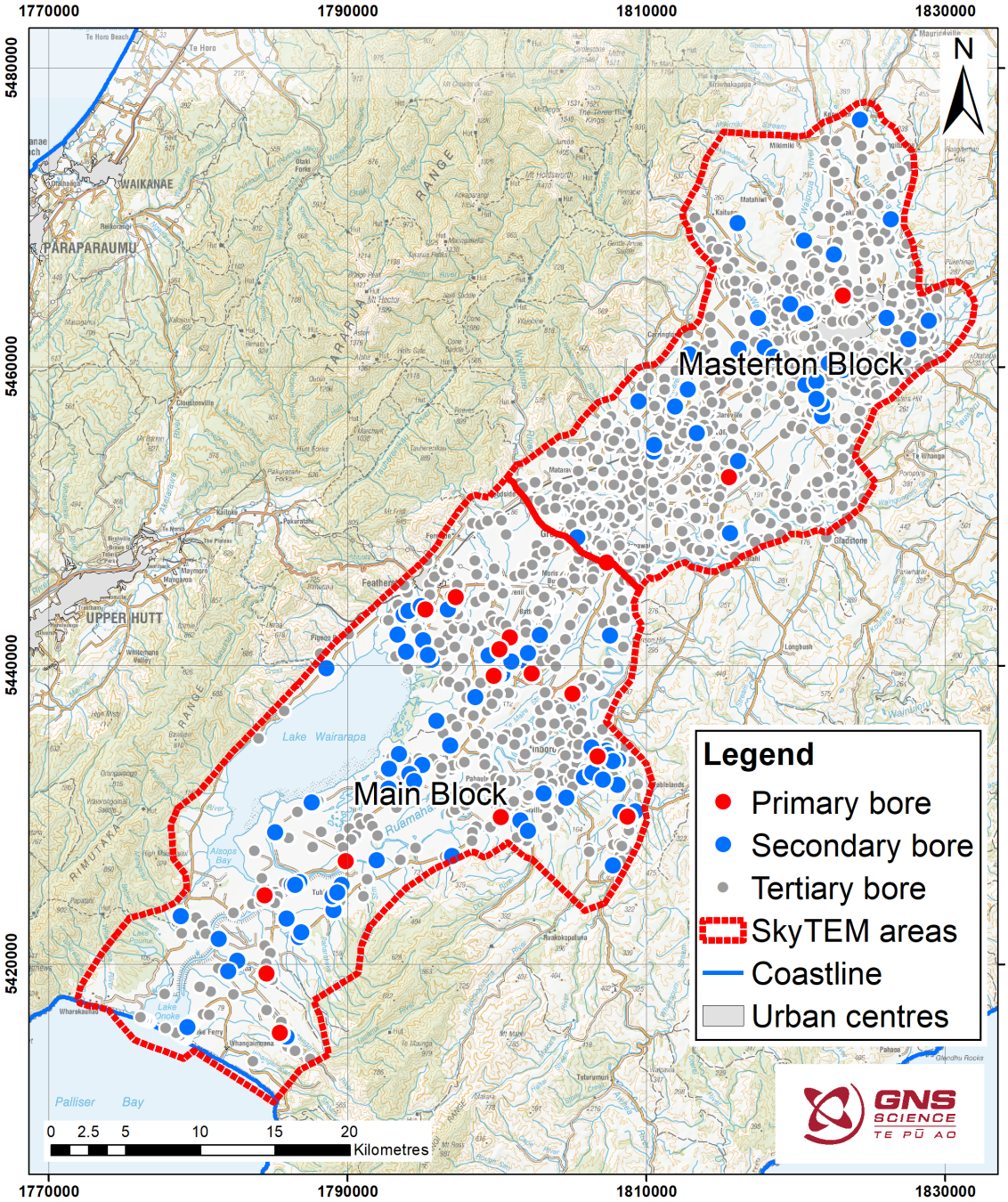

Figure 7.9 Location of the boreholes used to support the review of the SkyTEM resistivity models. The dataset comprises three sub-sets (Primary, Secondary, Tertiary) based on borehole depth and the quality of the lithological descriptions.

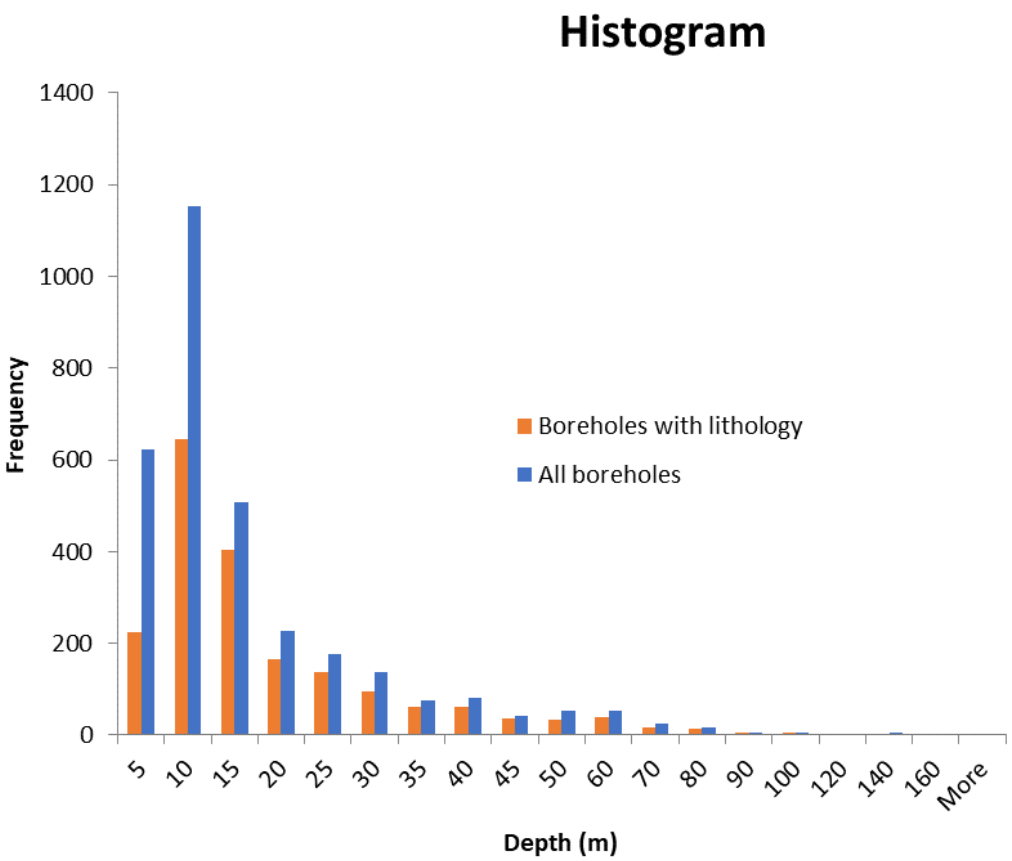

Figure 7.10 Histogram of borehole depths. There are 3195 boreholes (blue) with depth information and 1953 boreholes with lithological information (orange). The average depth of all boreholes is 15 m, and the deepest borehole is 177 m deep.

8.0 CONCLUSION

Between 28 January and 2 March 2023, 5684 km of SkyTEM data were collected over the Ruamāhanga Catchment in the Wairarapa Valley. Both automatic and manual data processing were carried out to remove electromagnetic noise from the low-moment and high-moment data. This processing was quality-checked, post-processing was undertaken to check for any remaining artefacts and then a final quality check was undertaken.

Using the retained data, spatially constrained inversions were performed, creating both a smooth and a sharp resistivity model result. Additionally, the system response modelling approach was used in the inversion of the data, enabling modelling of five extra time gates in the ramp-down time and thus providing higher resolution in the near surface.

The SkyTEM survey reveals a detailed 3D resistivity picture of the subsurface. The resistivity models have layer thicknesses of 1 m in the near-surface, increasing to 59 m at 541–600 m depth (Table 4.2). The standard depth of investigation varies from 22 m to 658 m, with a mean of 382 m for the smooth model.

The resistivity model was evaluated during a series of workshops with GWRC and its consultants using resistivity slices and key cross-sections. Images of the resistivity model are made available in this report. Additional geoscience data. such as GroundTEM, DC resistivity soundings and boreholes, were used to evaluate the resistivity models.

The final resistivity models are provided to GWRC as digital datasets in a range of formats suitable for display in modelling and GIS software. The layers contain some vertical averaging to smooth out variations across the entire area. The shallowest layer is 4 m thick. For the model presented in elevation above/below sea level, the 4 m thickness is retained to maintain vertical resolution between -100 m and 360 m. The layer thicknesses increase gradually to -500 m elevation, but the models are clipped at the standard DOI.

Hydrogeological interpretation of the 3D resistivity models is needed to make full use of the SkyTEM survey results. This follow-on work will be described within a separate report.

9.0 ACKNOWLEDGEMENTS

This work has been jointly funded by the New Zealand Government's Kānoa – Regional Economic Development & Investment Unit (formerly the Provincial Development Unit), Greater Wellington Regional Council (GWRC), Masterton District Council, Carterton District Council and South Wairarapa District Council.

Thank you to Bruce Geden, Rebecca Morris, Lindsay Annear, Mike Thompson and Rob van der Raaij of Greater Wellington Regional Council for their contributions to this project.

Andy Kass and Nicolaj Foged provided valuable training and critical reviews.

Thank you to Chris Worts and Kate Osborn for business partnerships support. Thank you to Rob Reeves and Zara Rawlinson for providing report reviews.

10.0 REFERENCES

Auken E, Christiansen AV, Westergaard JH, Kirkegaard C, Foged N, Viezzoli A. 2009. An integrated processing scheme for high-resolution airborne electromagnetic surveys, the SkyTEM system. *Exploration Geophysics*. 40(2):184–192. https://doi.org/10.1071/EG08128

Auken E, Christiansen AV, Kirkegaard C, Fiandaca G, Schamper C, Behroozmand AA, Binley A, Nielsen E, Effersø F, Christensen NB, et al. 2015. An overview of a highly versatile forward and stable inverse algorithm for airborne, ground-based and borehole electromagnetic and electric data. *Exploration Geophysics*. 46(3):223–235. https://doi.org/10.1071/EG13097

Auken E, Foged N, Andersen KR, Nyboe NS, Christiansen AV. 2020. On-time modelling using system response convolution for improved shallow resolution of the subsurface in airborne TEM. *Exploration Geophysics*. 51(1):4–13. https://doi.org/10.1080/08123985.2019.1662292

Begg JG, Johnston MR, compilers. 2000. Geology of the Wellington area [map]. Lower Hutt (NZ): Institute of Geological & Nuclear Sciences. 1 sheet + 64 p., scale 1:250,000. (Institute of Geological & Nuclear Sciences 1:250,000 geological map; 10).

Cape CD. 1989. Geophysical profiling of the Wairarapa Basin, New Zealand. Wellington (NZ): Department of Scientific and Industrial Research, Geophysics Division. 40 p. Research Report 227.

Cape CD, Lamb SH, Vella P, Wells PE, Woodward DJ. 1990. Geological structure of Wairarapa Valley, New Zealand, from seismic reflection profiling. *Journal of the Royal Society of New Zealand*. 20(1):85–105. https://doi.org/10.1080/03036758.1990.10426734

Christiansen AV, Auken E. 2012. A global measure for depth of investigation. *Geophysics*. 77(4):WB171–WB177. https://doi.org/10.1190/geo2011-0393.1

Cockett R, Kang S, Heagy LJ, Pidlisecky A, Oldenburg DW. 2015. SimPEG: an open source framework for simulation and gradient based parameter estimation in geophysical applications. *Computers & Geosciences*. 85:142–154. https://doi.org/10.1016/j.cageo.2015.09.015

Dahlin T. 2001. The development of DC resistivity imaging techniques. *Computers & Geosciences*. 27(9):1019–1029. https://doi.org/10.1016/S0098-3004(00)00160-6

Excel Geophysical Services Ltd. 2013. Seismic data processing report for PEP 53674. Located at: Ministry of Business, Innovation & Employment, Wellington, NZ. New Zealand Unpublished Petroleum Report 4823.

Heise W, Caldwell TG, Bertrand EA, Hill GJ, Bennie SL, Ogawa Y. 2013. Changes in electrical resistivity track changes in tectonic plate coupling. *Geophysical Research Letters*. 40(19):5029–5033. https://doi.org/10.1002/grl.50959

Heron DW, custodian. 2024. Geological map of New Zealand. 4th ed. Lower Hutt (NZ): GNS Science. 1 USB, scale 1:250,000. (GNS Science 1:250,000 geological map; 1).

[HGG] HydroGeophysics Group. 2011. Guideline and standards for SkyTEM measurements, processing and inversion. Aarhus (DK): Aarhus University; [accessed 2020 Nov]. https://hgg.au.dk/fileadmin/HGGfiles/Reports/Guide_SkyTEMGuide_ENG.pdf

[HGG] HydroGeophysics Group. 2017. SkyTEM survey Drenthe. Aarhus (DK): Aarhus University. 25 p. + appendices. Report 15-06-2017.

Hicks SR. 1974. Shallow seismic surveys at Wainuiomata, Waikanae and Whangaimoana. Wellington (NZ): Department of Scientific and Industrial Research, Geophysics Division. 33 p. Report 93.

Holdgate G. 2008. A review of the geology & geophysics for PEP38350 East Coast Basin, North Island, New Zealand. Located at: Ministry of Business, Innovation & Employment, Wellington, NZ. 79 p. New Zealand Unpublished Petroleum Report 3881.

Ingham M. 2014. Magnetotelluric survey of the Chester, Tiffin/Peter Cooper and Gladstone anticlines. Located at: Ministry of Business, Innovation & Employment, Wellington, NZ. New Zealand Unpublished Petroleum Report 4962.

Ingham M, Whaler K, McKnight D. 2001. Magnetotelluric sounding of the Hikurangi Margin, New Zealand. *Geophysical Journal International*. 144(2):343–355. https://doi.org/10.1046/j.0956-540X.2000.01330.x

Jørgensen F, Lykke-Andersen H, Sandersen PBE, Auken E, Nørmark E. 2003. Geophysical investigations of buried Quaternary valleys in Denmark: an integrated application of transient electromagnetic soundings, reflection seismic surveys and exploratory drillings. *Journal of Applied Geophysics*. 53(4):215–228. http://doi.org/10.1016/j.jappgeo.2003.08.017

Kellett RL, Rawlinson ZJ, Brakenrig T, Macdonald N. 2020. Ruamahanga ground TEM soundings for SkyTEM survey planning. Lower Hutt (NZ): GNS Science. 12 p. Consultancy Report 2020/100LR. Prepared for Greater Wellington Regional Council.

Kellett RL, Begg JG, Brakenrig T, Macdonald N, Boyes AF. 2022. Ground geophysical and geological investigations of aquifer characteristics in southern Wairarapa. Lower Hutt (NZ): GNS Science. 73 p. Consultancy Report 2022/69. Prepared for Greater Wellington Regional Council.

Kellett RL, Kirkby AL, Keats BS, Brakenrig T. 2023. Review of the Wairarapa airborne electromagnetic survey acquisition and deliverables. Lower Hutt (NZ): GNS Science. 4 p. Consultancy Report 2023/40LR. Prepared for Greater Wellington Regional Council.

Lee JM, Begg JG, compilers. 2002. Geology of the Wairarapa area [map]. Lower Hutt (NZ): Institute of Geological & Nuclear Sciences. 1 folded map + 66 p., scale 1:250,000. (Institute of Geological & Nuclear Sciences 1:250,000 geological map; 11).

[LINZ] Toitū Te Whenua Land Information New Zealand. 2011. NZ Topo250 Maps. Wellington (NZ): LINZ; [updated 2024 Mar 20; accessed 2024 Jun]. https://data.linz.govt.nz/layer/50798-nz-topo250-maps/

McLoughlin C, Ingham M, Whaler K, McKnight JD. 2002. A magnetotelluric transect of the Wairarapa region, New Zealand. *New Zealand Journal of Geology and Geophysics*. 45(2):257–269. https://doi.org/10.1080/00288306.2002.9514972

Nabighian MN, Macnae JC. 1991. Time domain electromagnetic prospecting methods. In: Nabighian MN, editor. *Electromagnetic methods in applied geophysics: volume 2, applications, part A and part B*. Tulsa (OK): Society of Exploration Geophysicists. p. 427–520. https://doi.org/10.1190/1.9781560802686.ch6

Nicol A, VanDissen R, Vella P, Alloway B, Melhuish A. 2002. Growth of contractional structures during the last 10 m.y. at the southern end of the emergent Hikurangi forearc basin, New Zealand. *New Zealand Journal of Geology and Geophysics*. 45(3):365–385. https://doi.org/10.1080/00288306.2002.9514979

Rawlinson ZJ, Foged N, Westerhoff RS, Kellet RL. 2021. Hawke's Bay 3D Aquifer Mapping Project: Heretaunga Plains SkyTEM data processing and resistivity models. Wairakei (NZ): GNS Science. 90 p. Consultancy Report 2021/93. Prepared for Hawke's Bay Regional Council. https://www.hbrc.govt.nz/assets/Document-Library/Reports/Hawkes-Bay-3D-Aquifer-Mapping-Project-Heretaunga-Plains-SkyTEM-data-processing-and-resistivity-models.pdf

Risk GF. 1974. Electrical resistivity soundings on the Heretaunga Plains. Wellington (NZ): Department of Scientific and Industrial Research, Geophysics Division. 28 p. Report 95.

Rollo JL. 1992. Geophysical investigations of the south western Wairarapa region of New Zealand [MSc thesis]. Wellington (NZ): Victoria University of Wellington. 178 p. https://doi.org/10.26686/wgtn.16992244.v1

SkyTEM Australia Pty Ltd. 2023. SkyTEM helicopter EM survey: Wairarapa 3D aquifer mapping AEM survey, Ruamāhanga Valley, Wairarapa, NZ. Malaga (AU): SkyTEM Australia Pty Ltd. 10088_NZL_Wellington_312. Prepared for Greater Wellington Regional Council.

Sørensen KI, Auken E. 2004. SkyTEM – a new high-resolution helicopter transient electromagnetic system. *Exploration Geophysics*. 35(3):194–202. https://doi.org/10.1071/EG04194

Streeter C. 2005. Liquefaction at the Blundell Barrage, Wairarapa. Christchurch (NZ): University of Canterbury. 80 p. Unpublished B. Eng. Report.

Tschritter C, Kellett RL, Rawlinson ZJ, Griffin AG. 2022. Hawke's Bay 3D Aquifer Mapping Project: Heretaunga Plains data and model inventory. Lower Hutt (NZ): GNS Science. 96 p. Consultancy Report 2021/113. Prepared for Hawke's Bay Regional Council. https://www.hbrc.govt.nz/assets/Document-Library/Reports/Hawkes-Bay-3D-Aquifer-Mapping-project-Heretaunga-Plains-data-and-model-inventory.pdf

Watson M. 2008a. Seismic Reflection Survey Line 1, Wairarapa. Whangārei (NZ): ScanTEC. 16 p. WR311 Part A. Unpublished Report for Greater Wellington Regional Council.

Watson M. 2008b. Seismic Reflection Survey Line 2, Wairarapa. Whangārei (NZ): ScanTEC. 18 p. WR311 Part B. Unpublished Report for Greater Wellington Regional Council.

White P. 1982. Resistivity surveys in the Pouawha area of Wairarapa. Wellington (NZ): Ministry of Works. 21 p. Unpublished Report.

This page left intentionally blank.

APPENDICES

This page left intentionally blank.

APPENDIX 1 LOCATION MAPS, QUALITY-CONTROL MAPS

This appendix includes maps of:

- Model moment indication (HI, LO or Both).
- Number of data points (number of data in the inversion at each measurement point).
- Flight altitude (elevation of the transmitter loop above the ground).
- Data residual (model mis-fit for the smooth and sharp inversions).
- Depth of investigation (DOI; standard for both smooth and sharp inversions).

In order to preserve the detail, the maps are shown as a southern sheet and a northern sheet with some overlap.

- Figure A1.1: Model moment indication South.
- Figure A1.2: Model moment indication North.
- Figure A1.3: NumData South.
- Figure A1.4: NumData North.
- Figure A1.5: Altitude above ground South.
- Figure A1.6: Altitude above ground North.
- Figure A1.7: Data residual smooth South.
- Figure A1.8: Data residual smooth North.
- Figure A1.9: Data residual sharp South.
- Figure A1.10: Data residual sharp North.
- Figure A1.11: DOI Standard smooth South.
- Figure A1.12: DOI Standard smooth North.
- Figure A1.13: DOI Standard sharp South.
- Figure A1.14: DOI Standard sharp North.
- Figure A1.15: Altitude Difference South smooth.
- Figure A1.16: Altitude Difference South sharp.
- Figure A1.17: Altitude Difference North smooth.
- Figure A1.18: Altitude Difference North sharp.

Figure A1.1 Model moment indication South.

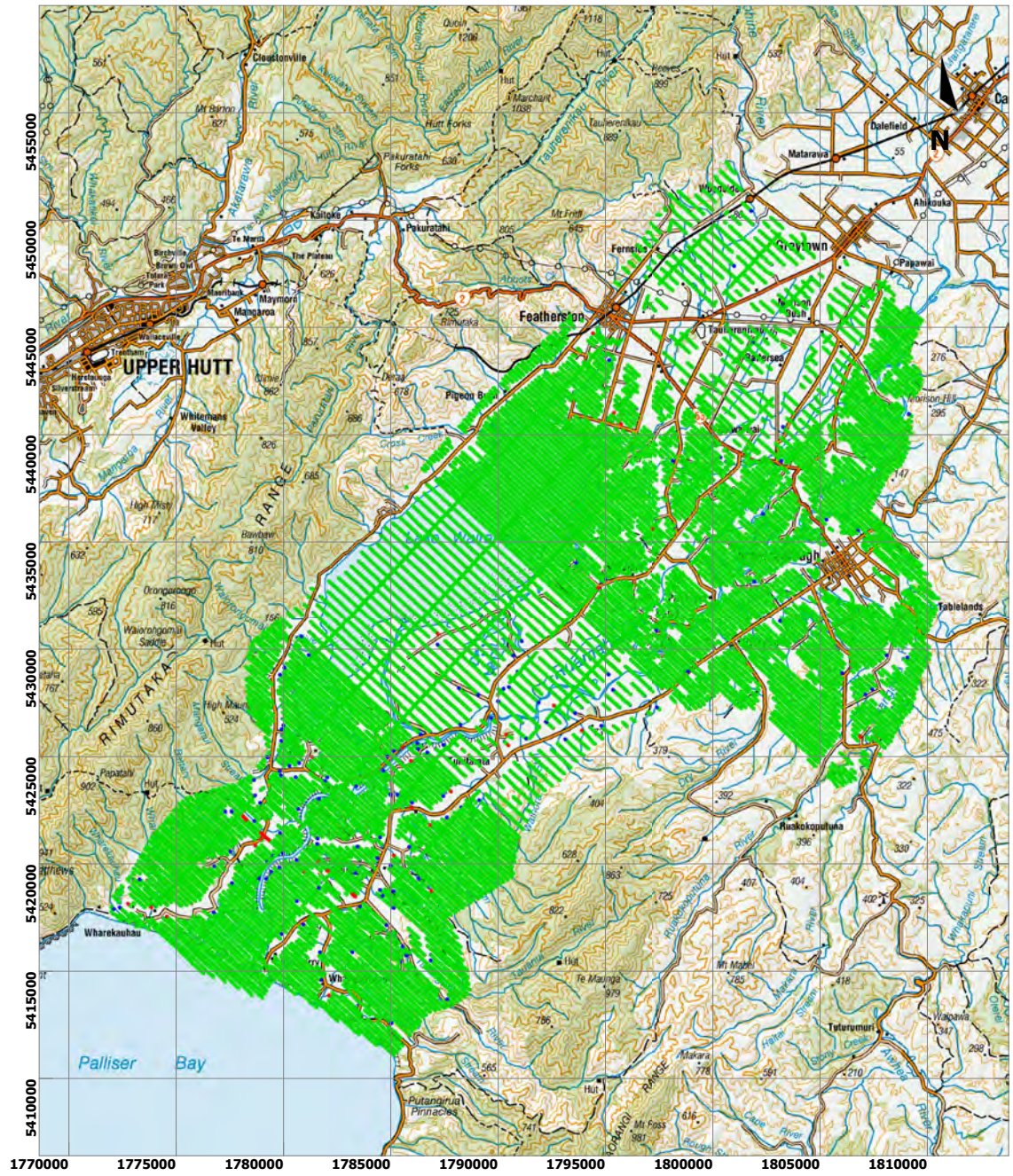

Figure A1.2 Model moment indication North.

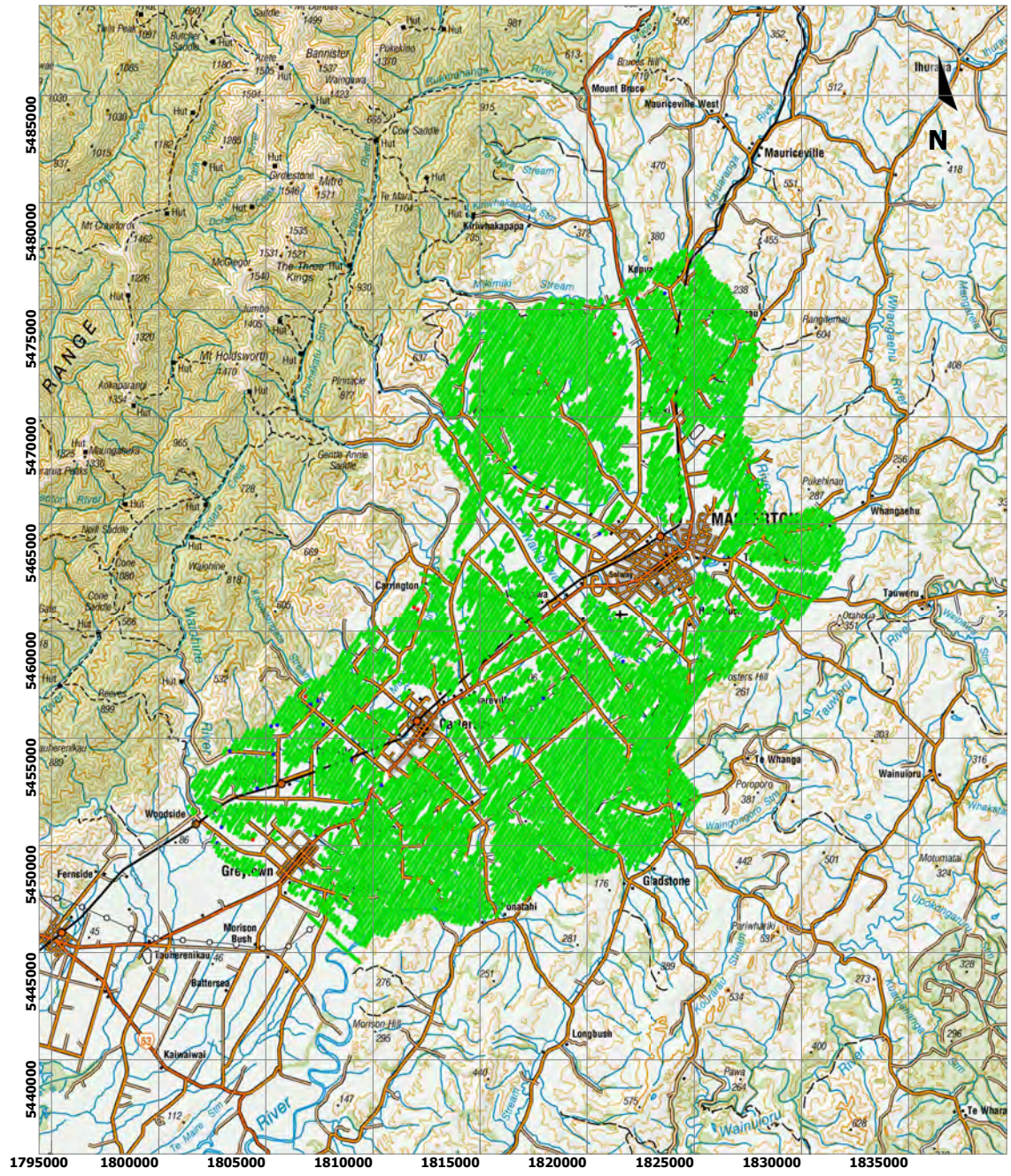

SkyTEM Survey
Ruamāhanga North

Model Moment Indication
Green: LM and HM; Red: LM only; Blue: HM only

0.0 5.0 10.0 15.0 20.0 25.0 30.0

NZTM2000

10000

Figure A1.3 NumData South.

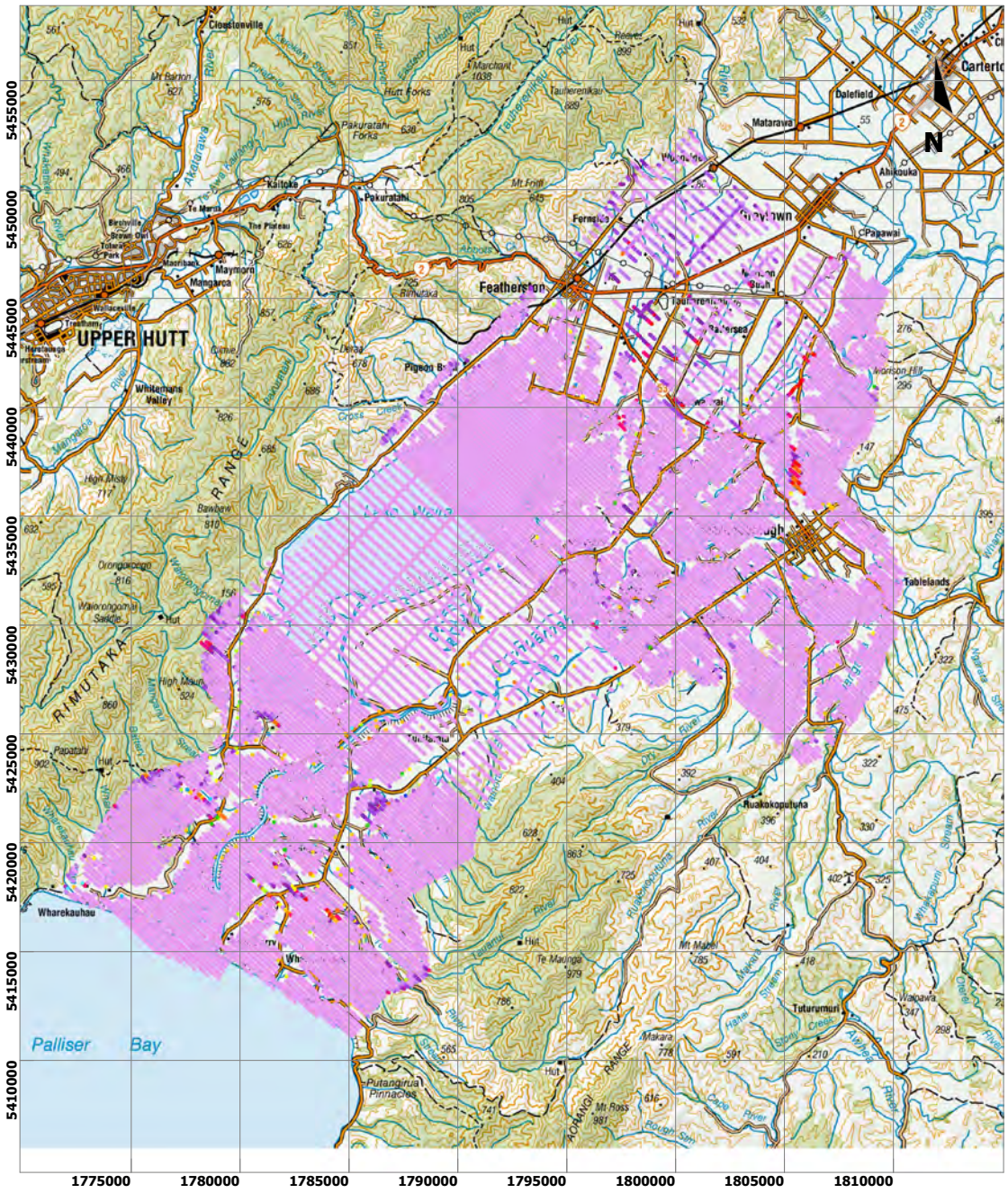

Figure A1.4 NumData North.

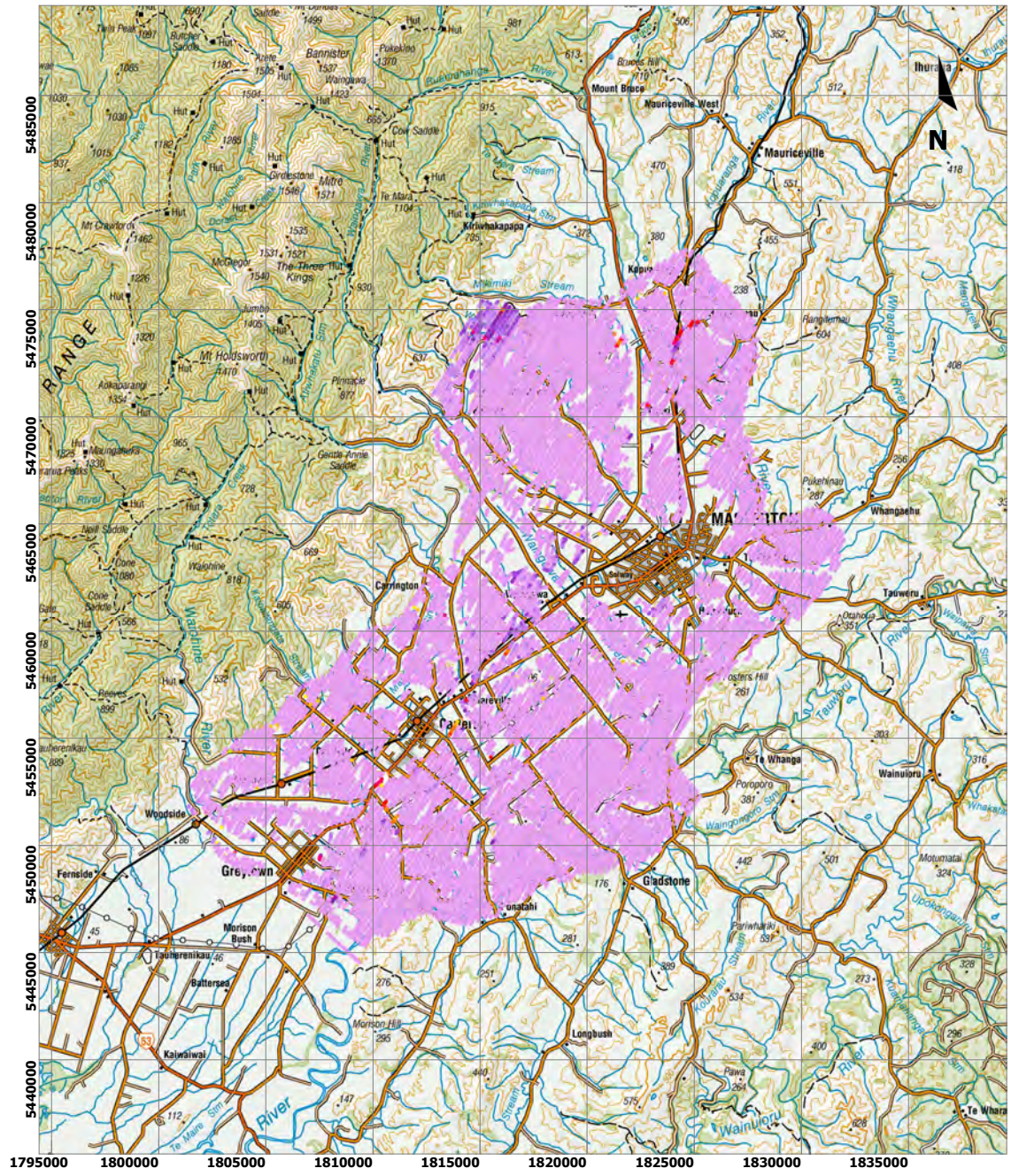

Figure A1.5 Altitude above ground South.

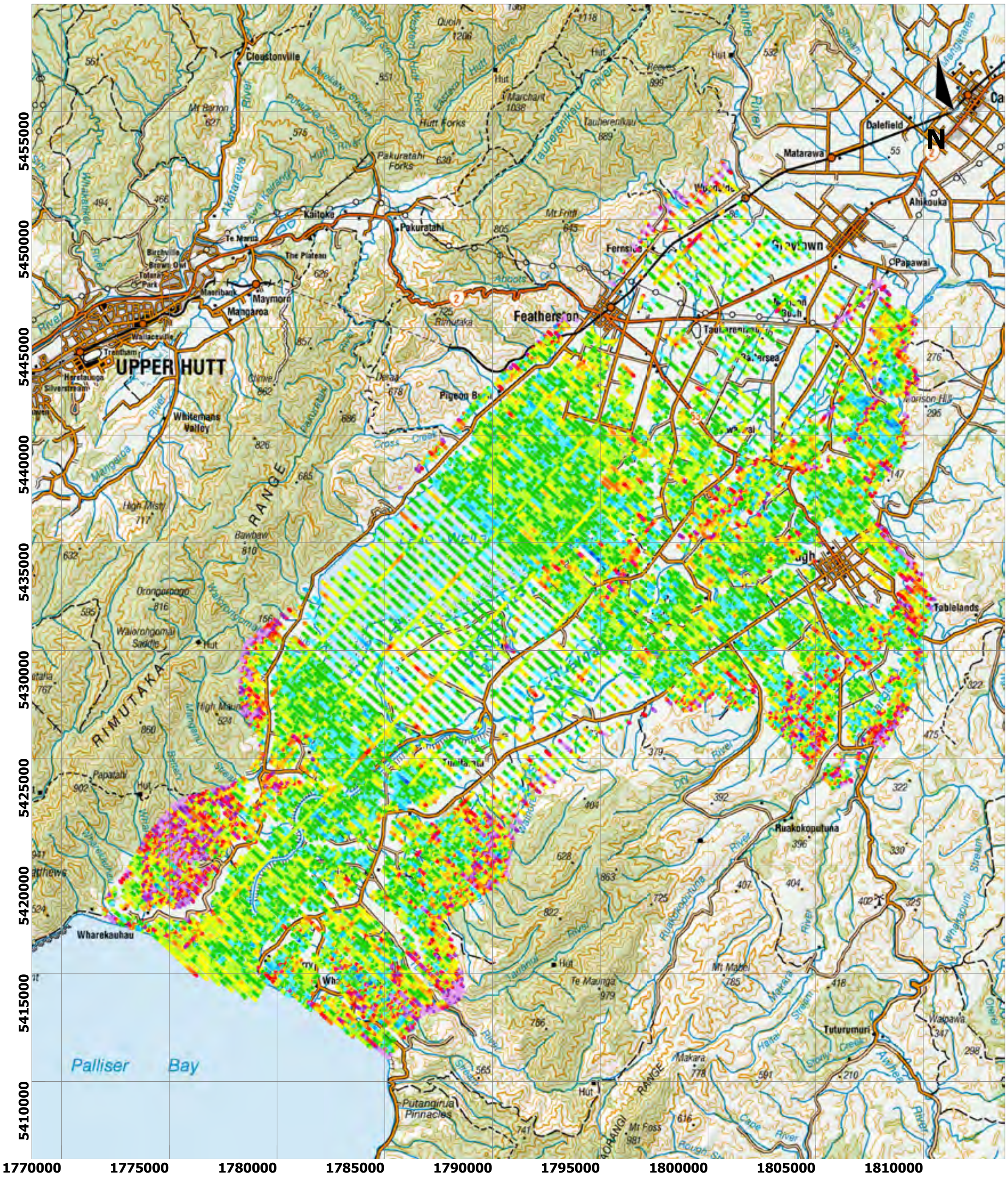

SkyTEM Survey Ruamāhanga South	Flight Altitude Elevation, metres
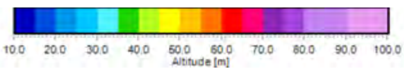	NZTM2000 10 km

Figure A1.6 Altitude above ground North.

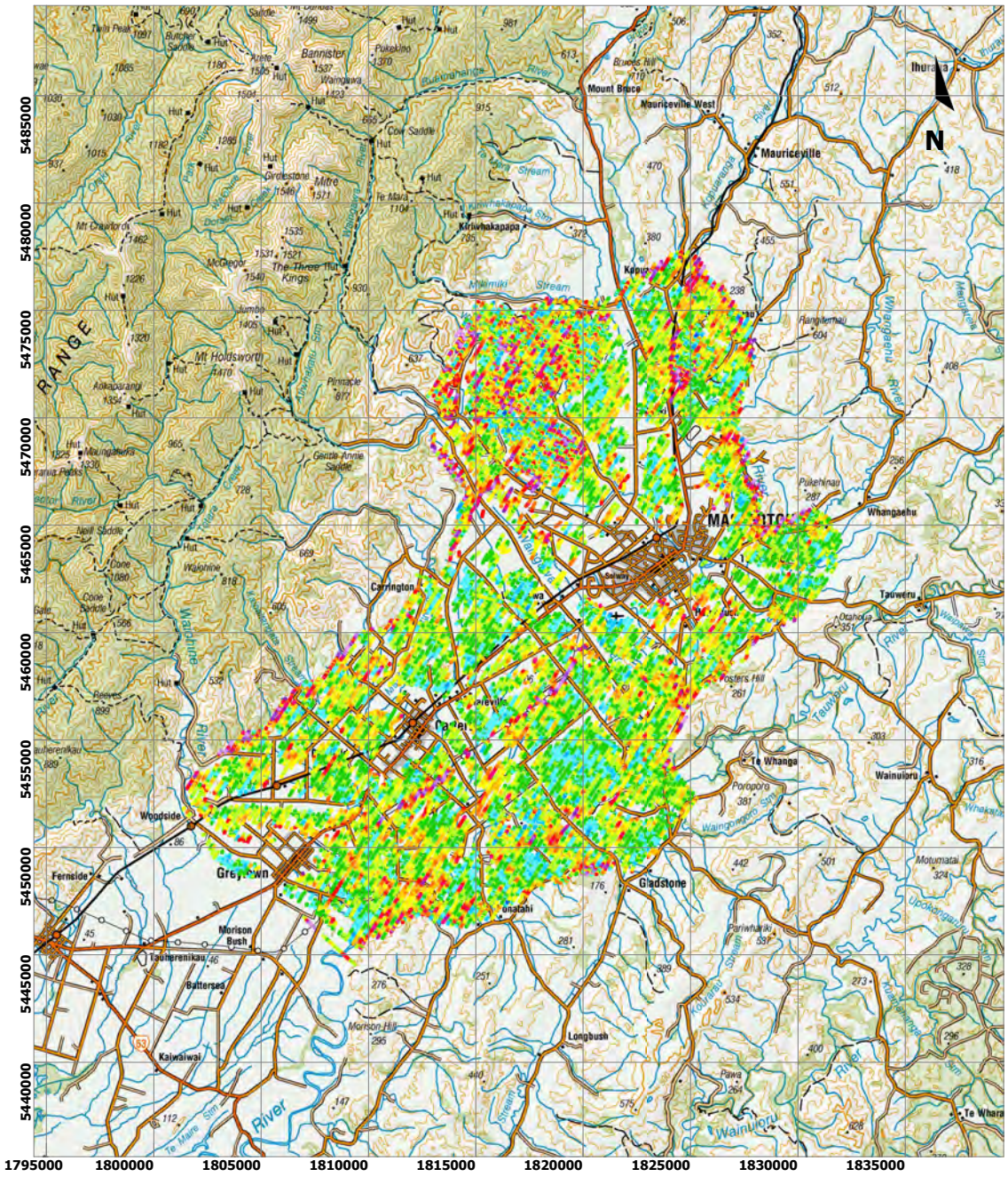

Figure A1.7 Data residual smooth South.

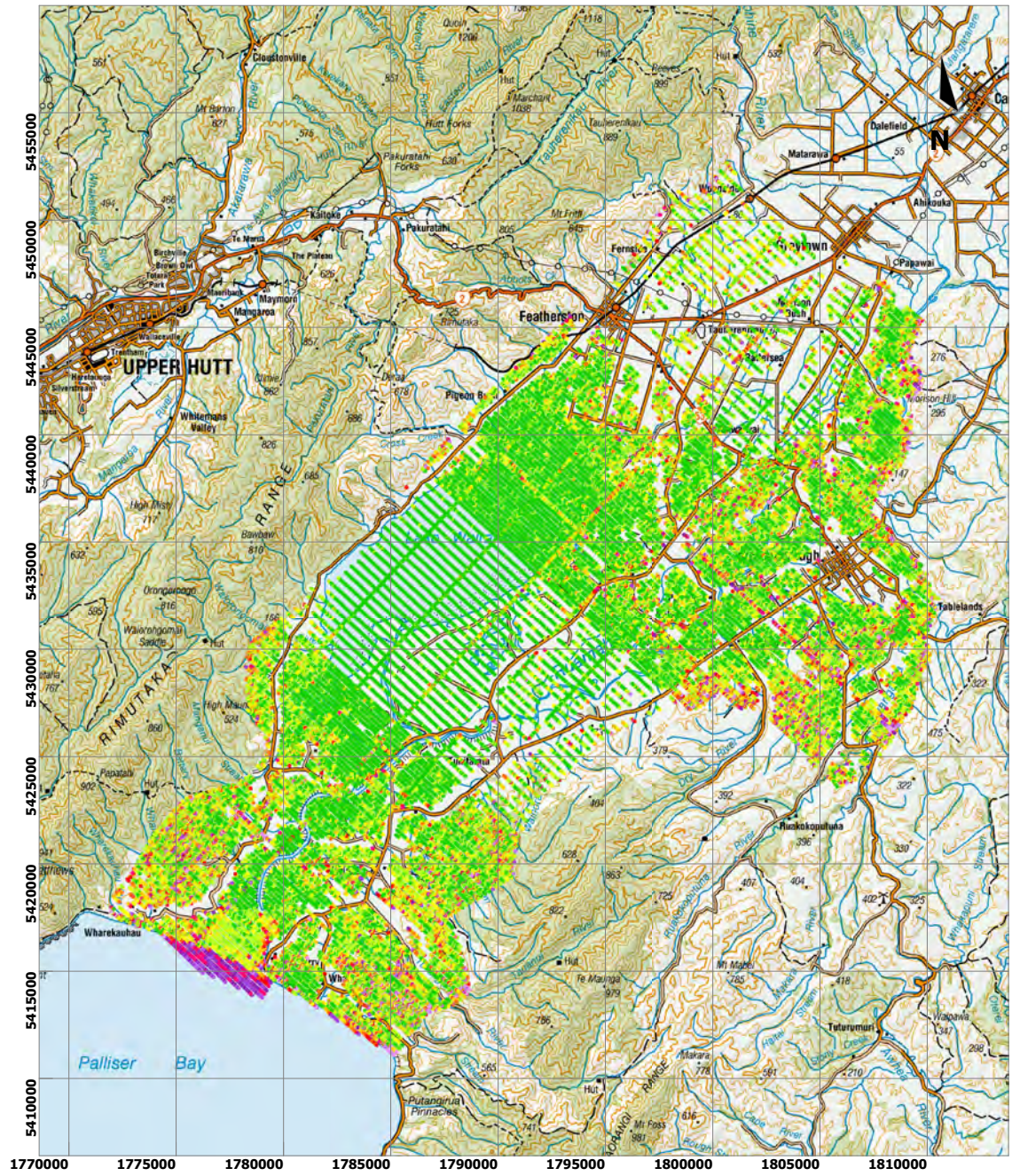

Figure A1.8 Data residual smooth North.

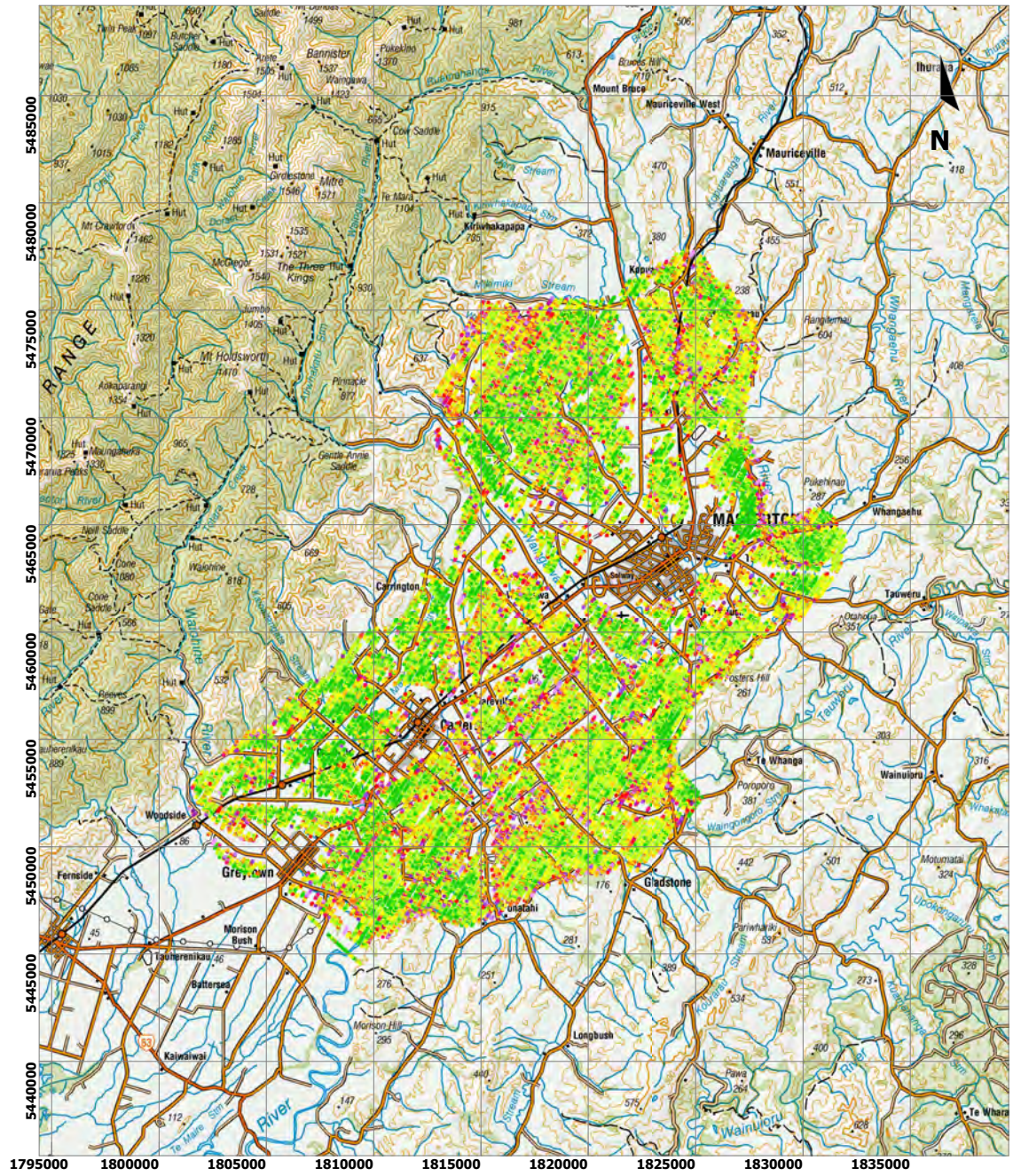

SkyTEM Survey
Ruamāhanga North

Data Residual, Smooth Inversion
Below one corresponds to a fit within one standard deviation

0.0 0.5 1.0 1.5 2.0 2.5 3.0 3.5

NZTM2000

10000

Figure A1.9 Data residual sharp South.

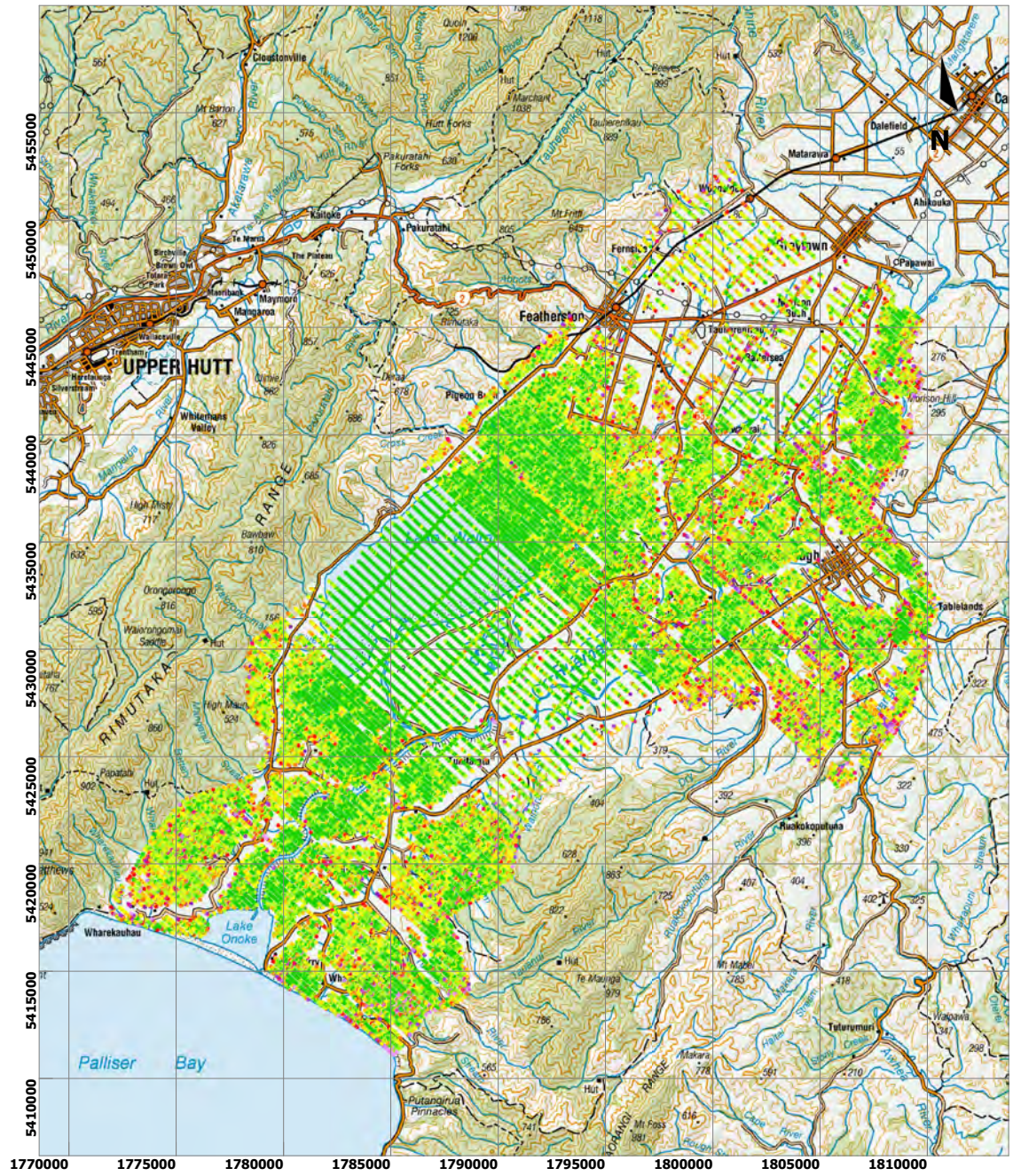

Figure A1.10 Data residual sharp North.

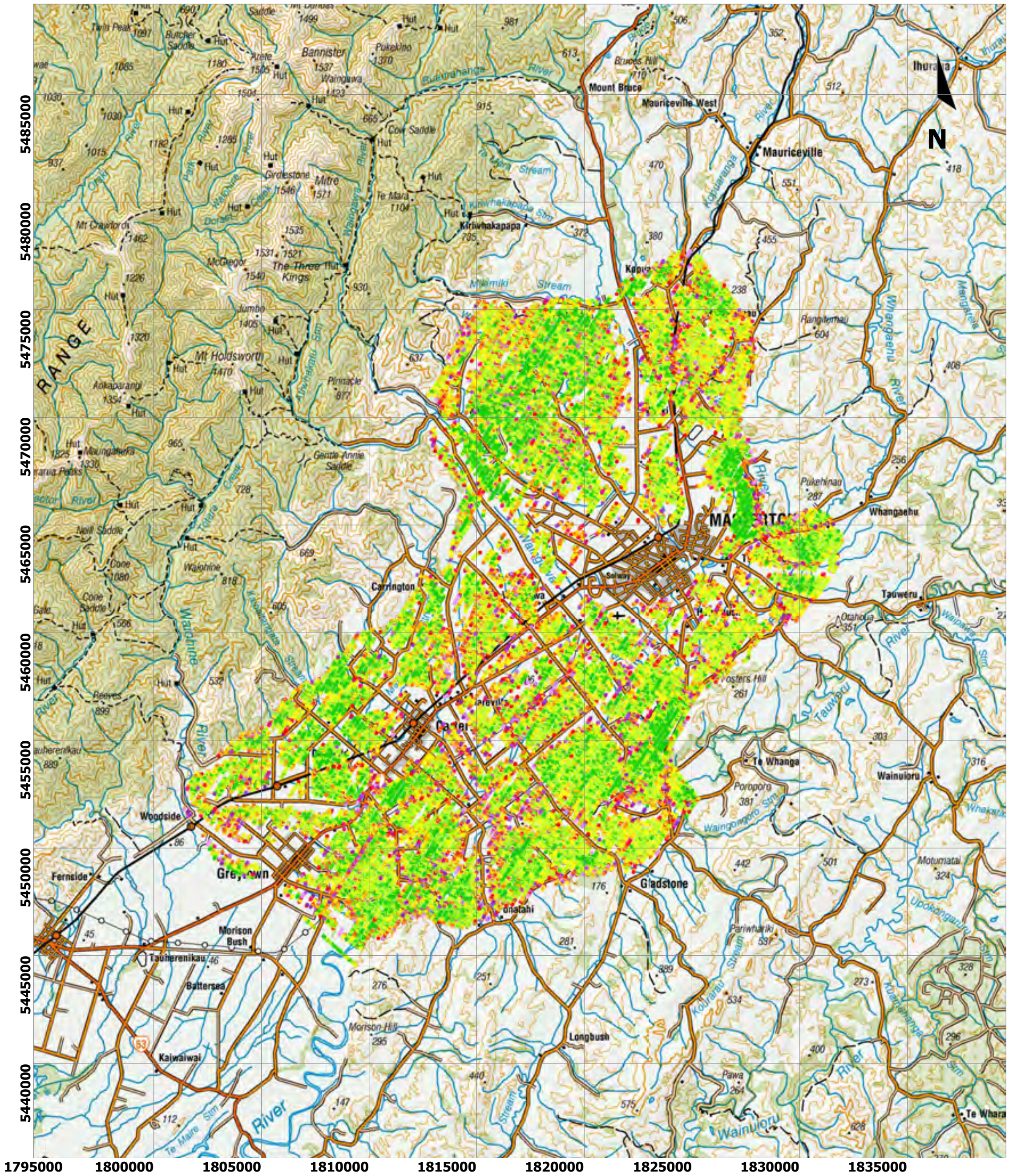

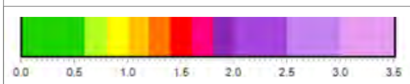

Data Residual, Sharp Inversion

Below one corresponds to a fit within one standard deviation

NZTM2000

10000

Figure A1.11 DOI Standard smooth South.

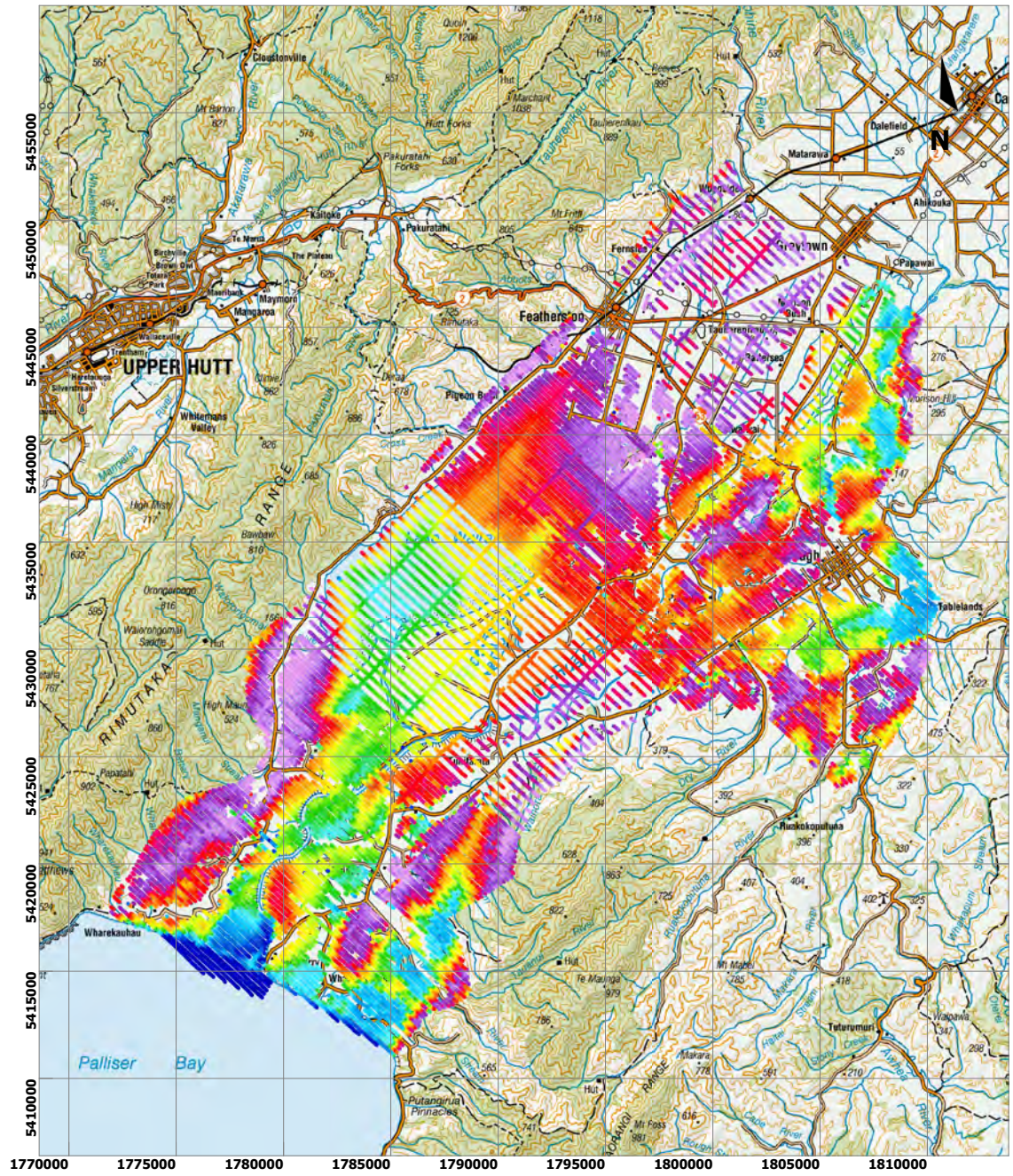

GNS SCIENCE TE PŪ AO	**SkyTEM Survey** **Ruamāhanga South**	Depth of Investigation, Smooth Inversion DOI Standard, metres
	100.0 200.0 300.0 400.0 500.0 600.0 Depth [m]	NZTM2000 10 km

Figure A1.12 DOI Standard smooth North.

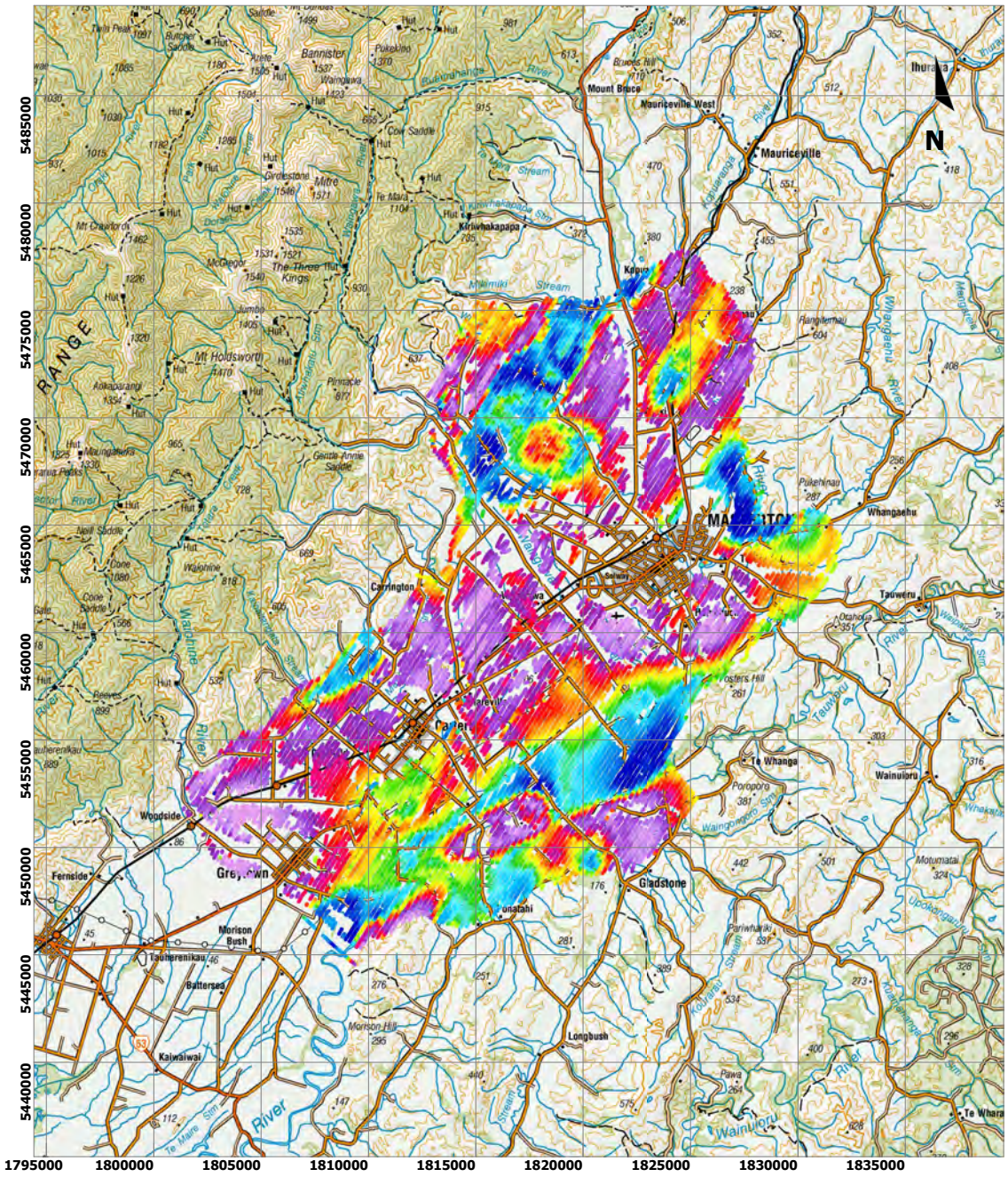

Figure A1.13 DOI Standard sharp South.

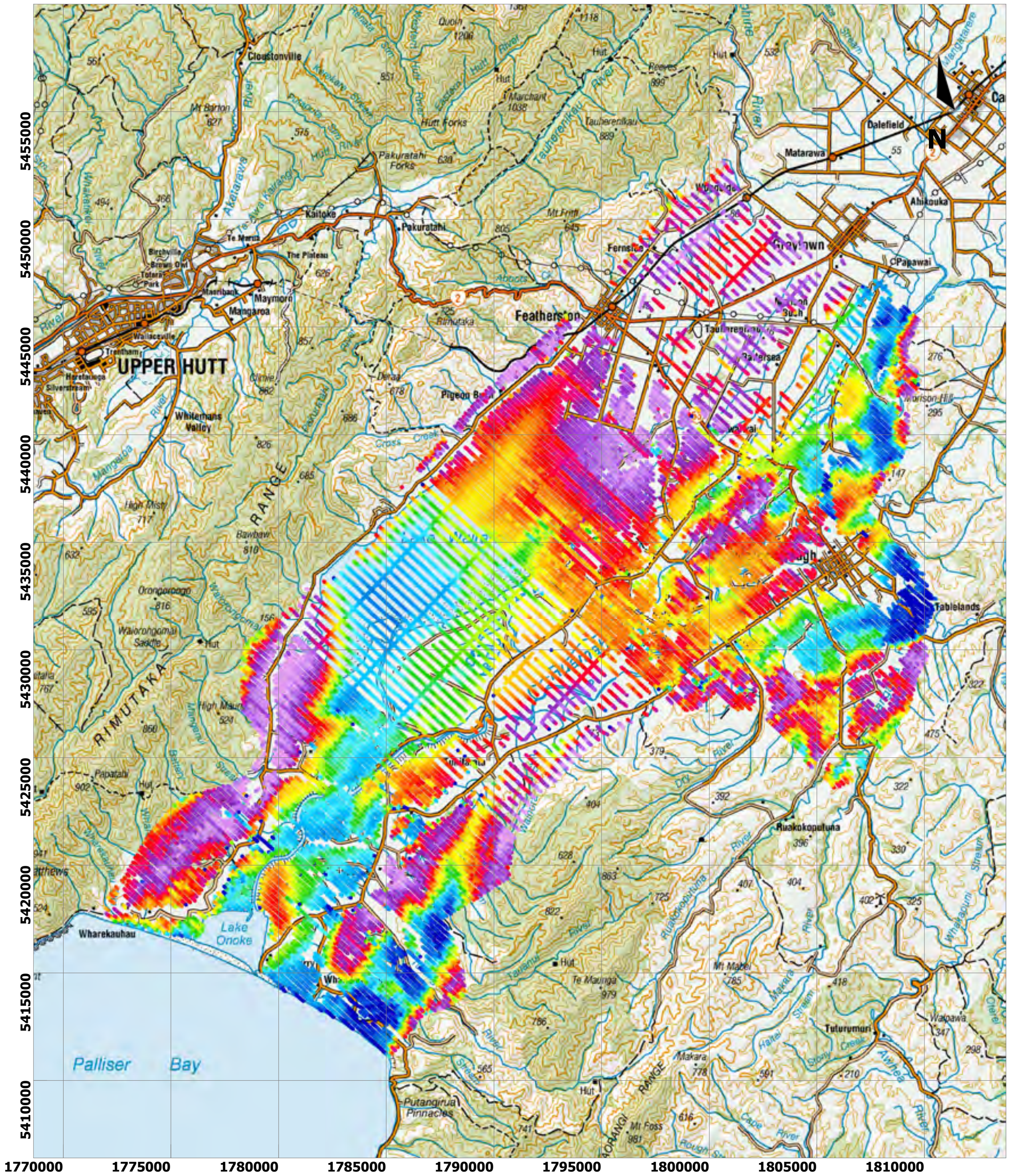

SkyTEM Survey
Ruamāhanga South

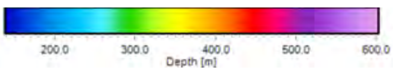

Depth of Investigation, Sharp Inversion

DOI Standard, metres

NZTM2000

10 km

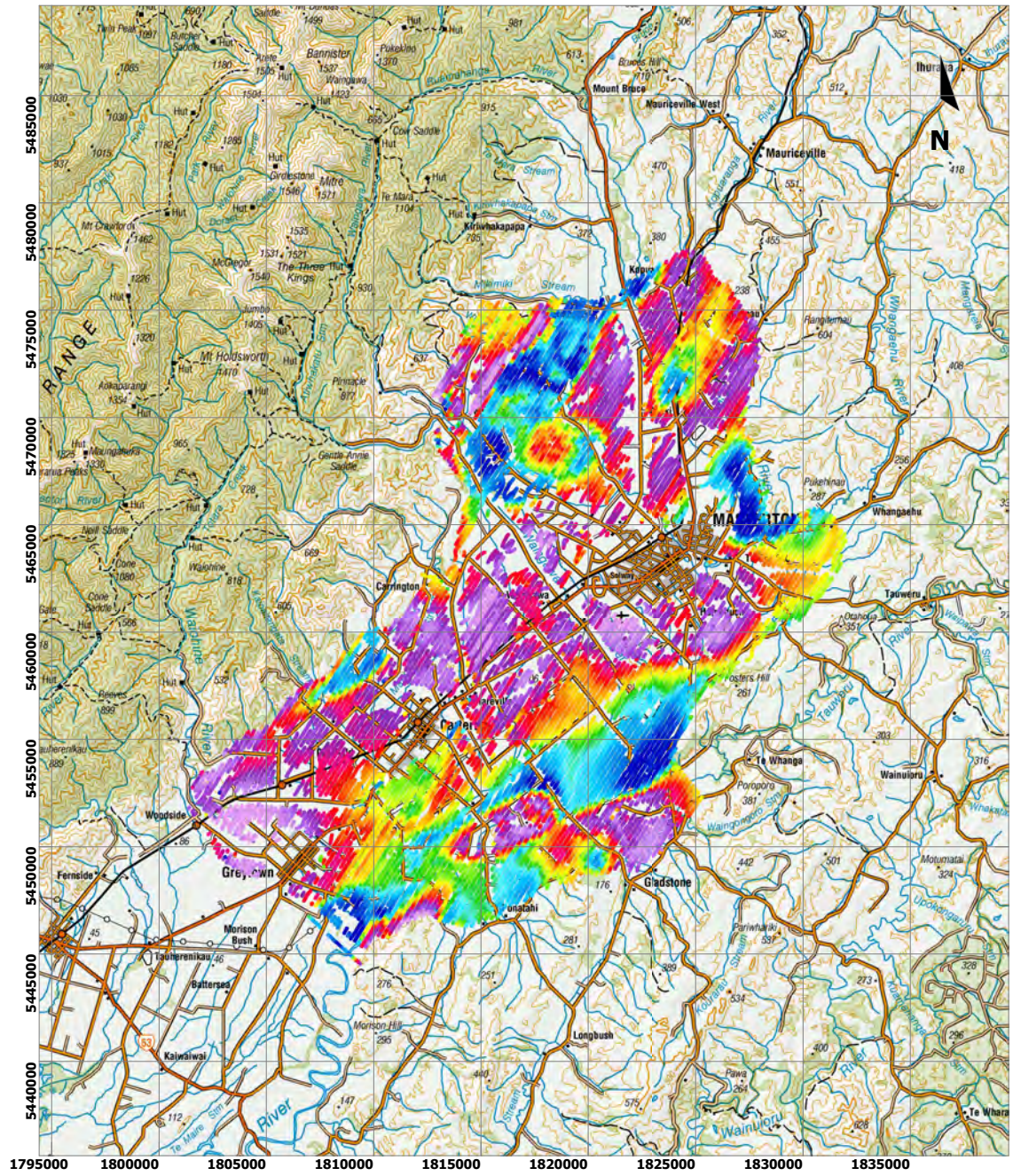

Figure A1.14 DOI Standard sharp North.

SkyTEM Survey
Ruamāhanga North

Depth of Investigation, Sharp Inversion

DOI Standard, metres

NZTM2000

10000

Figure A1.15 Altitude Difference South smooth.

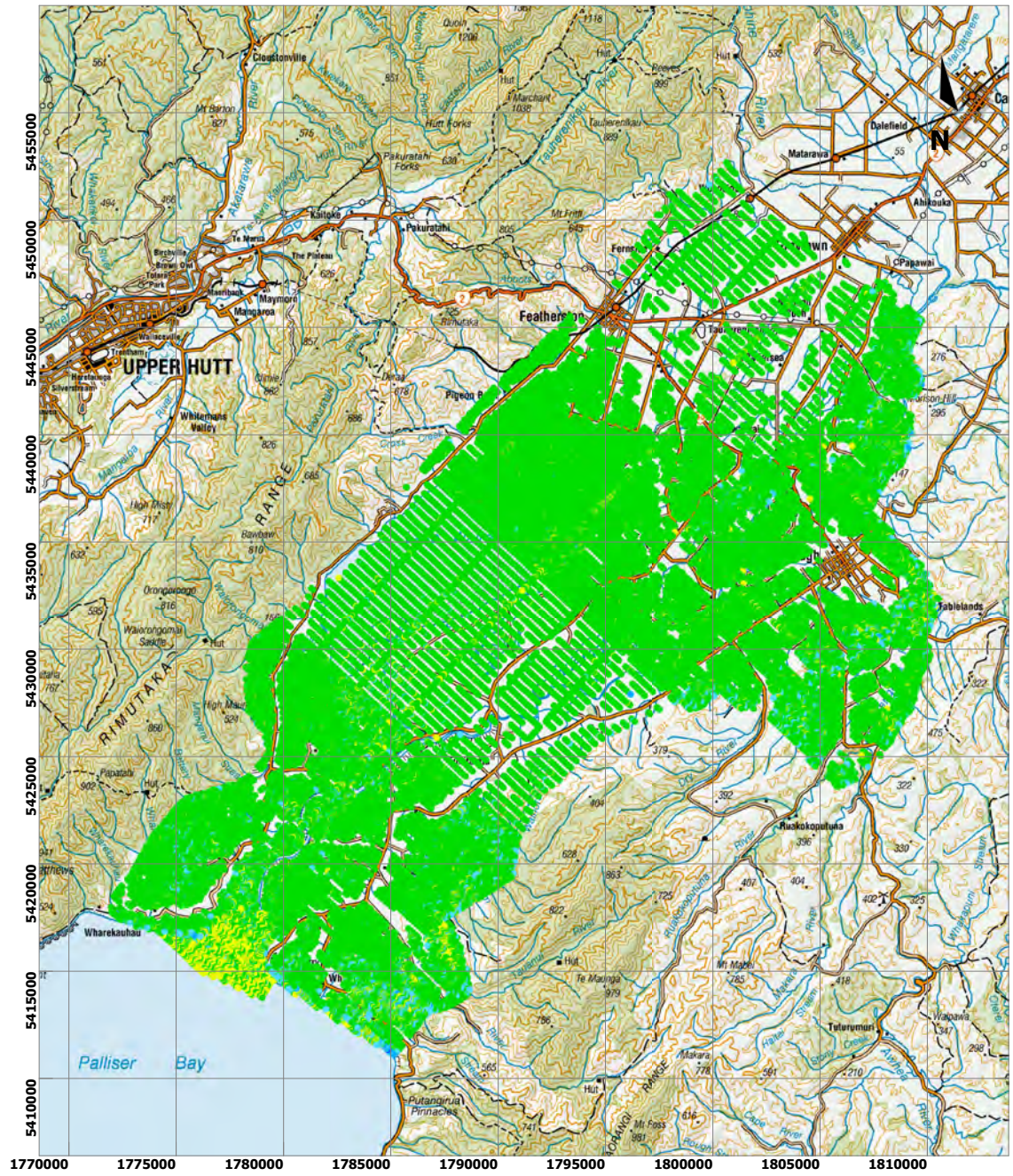

SkyTEM Survey
Ruamāhanga South

Modelled altitude difference, smooth inversion
Elevation difference from prior altitude, metres

-15.0 -10.0 -5.0 -2.5 -0.5 2.5 5.0 10.0 15.0
Altitude [m]

NZTM2000
10 km

Figure A1.16 Altitude Difference South sharp.

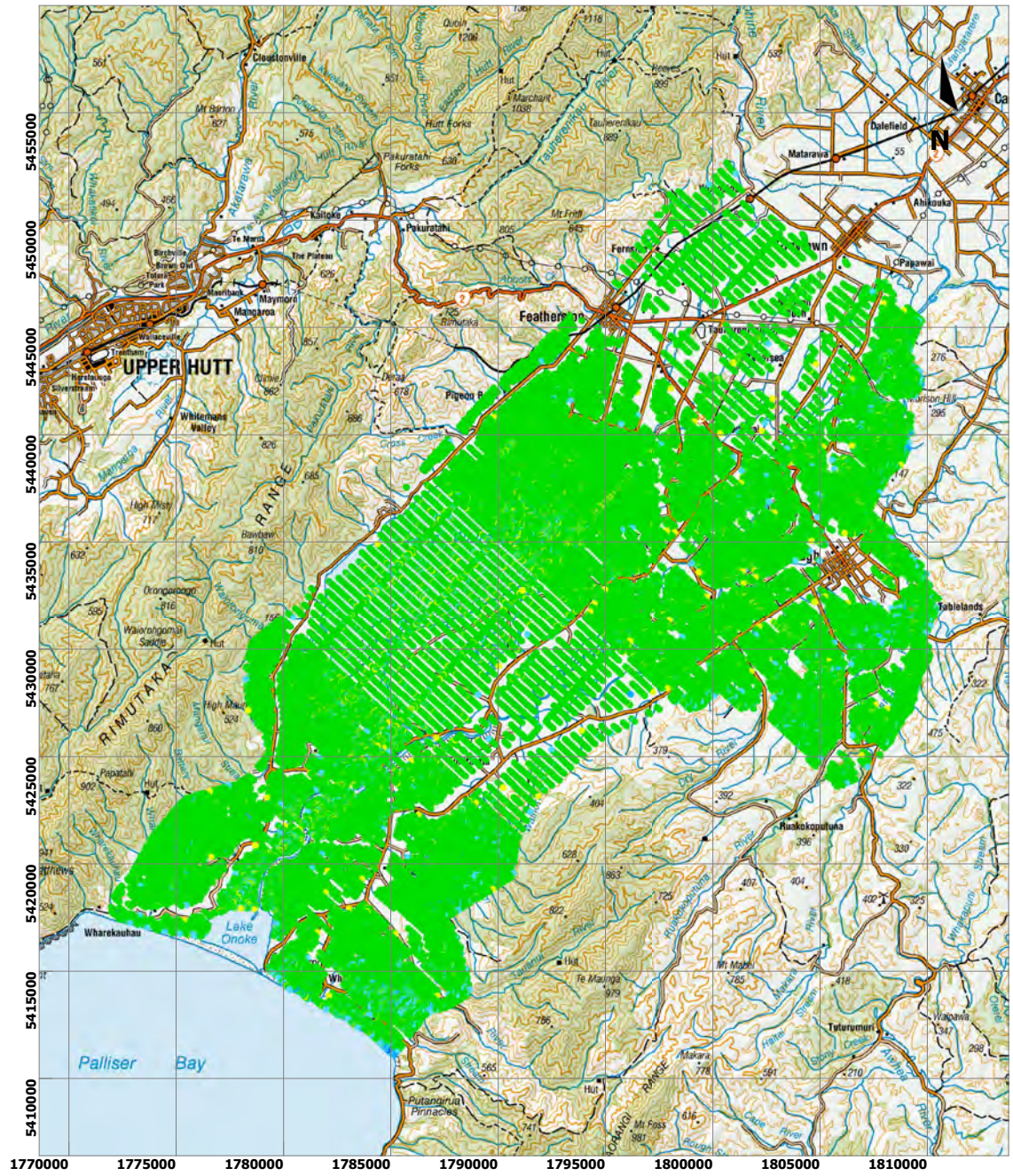

GNS SCIENCE TE PŪ AO	**SkyTEM Survey** **Ruamāhanga South**	Modelled altitude difference, sharp inversion Elevation difference from prior altitude, metres
		NZTM2000 10 km

Figure A1.17 Altitude Difference North smooth.

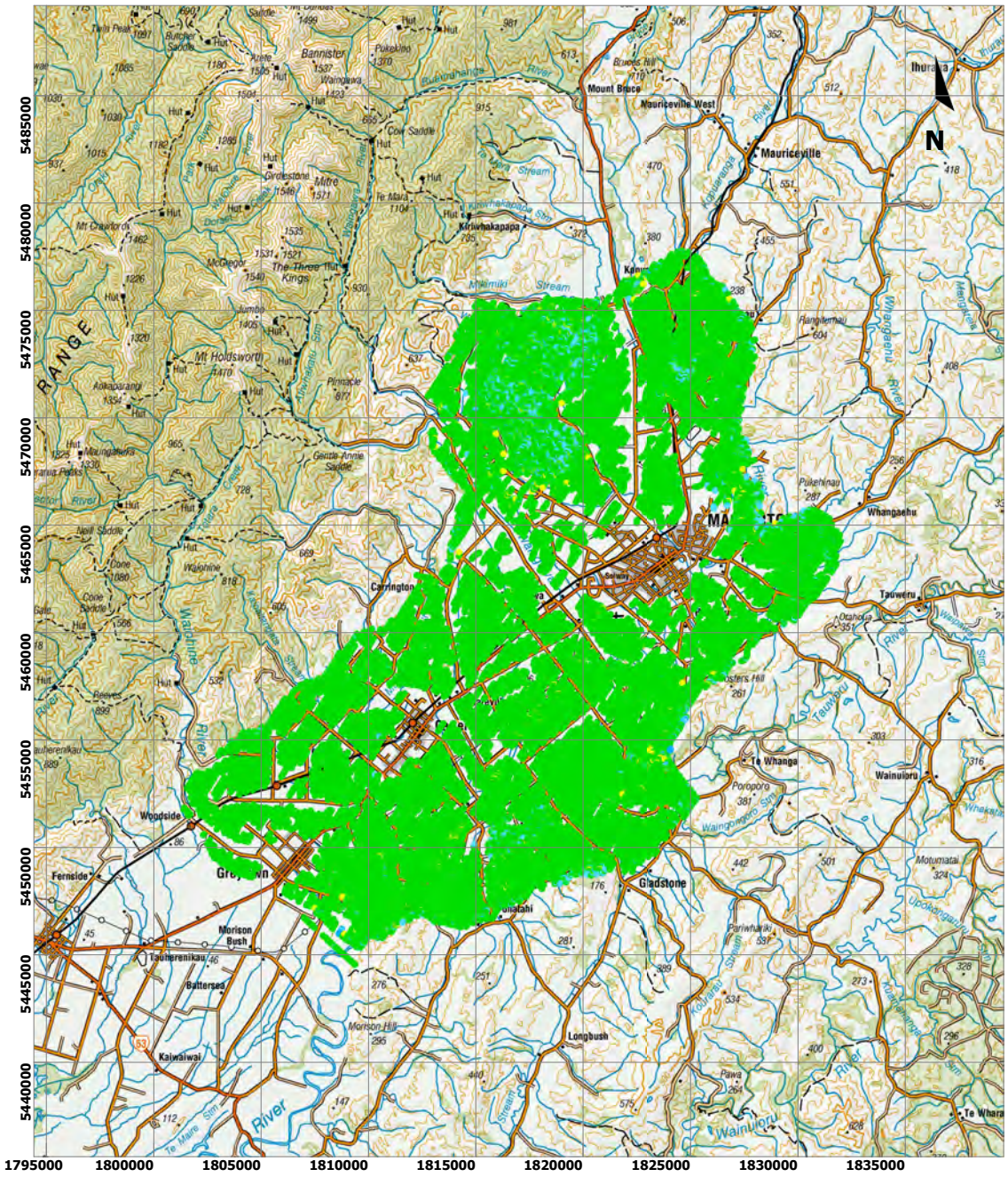

SkyTEM Survey
Ruamāhanga North

Modelled flight altitude difference, smooth
Elevation difference from prior altitude, metres

-15.0 -10.0 -5.0 -2.5 -0.5 0.5 2.5 5.0 10.0 15.0
Altitude [m]

NZTM2000
10000

Figure A1.18 Altitude Difference North sharp.

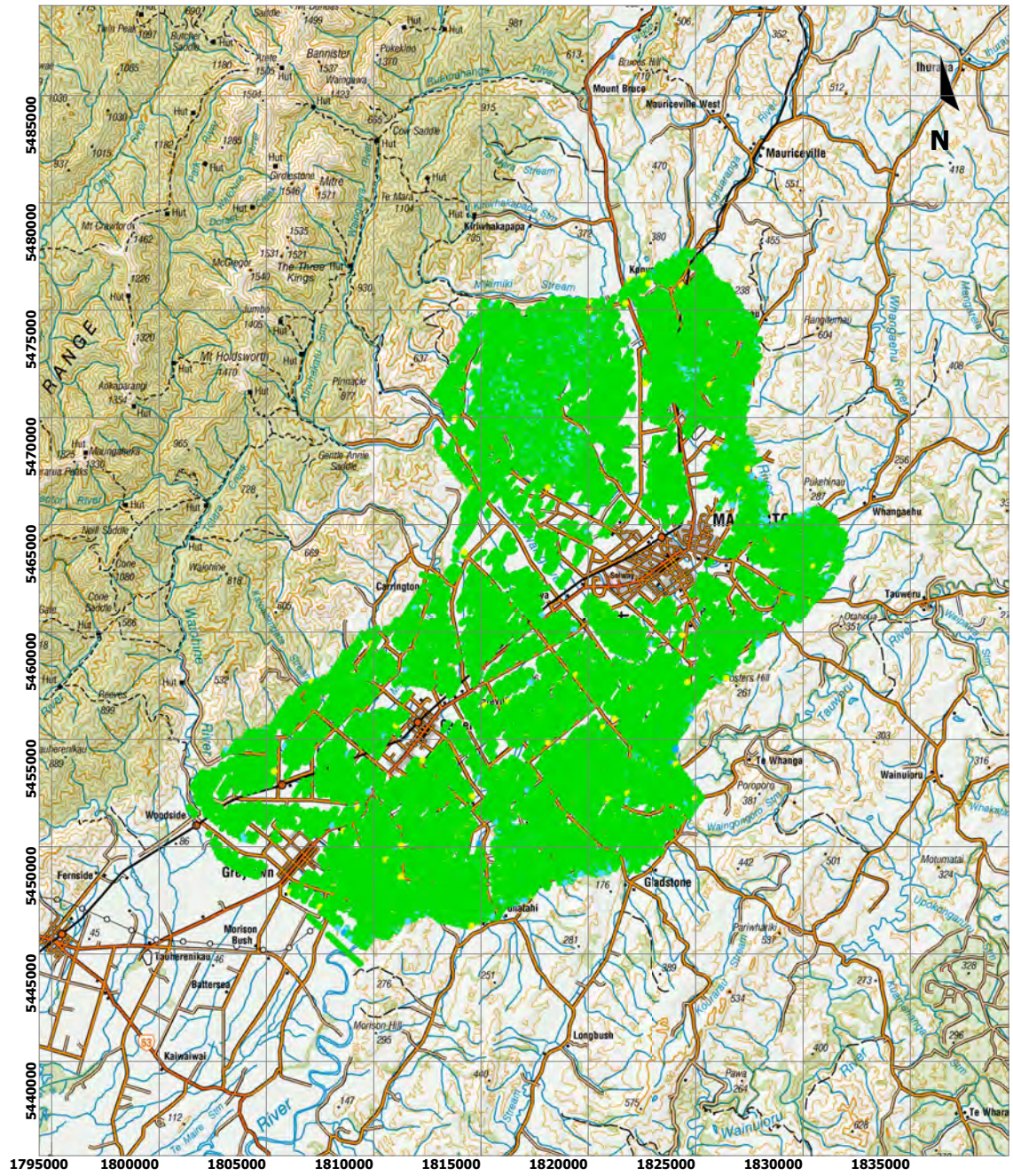

APPENDIX 2 CROSS-SECTIONS

Selected cross-sections for the smooth inversion are included. Each section shows the 1D models blanked at the depth of investigation standard value.

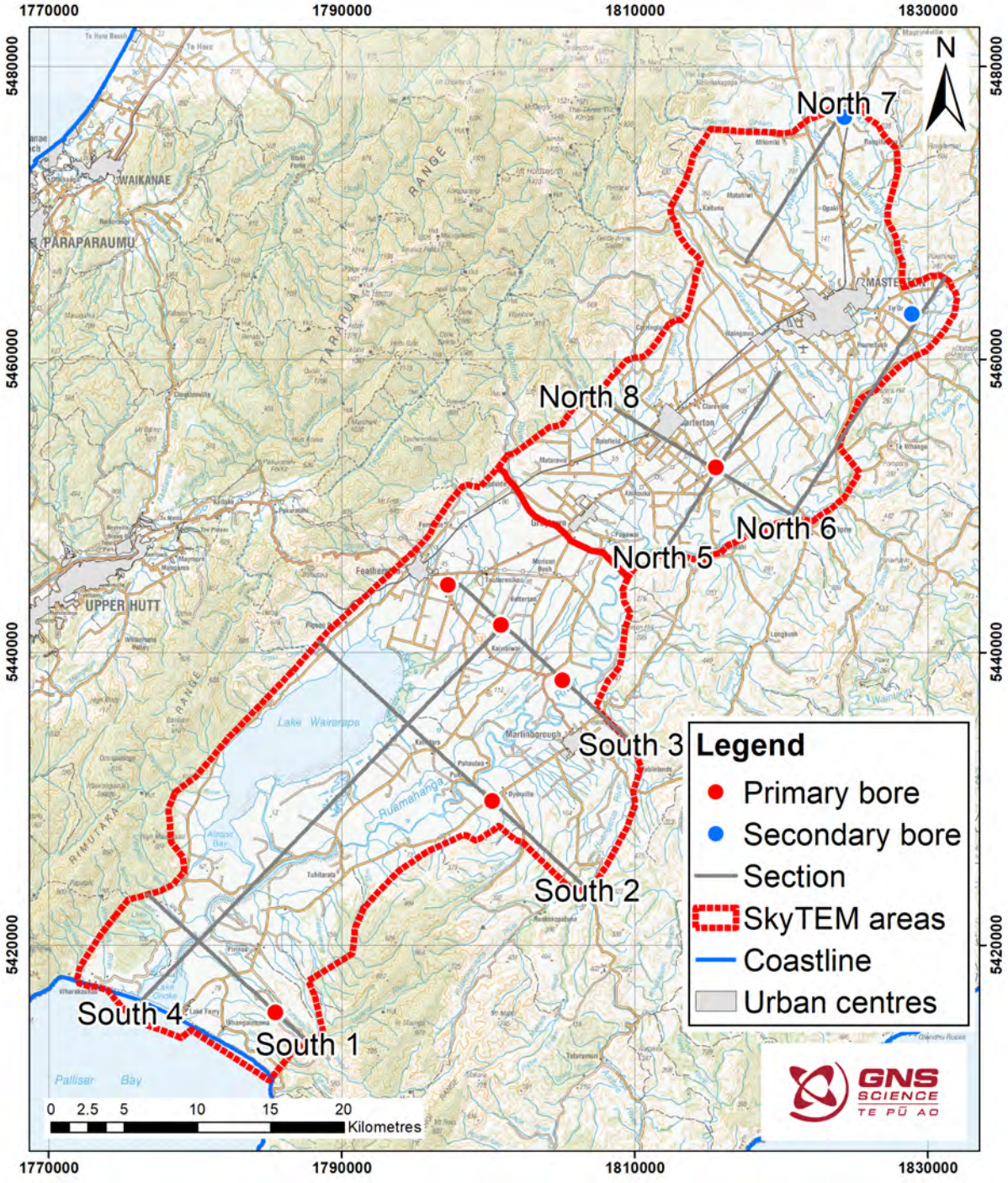

Figure A2.1 Map showing locations of the eight cross-sections used to illustrate the resistivity models. The boreholes shown are from primary and secondary sets and are used on the sections to illustrate the correlation of the geophysical data with lithology.

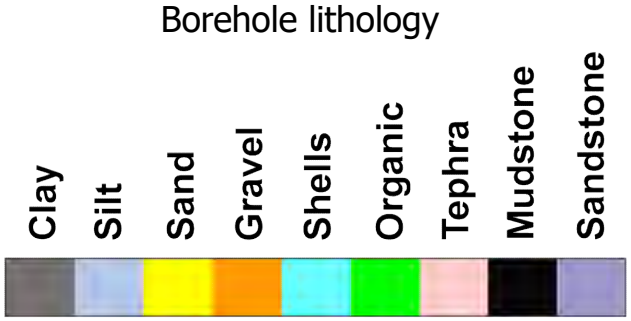

(West to East)

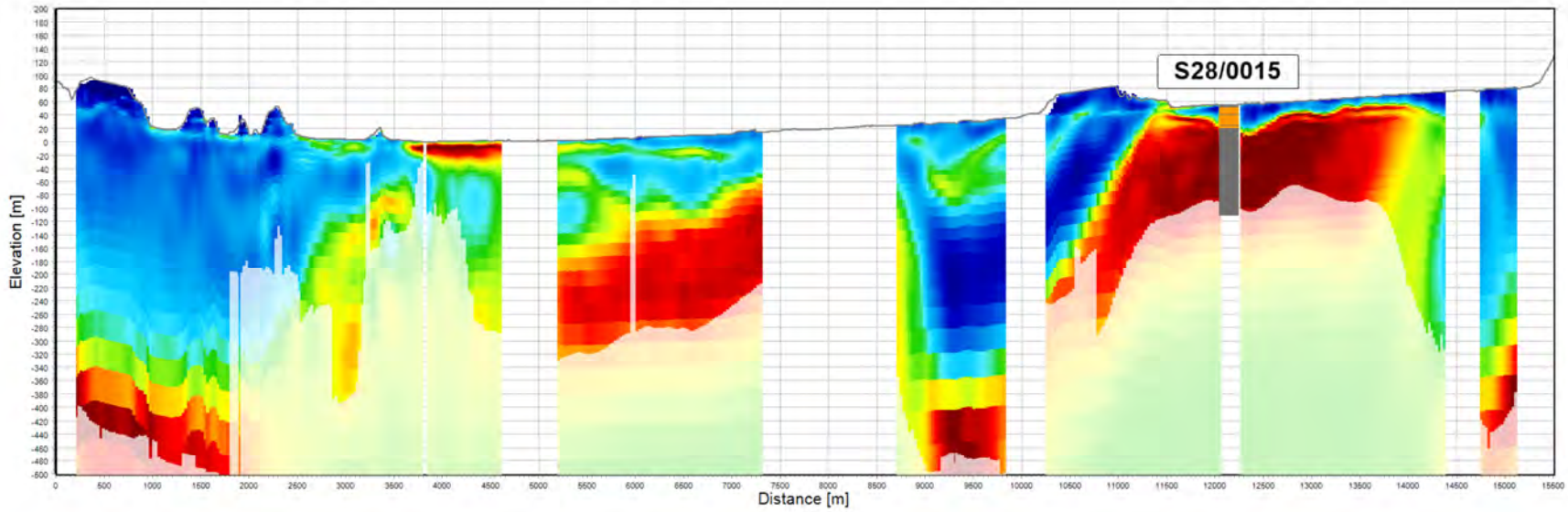

Figure A2.2 Section South_1

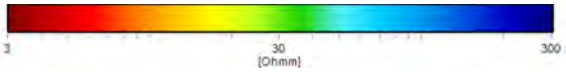

Resistivity profiles (ohm.m)
SCI smooth model

Models have been blanked by 75% below the DOI Standard.

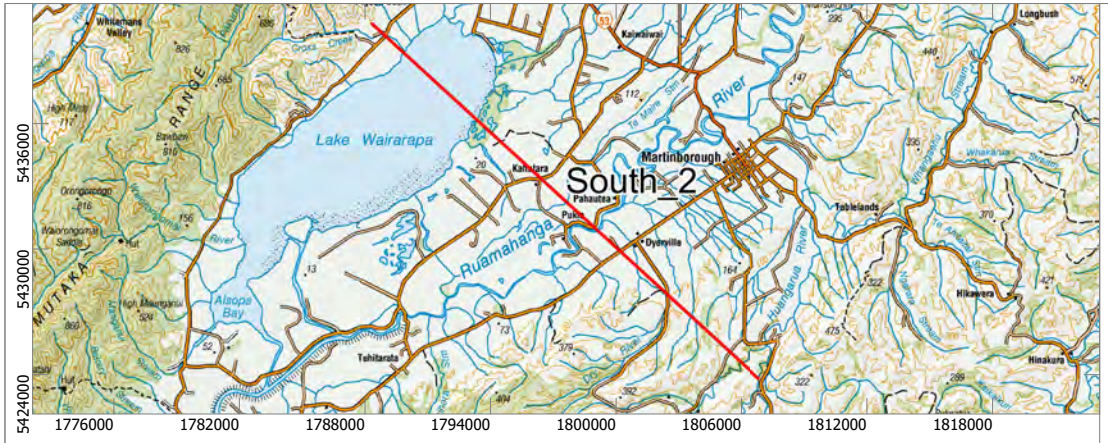

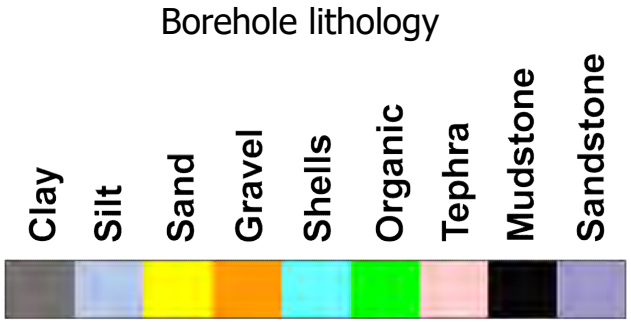

(West to East)

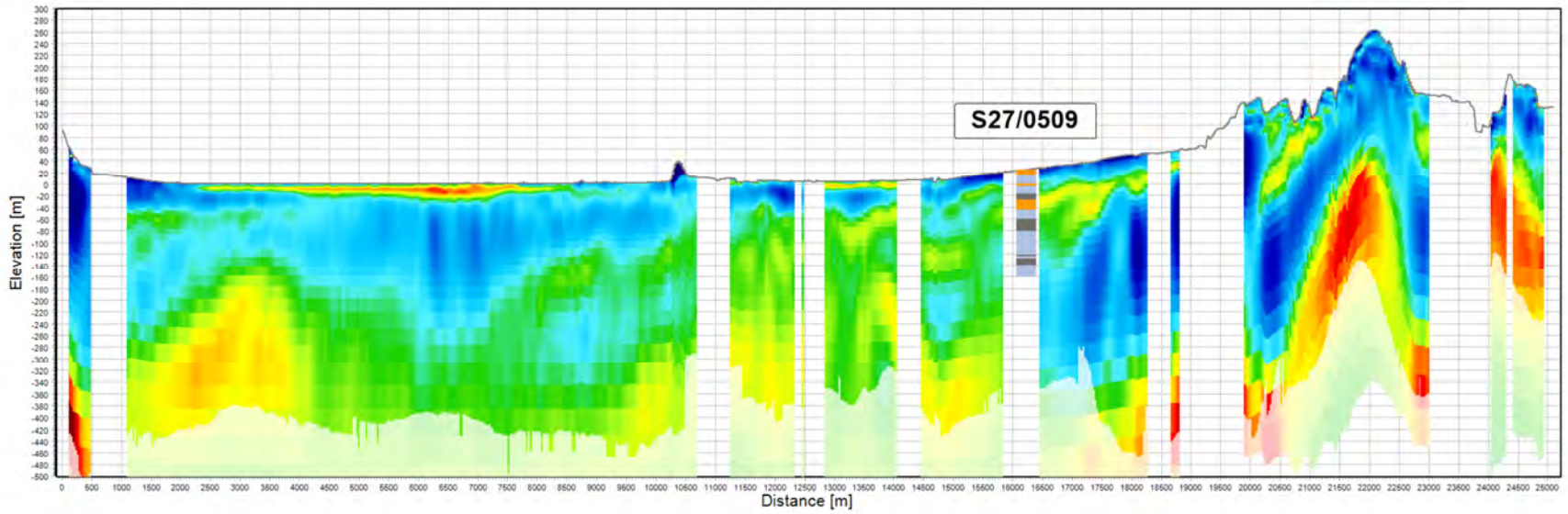

Figure A2.3 Section South_2

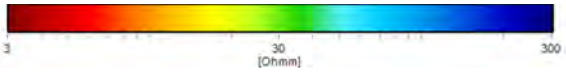

Resistivity profiles (ohm.m)
SCI smooth model

Models have been blanked by 75% below the DOI Standard.

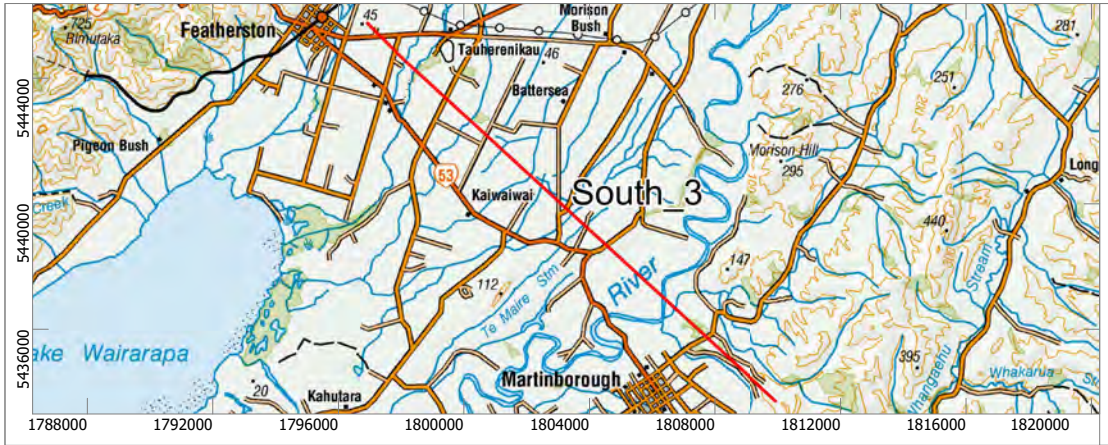

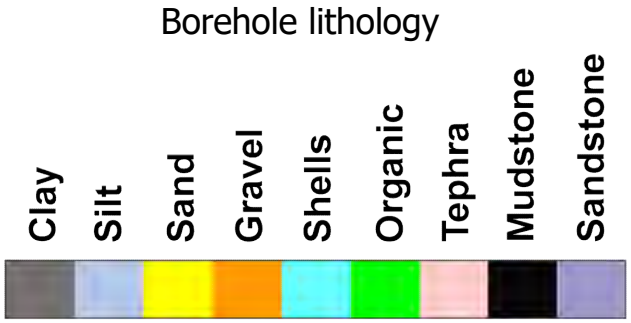

(West to East)

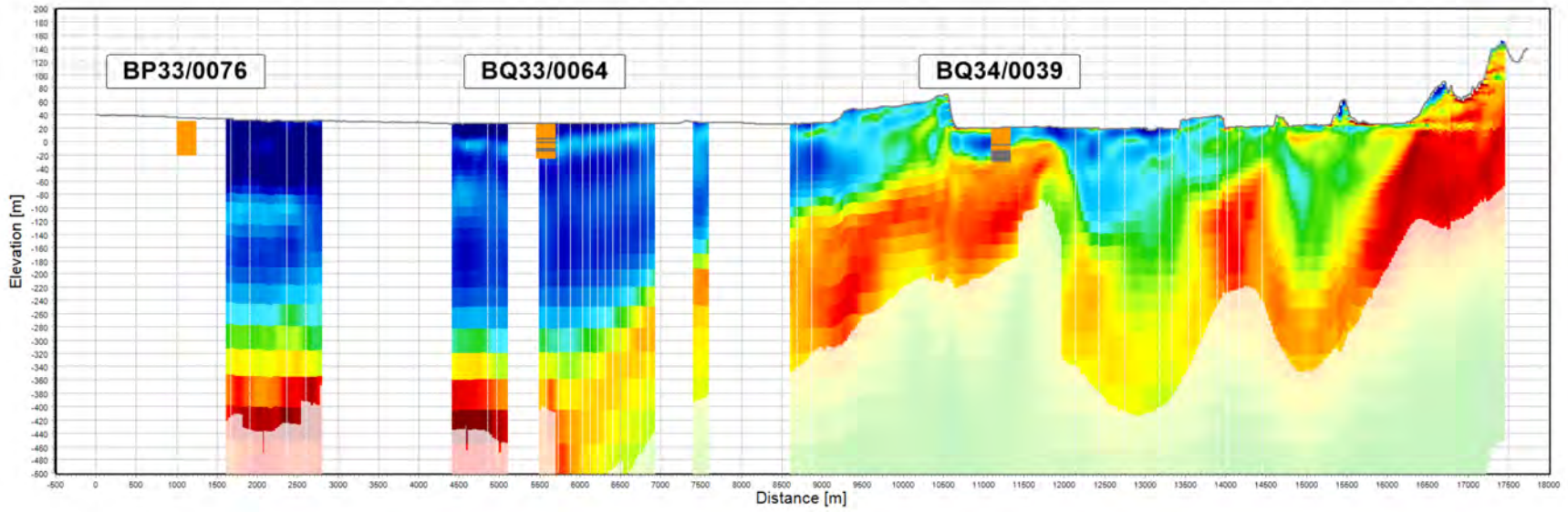

Figure A2.4 Section South_3

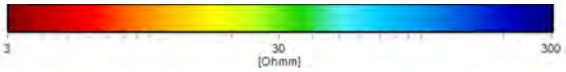

Resistivity profiles (ohm.m)
SCI smooth model

Models have been blanked by 75% below the DOI Standard.

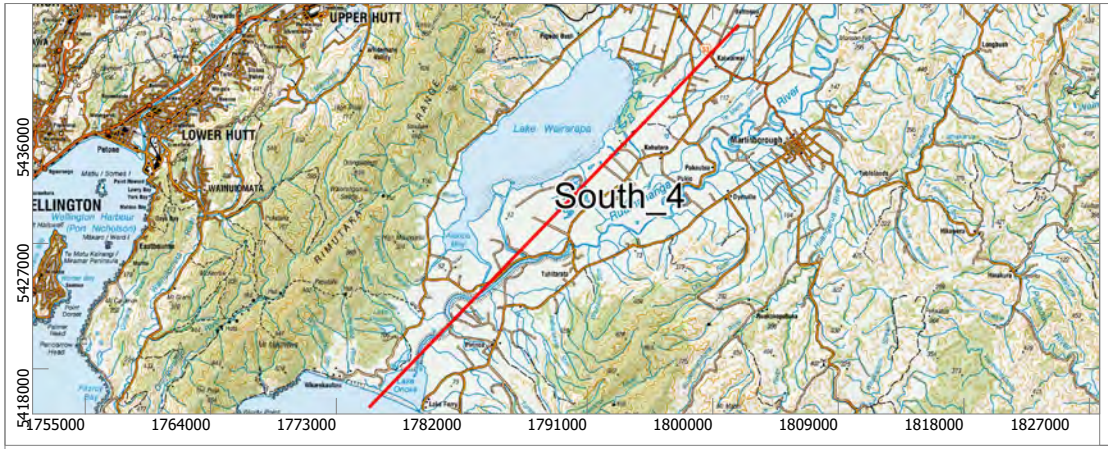

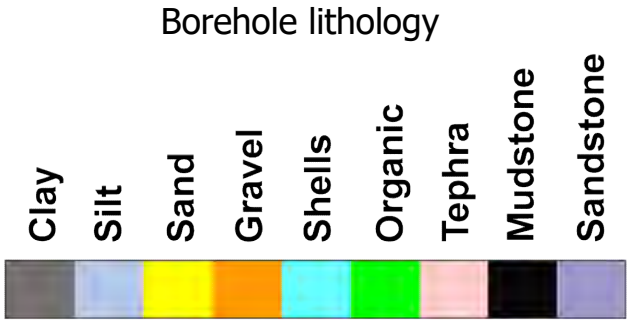

(South to North)

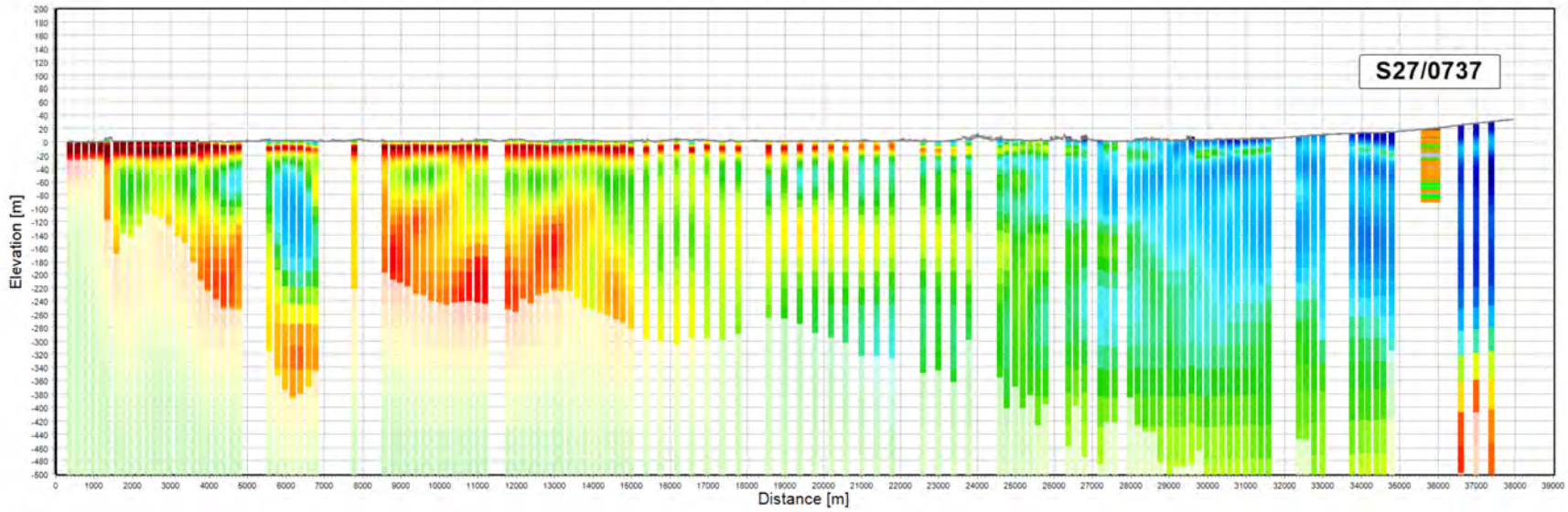

Figure A2.5 Section South_4

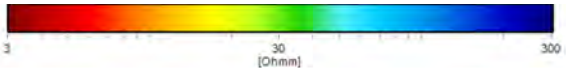

Resistivity profiles (ohm.m)
SCI smooth model

Models have been blanked by 75% below the DOI Standard.

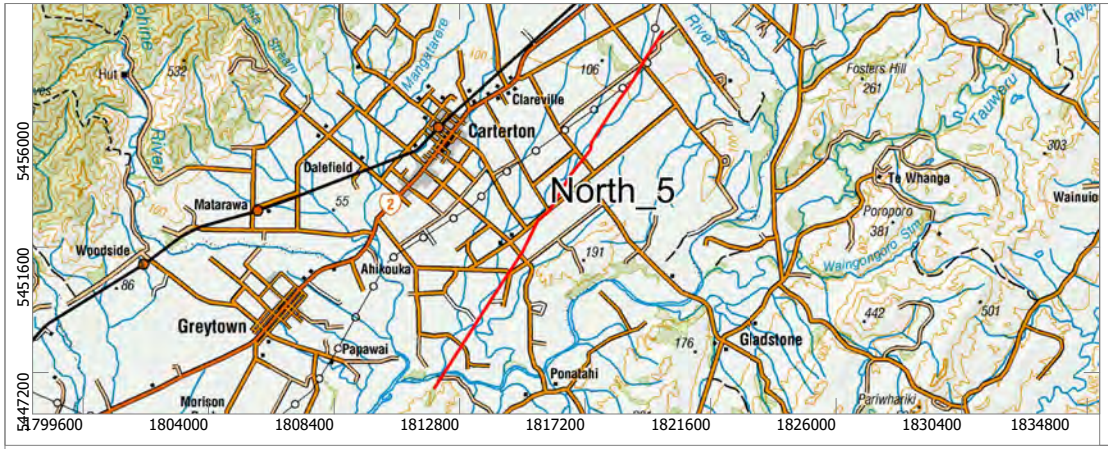

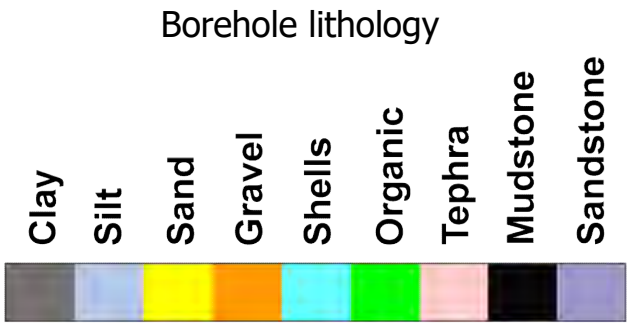

(South to North)

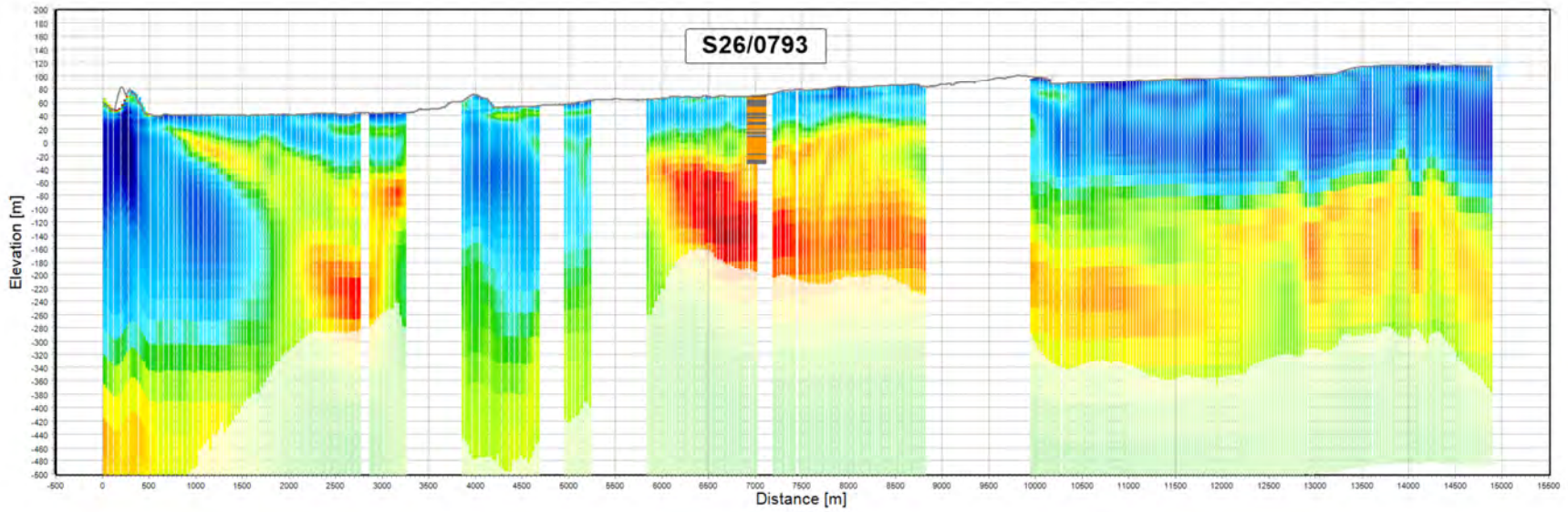

Figure A2.6 Section North_5

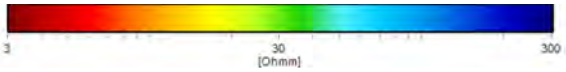

Resistivity profiles (ohm.m)
SCI smooth model

Models have been blanked by 75% below the DOI Standard.

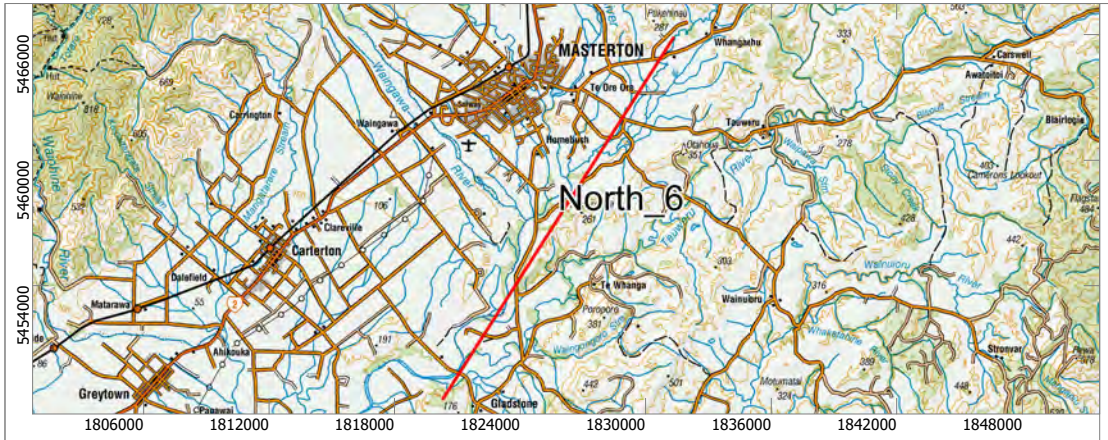

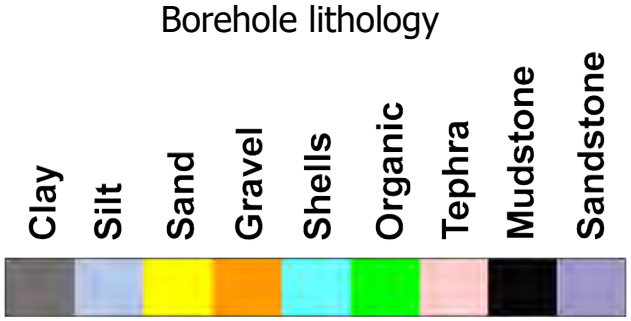

(South to North)

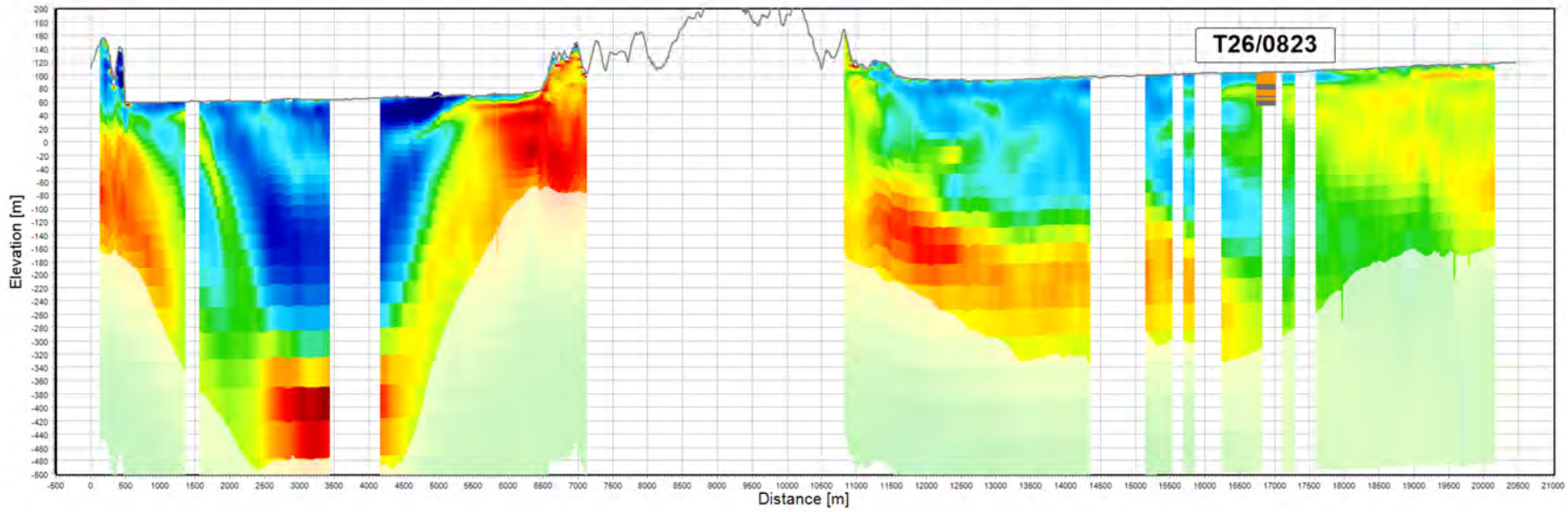

Figure A2.7 Section North_6

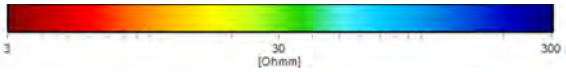

Resistivity profiles (ohm.m)
SCI smooth model

Models have been blanked by 75% below the DOI Standard.

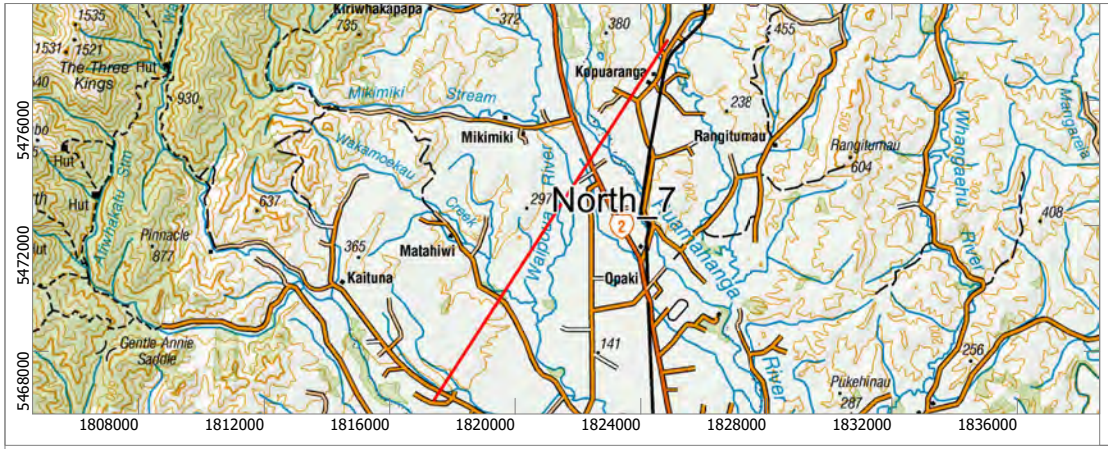

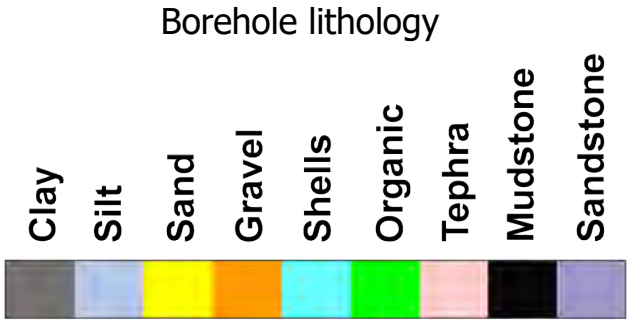

(South to North)

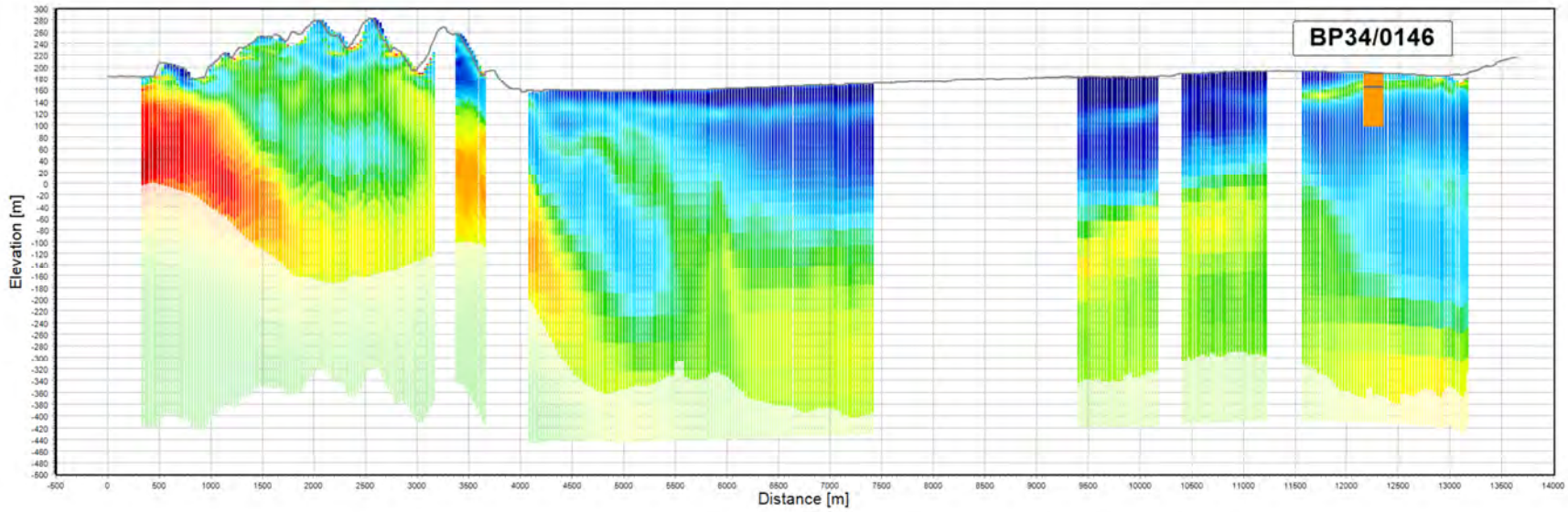

Figure A2.8 Section North_7

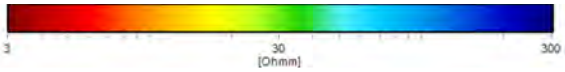

Resistivity profiles (ohm.m)
SCI smooth model

Models have been blanked by 75% below the DOI Standard.

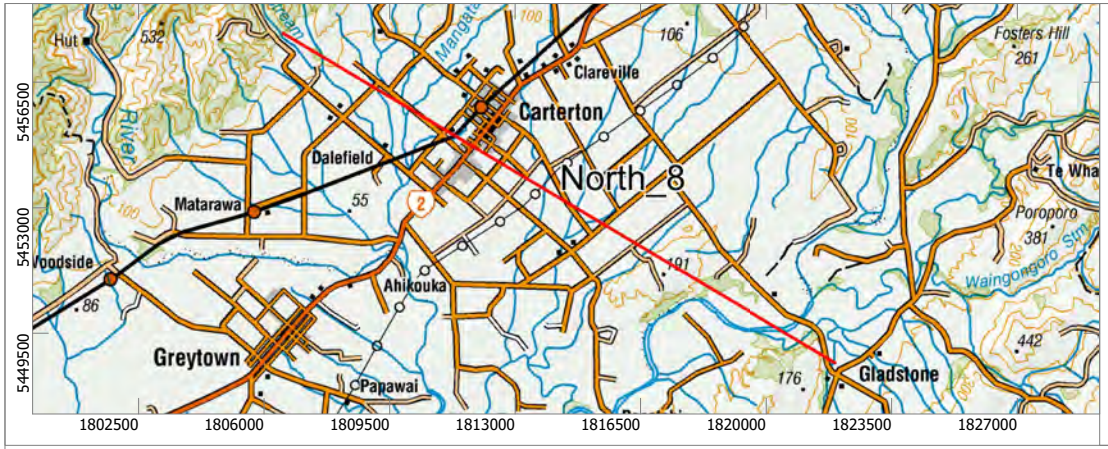

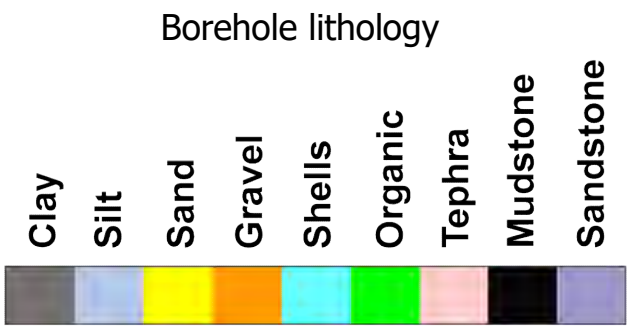

(West to East)

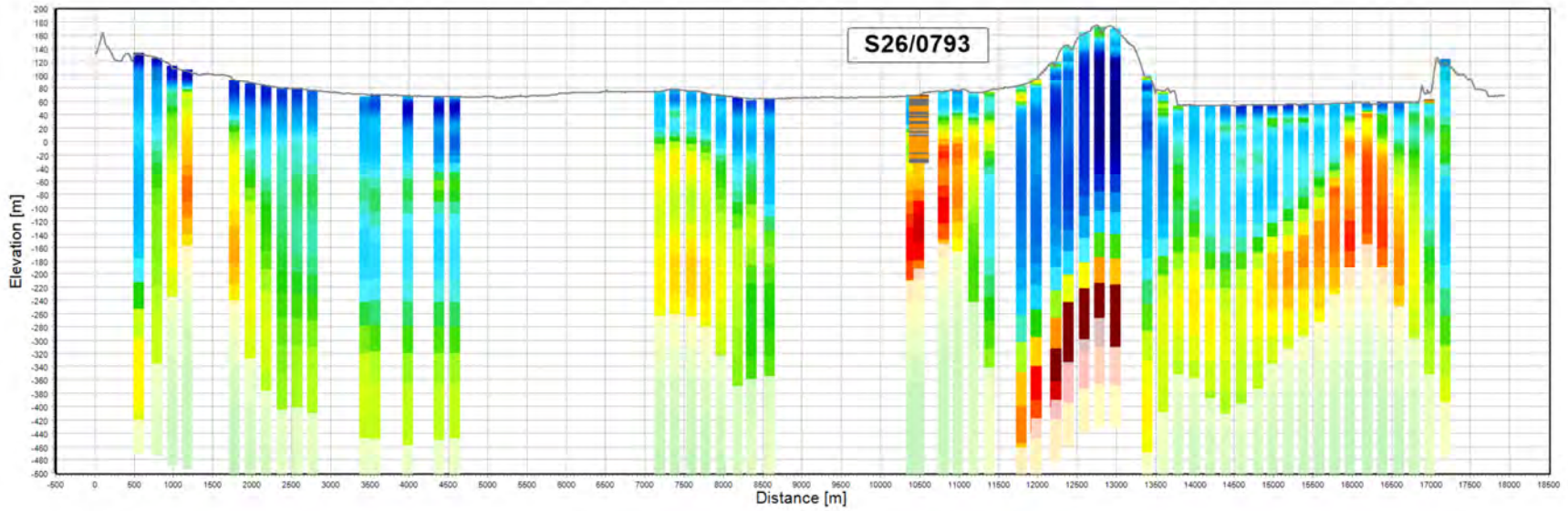

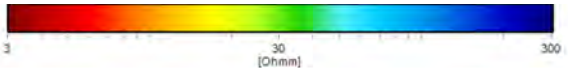

Figure A2.9 Section North_8

Resistivity profiles (ohm.m)
SCI smooth model

Models have been blanked by 75% below the DOI Standard.

APPENDIX 3 MEAN RESISTIVITY MAPS

This appendix includes mean resistivity maps generated from the smooth-model inversion set at depths below ground surface. Four representative depths are shown:

- Figure A3.1: Mean resistivity map smooth model depth 4–6 m (South).
- Figure A3.2: Mean resistivity map smooth model depth 4–6 m (North).
- Figure A3.3: Mean resistivity map smooth model depth 20–23 m (South).
- Figure A3.4: Mean resistivity map smooth model depth 20–23 m (North).
- Figure A3.5: Mean resistivity map smooth model depth 60–68 m (South).
- Figure A3.6: Mean resistivity map smooth model depth 60–68 m (North).
- Figure A3.7: Mean resistivity map smooth model depth 139–156 m (South).
- Figure A3.8: Mean resistivity map smooth model depth 139–156 m (North).

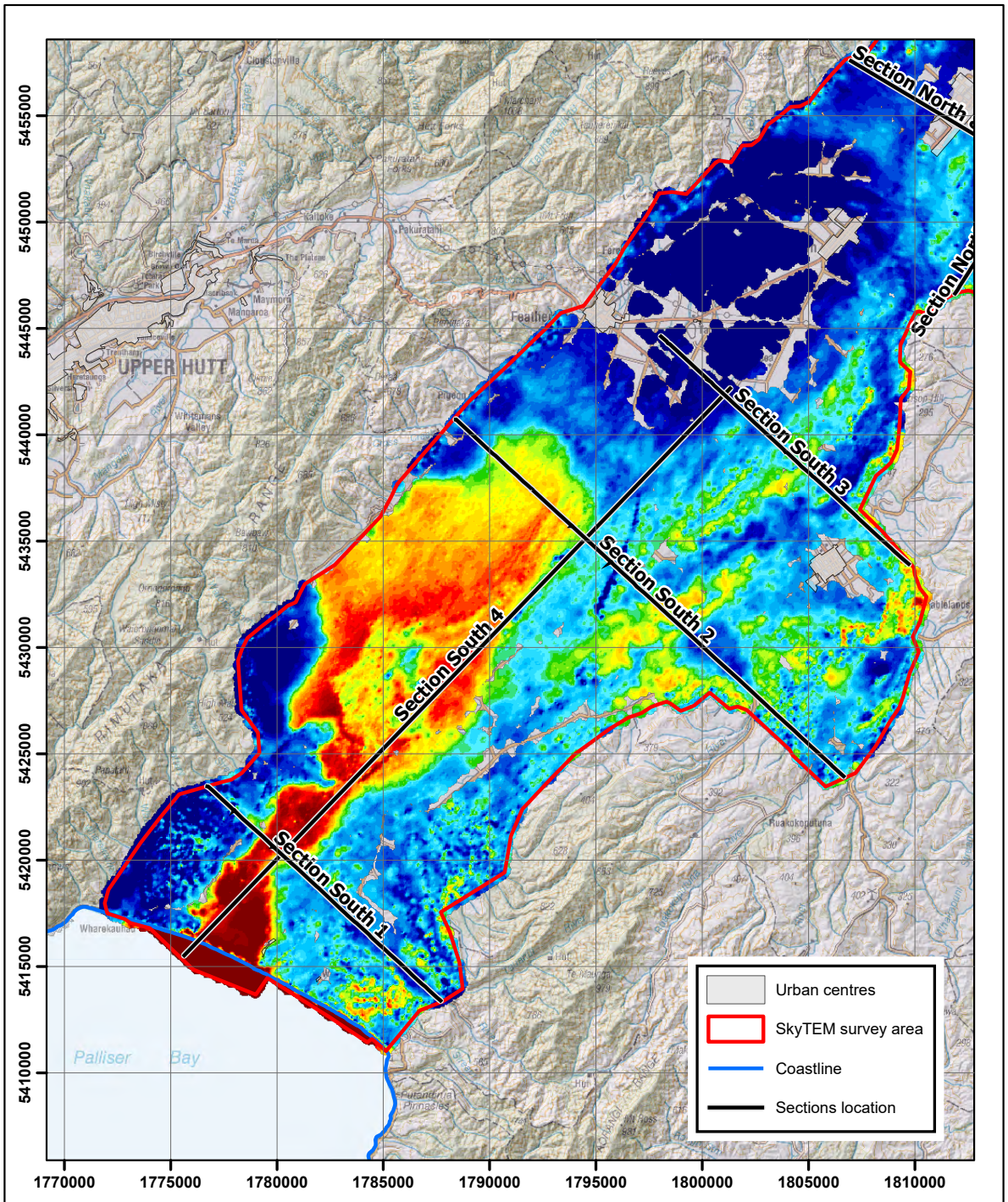

SkyTEM Survey Ruamāhanga South
Mean resistivity map, smooth model at depth 4 - 6 m

Appendix 3

Map No. 1

GNS SCIENCE TE PŪ AO

Mean resistivity (ohm.m)

< 3.5	15.5 - 18.3	80.5 - 95.0
3.5 - 4.2	18.3 - 21.6	95.0 - 112
4.2 - 4.9	21.6 - 25.5	112 - 132
4.9 - 5.8	25.5 - 30.0	132 - 155
5.8 - 6.8	30.0 - 35.4	155 - 183
6.8 - 8.1	35.4 - 41.7	183 - 216
8.1 - 9.5	41.7 - 49.1	216 - 255
9.5 - 11.2	49.1 - 57.9	> 255
11.2 - 13.2	57.9 - 68.3	
13.2 - 15.5	68.3 - 80.5	

N

NZTM2000

0 2.5 5 Km

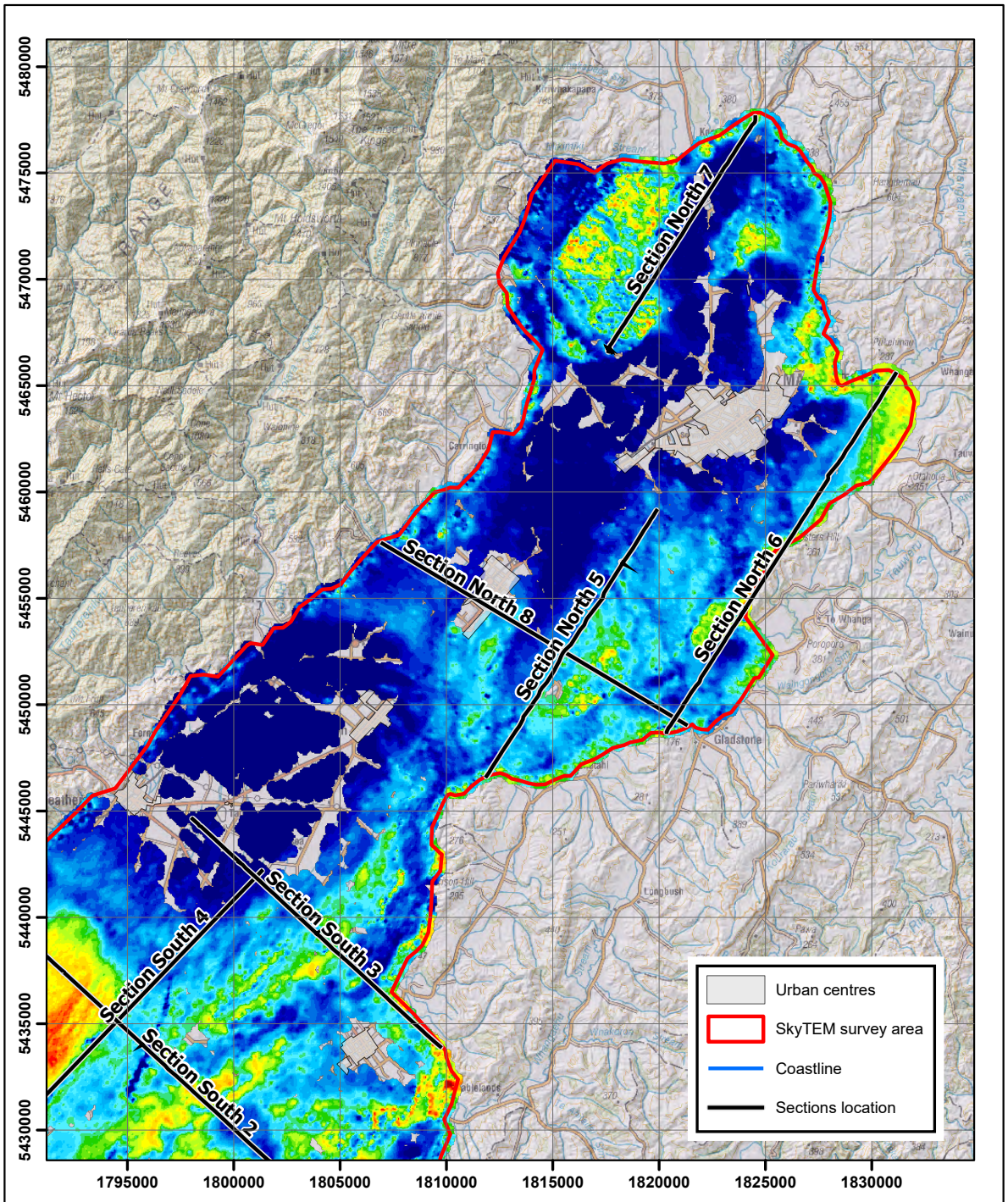

SkyTEM Survey Ruamāhanga North
Mean resistivity map, smooth model at depth 4 - 6 m

Appendix 3

Map No. 2

GNS SCIENCE TE PŪ AO

Mean resistivity (ohm.m)

< 3.5	15.5 - 18.3	80.5 - 95.0
3.5 - 4.2	18.3 - 21.6	95.0 - 112
4.2 - 4.9	21.6 - 25.5	112 - 132
4.9 - 5.8	25.5 - 30.0	132 - 155
5.8 - 6.8	30.0 - 35.4	155 - 183
6.8 - 8.1	35.4 - 41.7	183 - 216
8.1 - 9.5	41.7 - 49.1	216 - 255
9.5 - 11.2	49.1 - 57.9	> 255
11.2 - 13.2	57.9 - 68.3	
13.2 - 15.5	68.3 - 80.5	

N

NZTM2000

0 2.5 5 Km

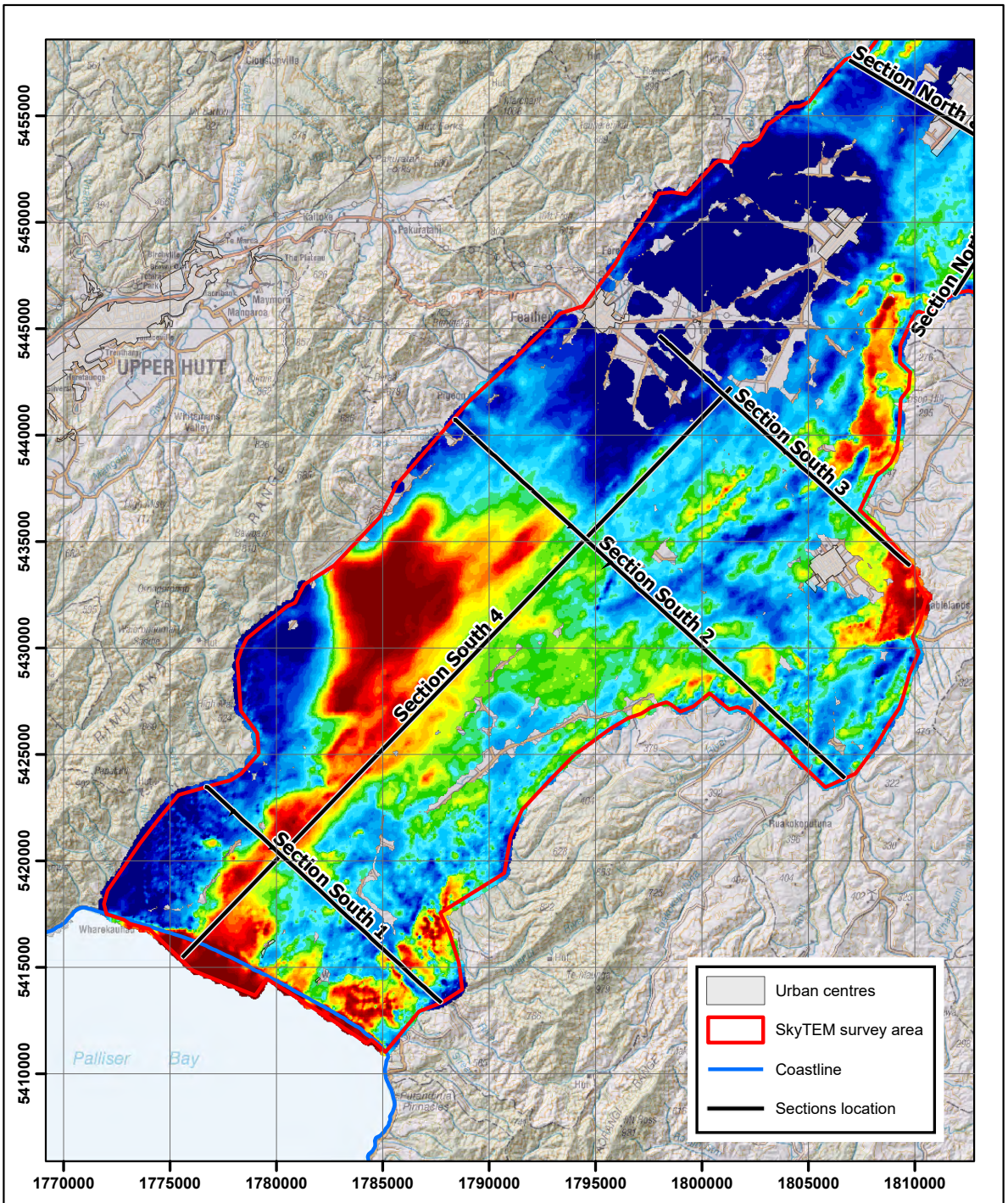

SkyTEM Survey Ruamāhanga South
Mean resistivity map, smooth model at depth 20 - 23 m

Appendix 3

Map No. 3

GNS SCIENCE TE PŪ AO

Mean resistivity (ohm.m)

< 3.5	15.5 - 18.3	80.5 - 95.0
3.5 - 4.2	18.3 - 21.6	95.0 - 112
4.2 - 4.9	21.6 - 25.5	112 - 132
4.9 - 5.8	25.5 - 30.0	132 - 155
5.8 - 6.8	30.0 - 35.4	155 - 183
6.8 - 8.1	35.4 - 41.7	183 - 216
8.1 - 9.5	41.7 - 49.1	216 - 255
9.5 - 11.2	49.1 - 57.9	> 255
11.2 - 13.2	57.9 - 68.3	
13.2 - 15.5	68.3 - 80.5	

N

NZTM2000

0 2.5 5 Km

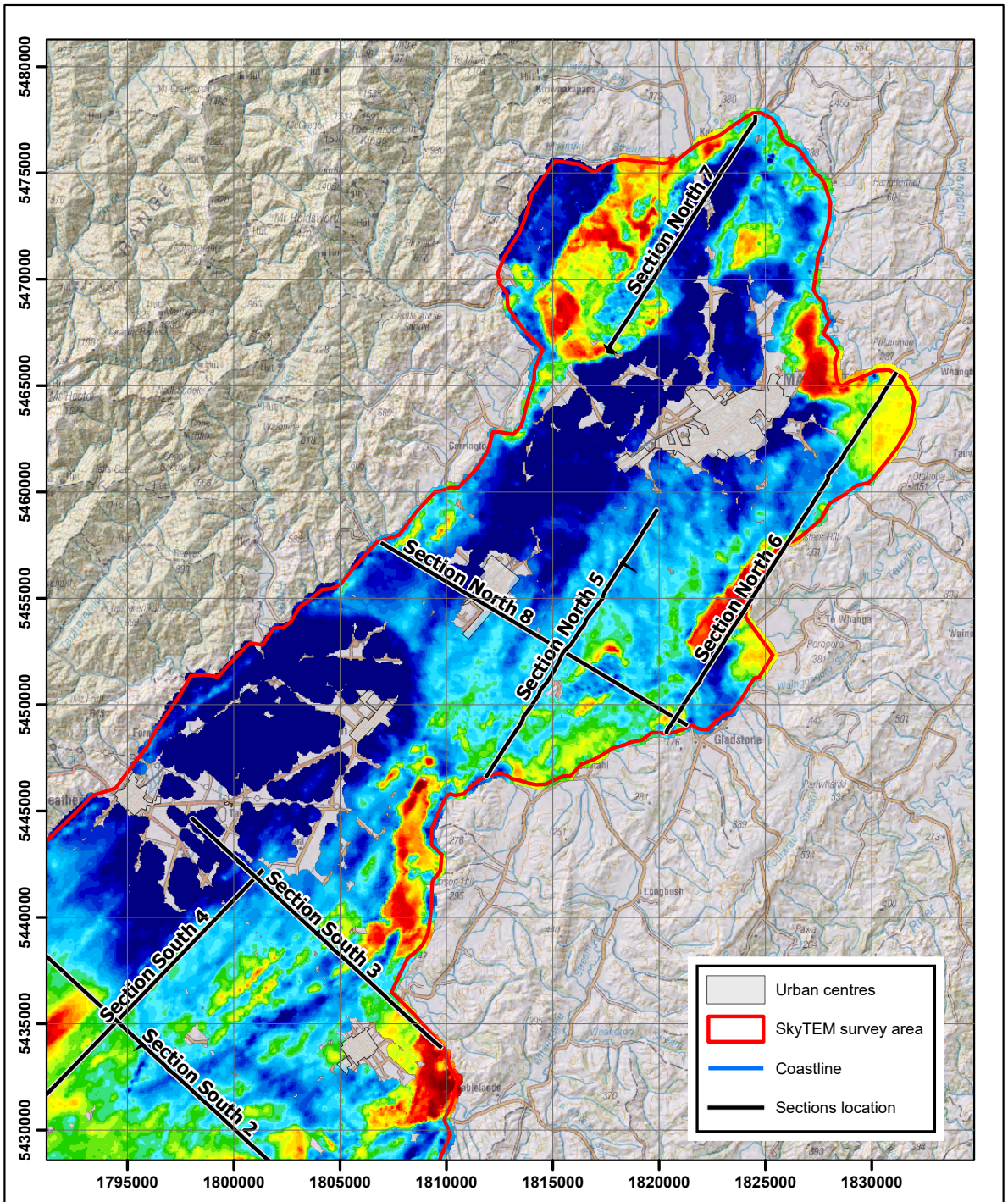

SkyTEM Survey Ruamāhanga North
Mean resistivity map, smooth model at depth 20 - 23 m

Appendix 3

Map No. 4

GNS SCIENCE TE PŪ AO

Mean resistivity (ohm.m)

< 3.5	15.5 - 18.3	80.5 - 95.0
3.5 - 4.2	18.3 - 21.6	95.0 - 112
4.2 - 4.9	21.6 - 25.5	112 - 132
4.9 - 5.8	25.5 - 30.0	132 - 155
5.8 - 6.8	30.0 - 35.4	155 - 183
6.8 - 8.1	35.4 - 41.7	183 - 216
8.1 - 9.5	41.7 - 49.1	216 - 255
9.5 - 11.2	49.1 - 57.9	> 255
11.2 - 13.2	57.9 - 68.3	
13.2 - 15.5	68.3 - 80.5	

N

NZTM2000

0 2.5 5 Km

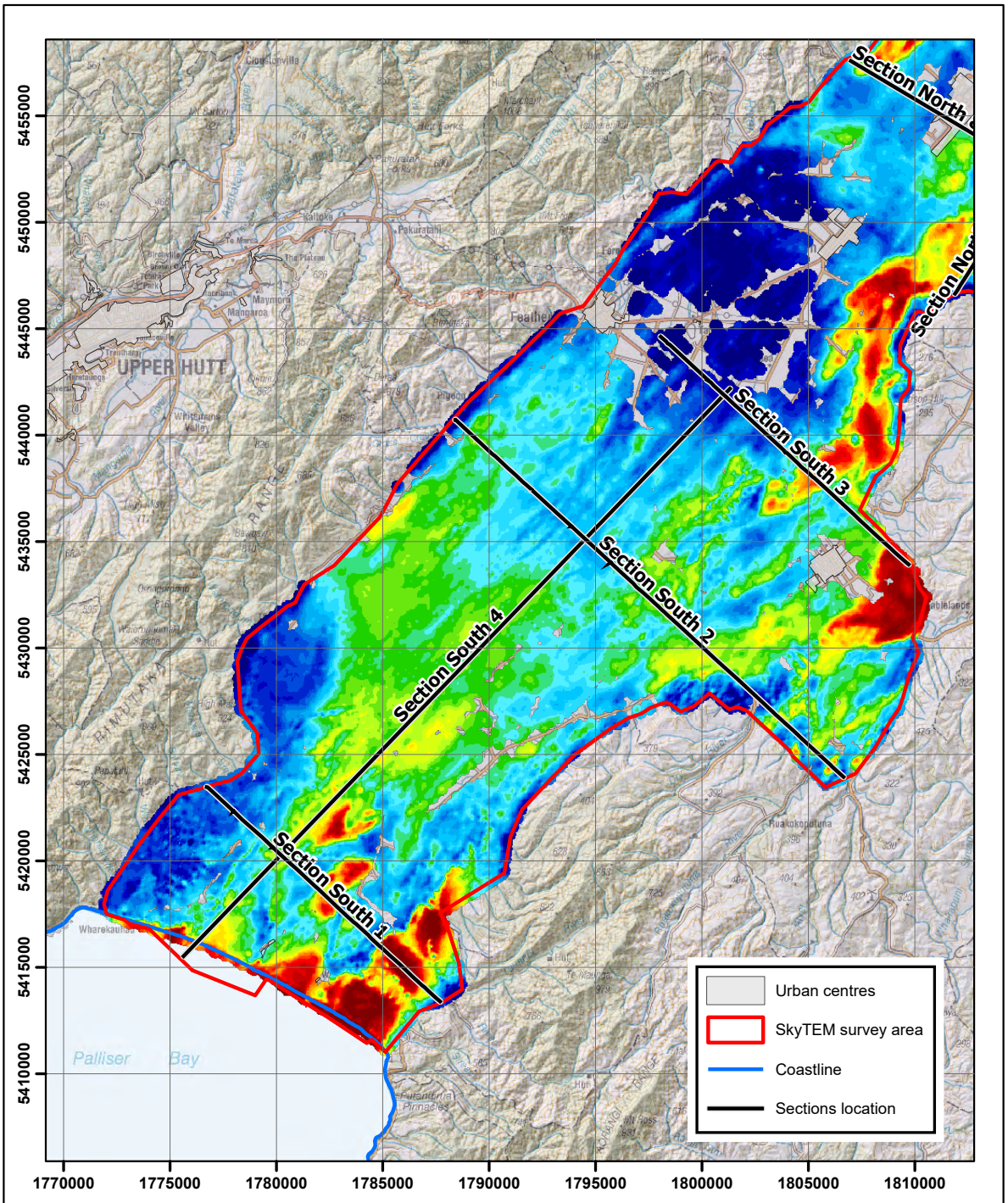

SkyTEM Survey Ruamāhanga South
Mean resistivity map, smooth model at depth 60 - 68 m

Appendix 3

Map No. 5

GNS SCIENCE TE PŪ AO

Mean resistivity (ohm.m)

< 3.5	15.5 - 18.3	80.5 - 95.0
3.5 - 4.2	18.3 - 21.6	95.0 - 112
4.2 - 4.9	21.6 - 25.5	112 - 132
4.9 - 5.8	25.5 - 30.0	132 - 155
5.8 - 6.8	30.0 - 35.4	155 - 183
6.8 - 8.1	35.4 - 41.7	183 - 216
8.1 - 9.5	41.7 - 49.1	216 - 255
9.5 - 11.2	49.1 - 57.9	> 255
11.2 - 13.2	57.9 - 68.3	
13.2 - 15.5	68.3 - 80.5	

N

NZTM2000

0 2.5 5 Km

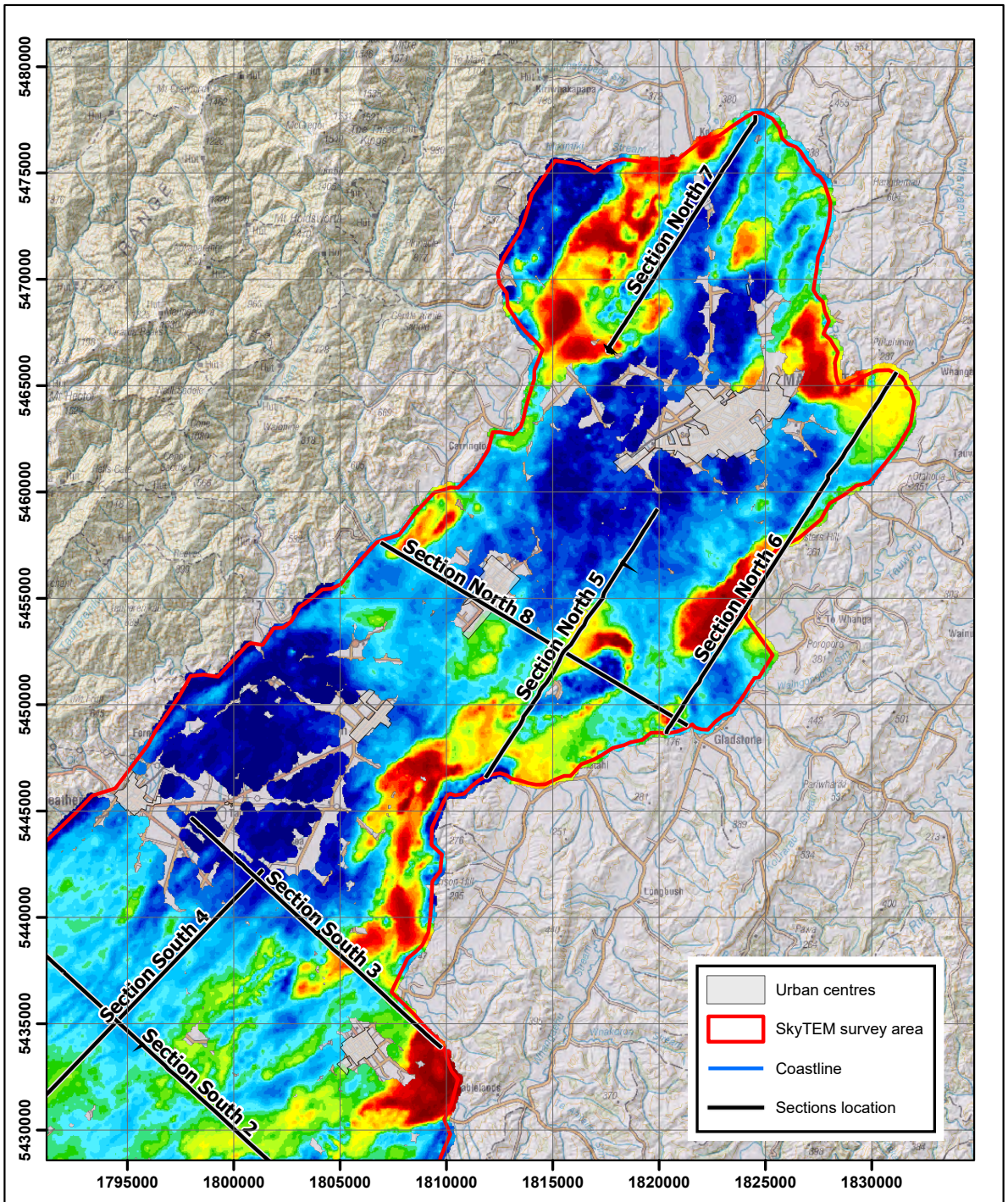

SkyTEM Survey Ruamāhanga North
Mean resistivity map, smooth model at depth 60 - 68 m

Appendix 3

Map No. 6

Mean resistivity (ohm.m)

< 3.5	15.5 - 18.3	80.5 - 95.0
3.5 - 4.2	18.3 - 21.6	95.0 - 112
4.2 - 4.9	21.6 - 25.5	112 - 132
4.9 - 5.8	25.5 - 30.0	132 - 155
5.8 - 6.8	30.0 - 35.4	155 - 183
6.8 - 8.1	35.4 - 41.7	183 - 216
8.1 - 9.5	41.7 - 49.1	216 - 255
9.5 - 11.2	49.1 - 57.9	> 255
11.2 - 13.2	57.9 - 68.3	
13.2 - 15.5	68.3 - 80.5	

N

NZTM2000

0 2.5 5 Km

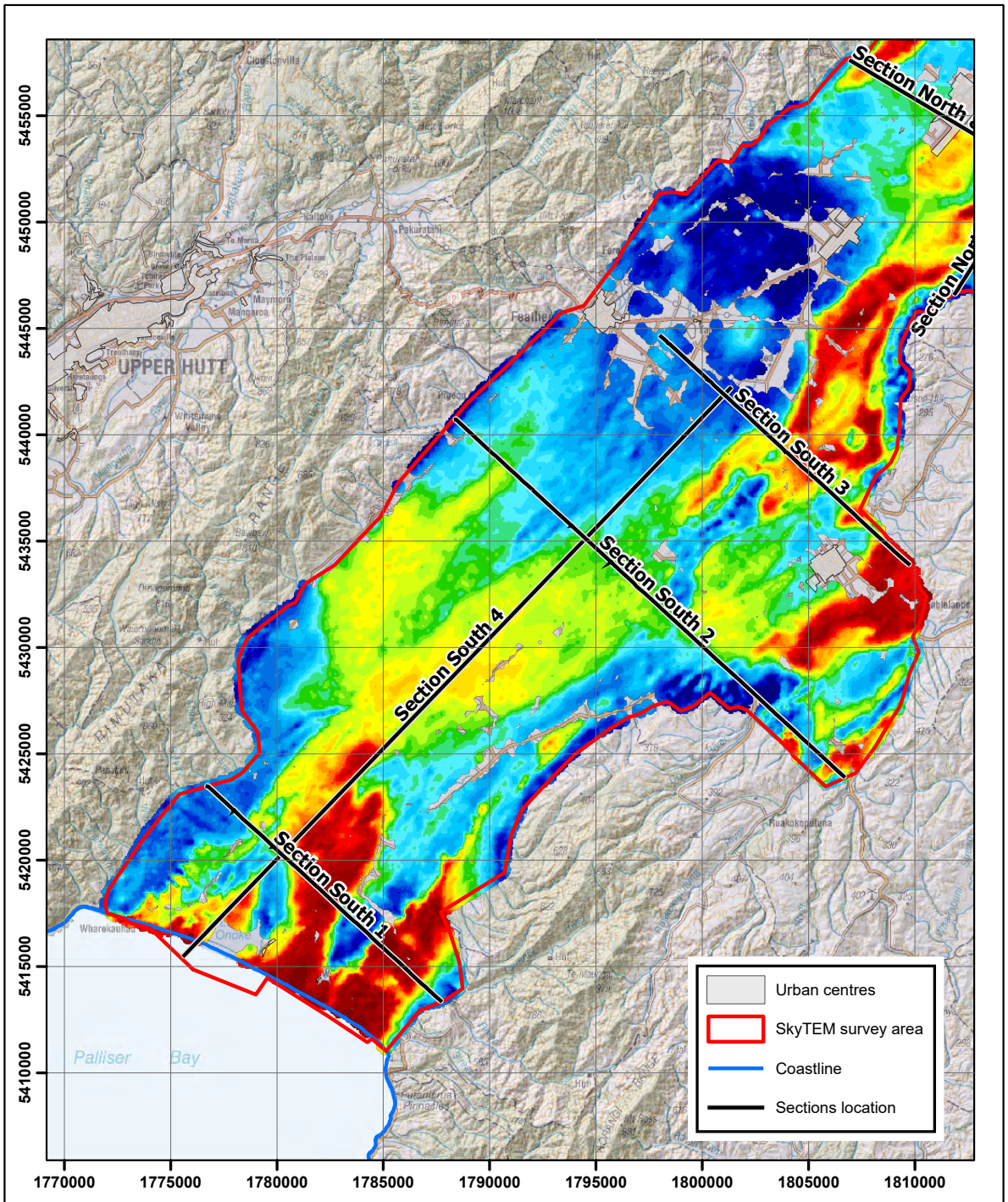

SkyTEM Survey Ruamāhanga South
Mean resistivity map, smooth model at depth 139 - 156 m

Appendix 3

Map No. 7

GNS SCIENCE TE PŪ AO

Mean resistivity (ohm.m)

< 3.5	15.5 - 18.3	80.5 - 95.0
3.5 - 4.2	18.3 - 21.6	95.0 - 112
4.2 - 4.9	21.6 - 25.5	112 - 132
4.9 - 5.8	25.5 - 30.0	132 - 155
5.8 - 6.8	30.0 - 35.4	155 - 183
6.8 - 8.1	35.4 - 41.7	183 - 216
8.1 - 9.5	41.7 - 49.1	216 - 255
9.5 - 11.2	49.1 - 57.9	> 255
11.2 - 13.2	57.9 - 68.3	
13.2 - 15.5	68.3 - 80.5	

N

NZTM2000

0 2.5 5 Km

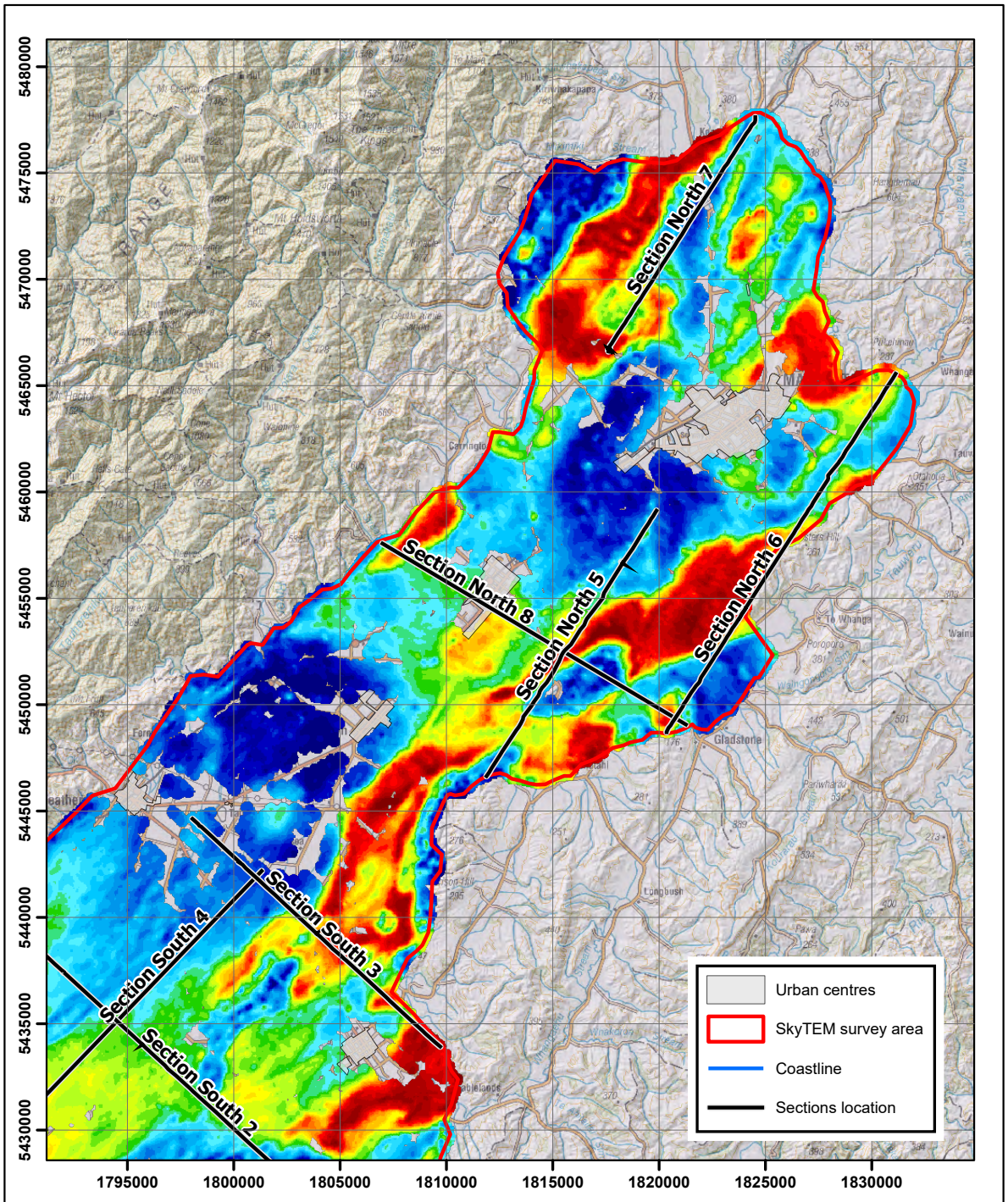

SkyTEM Survey Ruamāhanga North
Mean resistivity map, smooth model at depth 139 - 156 m

Appendix 3

Map No. 8

GNS SCIENCE TE PŪ AO

Mean resistivity (ohm.m)

< 3.5	15.5 - 18.3	80.5 - 95.0
3.5 - 4.2	18.3 - 21.6	95.0 - 112
4.2 - 4.9	21.6 - 25.5	112 - 132
4.9 - 5.8	25.5 - 30.0	132 - 155
5.8 - 6.8	30.0 - 35.4	155 - 183
6.8 - 8.1	35.4 - 41.7	183 - 216
8.1 - 9.5	41.7 - 49.1	216 - 255
9.5 - 11.2	49.1 - 57.9	> 255
11.2 - 13.2	57.9 - 68.3	
13.2 - 15.5	68.3 - 80.5	

N

NZTM2000

0 2.5 5 Km

APPENDIX 4 DELIVERABLE FILE DESCRIPTIONS

In all cases, STD refers to Standard Deviation and UTC refers to Coordinated Universal Time.

Table A4.1 Format of the resistivity model XYZ-ASCII files for both the sharp and smooth models.

Attribute	Description
LINE_NO	Line number
UTMX	Easting NZTM
UTMY	Northing NZTM
TIMESTAMP	Time (days) using epoch starting 30 December 1899, in UTC
FID	Fiducial
RECORD	Record
ELEVATION	Topography (m; from imported DEM)
ALT	Input altitude (metres above ground level)
INVALT	Inverted altitude (metres above ground level)
INVALTSTD	STD on inverted altitude
DELTAALT	Difference between input and inverted altitude (m; inverted – input altitude)
TILT	N/A (not utilised by SkyTEM Z-component inversion)
INVTILT	N/A (not utilised by SkyTEM Z-component inversion)
INVTILTSTD	N/A (not utilised by SkyTEM Z-component inversion)
SHIFT	N/A (not utilised by SkyTEM Z-component inversion)
INVSHIFT	N/A (not utilised by SkyTEM Z-component inversion)
INVSHIFTSTD	N/A (not utilised by SkyTEM Z-component inversion)
NUMDATA	Number of gates inverted (number of data points)
SEGMENTS	Moment ID (low moment = 1, high moment = 2, both = 12 or 21)
RESDATA	Data mis-fit (for each 1D inversion)
RESTOTAL	Total mis-fit (for the entire inversion)
RHO_I_1	Resistivity (Ohm m) for layer_1
RHO_I_2	Resistivity (Ohm m) for layer_2
…	…
RHO_I_N	Resistivity (Ohm m) for layer N
RHO_I_STD_1	STD on resistivity for layer_1
RHO_I_STD_2	STD on resistivity for layer_2
…	…
RHO_I_STD_N	STD on resistivity for layer_N
SIGMA_I_1	Conductivity (mS/m) for layer_1
SIGMA_I_2	Conductivity (mS/m) for layer_2
…	…
SIGMA_I_N	Conductivity (mS/m) for layer_N
DEP_TOP_1	Depth (m) to top of layer_1

Attribute	Description
DEP_TOP_2	Depth (m) to top of layer_2
…	…
DEP_TOP_N	Depth (m) to top of layer_N
DEP_BOT_1	Depth (m) to bottom of layer_1
DEP_BOT_2	Depth (m) to bottom of layer_2
…	…
DEP_BOT_N-1	Depth (m) to bottom of layer_N-1
THK_1	Thickness (m) of layer_1
THK_2	Thickness (m) of layer_2
…	…
THK_N-1	Thickness (m) of layer_N-1
THK_STD_1	STD on thickness of layer_1
THK_STD_2	STD on thickness of layer_2
…	…
THK_STD_N-1	STD on thickness of layer_N-1
DEP_BOT_STD_1	STD on depth bottom of layer_1
DEP_BOT_STD_2	STD on depth bottom of layer_2
…	…
DEP_BOT_STD_N-1	STD on depth bottom of layer_N-1
DOI_CONSERVATIVE	DOI Conservative for resistivity (m)
DOI_STANDARD	DOI Standard for resistivity (m)

Leapfrog requires three files to import a resistivity model as an effective borehole log.

- *Merged_SCI_smooth_MOD_collar.csv* – location information for each model point.
- *Merged_SCI_smooth_MOD_survey.csv* – uniformly set to vertical for the 1D models.
- *Merged_SCI_smooth_MOD.csv* – resistivity data saved as interval information.

Only the smooth model has been delivered as a LeapFrog pseudo borehole database.

Table A4.2 Collar file for resistivity models in Seequent Leapfrog Pseudo borehole format (e.g. for importing into Leapfrog Software). The file is semi-colon delimited.

Attribute	Description
holeID	Model ID
x	Easting NZTM
y	Northing NZTM
z	Elevation of the surface location at the model location (m)

Table A4.3 Survey file for resistivity models in Seequent Leapfrog Pseudo borehole format (e.g. for importing into Leapfrog Software). All pseudo boreholes are assumed to be vertical. The file is semi-colon delimited.

Attribute	Description
holeID	Model ID
depth	Set to 0
dip	Set to 90
azimuth	Set to 0

Table A4.4 Data file for resistivity models in Seequent Leapfrog Pseudo borehole format (e.g. for importing into Leapfrog Software). All pseudo boreholes are assumed to be vertical.

Attribute	Description
holeID	Model ID
from	Top of interval
to	Base of interval
Res(ohmm)h	Resistivity of the interval
ResSTD	Standard deviation of the resistivity
Cond(ms/m)	Conductivity of the interval

The smooth and sharp models were delivered as ESRI ASCII grids for both the data presented as layers below ground surface and as elevation (above and below sea level). Each file comes as a data file (**.asc*) and the projection file (**.prj*). The grids contain the resistivity in Ohm.m.

Table A4.5 Format of the header of the mean resistivity files as ESRI ASCII grids.

Attribute	Description
ncols	Number of rows in the grid 1211
nrows	Number of columns in the grid 1344
xllcorner	Lower left corner x co-ordinate 1771675.0
yllcorner	Lower left corner y co-ordinate 5410825.0
cellsize	Grid size from interpolation 50 m
Nodata_value	Blank pixels -9999.0

The same layers have been produced as layer files for direct import into an ARC Pro project. Each grid is classified into 28 levels from 3 to 300 ohm.m in a logarithmic scale for resistivity (ohm.m).

www.gns.cri.nz

Principal Location

1 Fairway Drive, Avalon
Lower Hutt 5010
PO Box 30368
Lower Hutt 5040
New Zealand
T +64-4-570 1444
F +64-4-570 4600

Other Locations

Dunedin Research Centre
764 Cumberland Street
Private Bag 1930
Dunedin 9054
New Zealand
T +64-3-477 4050
F +64-3-477 5232

Wairakei Research Centre
114 Karetoto Road
Private Bag 2000
Taupo 3352
New Zealand
T +64-7-374 8211
F +64-7-374 8199

National Isotope Centre
30 Gracefield Road
PO Box 30368
Lower Hutt 5040
New Zealand
T +64-4-570 1444
F +64-4-570 4657